The Thesis Committee for Sarah M. Prentice
Certifies that this is the approved version of the following Thesis:

The Effect of Methane and Fluid Geometry on CO_2 Enhanced Oil Recovery

APPROVED BY
SUPERVISING COMMITTEE:

Susan Hovorka, Supervisor

William L. Fisher, Co-Supervisor

Timothy A. Meckel

The Effect of Methane and Fluid Geometry on CO_2 Enhanced Oil Recovery

by

Sarah M. Prentice

Thesis

Presented to the Faculty of the Graduate School of

The University of Texas at Austin

in Partial Fulfillment

of the Requirements

for the Degree of

Master of Science in Energy and Earth Resources

The University of Texas at Austin

May 2019

Dedication

To my parents for encouraging a love of science and learning from a young age.

Acknowledgements

I would like to acknowledge my thesis committee, Dr. Susan Hovorka, Dr. William Fisher, and Tip Meckel, for their endless support, encouragement and effort throughout my time at the University of Texas. I will be eternally grateful for your mentorship and wisdom.

I would like to thank the Gulf Coast Carbon Center of the Bureau of Economic Geology at The University of Texas at Austin, which sponsored me and every single person there because they all helped me in some form along the way.

I want express gratitude to the staff and faculty of the Jackson School of Geosciences and Energy and Earth Resources who have been such significant contributors to my educational career.

Lastly a special thanks to my family, friends and Jack, who have supported me throughout not just my master's degree but also my life.

Abstract

The Effect of Methane and Fluid Geometry on CO_2 Enhanced Oil Recovery

Sarah M. Prentice, M.S.E.E.R.

The University of Texas at Austin, 2019

Supervisor: Susan Hovorka

Co-Supervisor: William L. Fisher

CO_2 Enhanced Oil Recovery (EOR) is a process that involves injecting large volumes of carbon dioxide as a supercritical fluid into hydrocarbon reservoirs in order to recover hydrocarbons that are not mobilized during primary or secondary production. Some of the injected CO_2 is produced with the produced hydrocarbons and then recycled by reinjection into the reservoir. Most CO_2 floods performed for EOR are miscible, which means the fluids mix to form a homogeneous mixture under a specific set of conditions. For a typical oil field, miscible floods are more efficient in recovering oil than immiscible floods. When recycled CO_2 includes a high percentage of methane, miscibility is significantly reduced. For a typical oil field, miscible floods are more efficient in recovering oil than immiscible floods. Calculations from produced fluid data base shows that at 18 mole percent methane, 28 percent of offshore oil reservoirs became immiscible (Ogbaubau, 2015). The effect was more pronounced in nearshore fields.

In this study, I assessed the fluid distribution in a study area to determine if methane production can be avoided by strategic completion of wells to avoid high methane areas. High Island 10L, High Island 24L and ST TR 60S were selected due to

availability of structural data. Using seismic, well log interpretation, and production data it was found that, of the wells evaluated, 94 percent had solution gas drive. A number of economic solutions to the problem were postulated; these included a methane separation facility, changes to CO_2 recycling, cutting CO_2 with another gas, and accepting immiscible flood conditions. The following equation was developed to estimate the increased cost for miscible CO_2 enhanced oil recovery:

$$
\begin{aligned}
&General\ Additional\ Costs\ of\ CO2\ Enhanced\ Oil\ Recovery \\
&\quad = (Cost\ of\ CO2\ Recycling\ Plant + Cost\ of\ Pipelines \\
&\quad + Cost\ of\ CO2\ to\ Offset\ Methane\ Immiscibility \\
&\quad + Transportation\ costs + O\&M\ costs + Pipeline\ Operation\ Costs) \\
&\quad - (Value\ of\ Storage\ Tax\ Credit)
\end{aligned}
$$

Where:

$$
\begin{aligned}
&Cost\ of\ CO2\ to\ Offset\ Methane\ Immiscibility \\
&\quad = \left(cost\ of\ \frac{CO2}{ton} * tons\ of\ CO2\ needed\ to\ offset\ Methane\right) \\
&Cost\ of\ Pipelines \\
&\quad = (cost\ of\ pipeline\ construction\ per\ mile * mumber\ of\ miles) \\
&Value\ of\ Storage\ Tax\ Credit \\
&\quad = (\frac{\$35}{ton} of\ CO2\ stored\ Tax\ Credit * tons\ of\ stored\ CO2)
\end{aligned}
$$

The equations parameters were then used to create a table showing how the economic solutions might affect the cost of CO_2 enhanced oil recovery.

Table of Contents

List of Tables

List of Figures

Chapter 1: Introduction

1.1 Production of Oil

Modern day oil drilling in the United States began in 1859 when Edwin Drake became the first American entrepreneur to successfully drill for oil, setting off a wave of businessmen to drill their own oil gushers and paving the way for oil to become the largest consumed energy source in the United States of America today (Latson, 2015). Today, we are far beyond the wasteful but iconic oil gushers of Drake's time, however, as much as two thirds of conventional crude oil remains unproduced due to the limitations of fluid flow physics (National Energy Technology Laboratory, n.d.). Enhanced oil recovery (EOR) technologies have been developed to recover more of the remaining unproduced oil.

The first phase of oil production produces only about 10 percent of original oil in place (Schlumberger, 2018). In primary production, there are five different drive mechanisms for production. A drive mechanism is a source of natural energy in a reservior that can be used to move a hydrocarbon towards the wellbore. The five different drives mechanisms are gas expansion drive, rock drive, gravity drainage, water drive, and solution gas drive, which can all be present in different combinations in the reservior. Gas expansion occurs in reservior systems with little to no water drive and free gas, such as a gas cap, is present. During production, the free gas expands and slows the rate of fluid pressure drop. In rock drive, as the fluid pressure declines, the net confining pressure increases and can cause a pore space collapse, thus expeling hydrocarbons. Gravity drainage requires high vertical permeability or steeply dipping beds and involves oil draining downward from the force of gravity. Water drive is caused by an aquifer being present in the reservior. As oil or gas is produced, the aquifer expands thereby displacing hydrocarbons towards the well and keeping the rate of pressure drop down. In solution gas drive, the reservior is surrounded by an impermeable seal allowing for high pressure above the bubblepoint in the reservior. Due to the high pressure, gas may dissolve in the oil. During production, once pressure is below the bubblepoint, some of the gas bubbles become free and

expand, pushing the oil to the wellbore while the still disolved gas bubbles reduce the oil viscosity, thus improving flow rate (AAPG, 2016; Petrowiki, 2015; Sills, 1993).

The second phase of oil production, or secondary recovery, involves reinjecting a reservoir fluid, typically water, into the reservoir to maintain reservoir pressure and can recover an additional 10 to 30 percent of original oil in place (Schlumberger, 2018; Department of Energy, n.d.). EOR, sometimes called tertiary recovery, can happen at any time along the lifespan of a field, and methods include gas floods, polymer floods, thermal methods, chemical floods, and microbial processes. Polymer flooding and thermal methods improve production through altering the mobility ratio by decreasing the mobility of the injected fluid and increasing the mobility of the hydrocarbon. Chemical flooding, microbial processes, and miscible gas flooding impact capillary forces and improve displacement efficiency (Bondor et al., 2005; Schlumberger, 2018). EOR methods can result in another 10 to 20 percent recovery resulting, along with primary and secondary recovery, a total of 30 to 60 percent of original in place oil produced (Department of Energy, n.d.). One of the methods of particular interest of the last few decades is CO_2 EOR, which the EIA estimates could recover 240 billion barrels of additional oil from US oil fields (EIA, 2011).

CO_2 EOR is a process that involves injecting large volumes of supercritical carbon dioxide into hydrocarbon reservoirs. When the gas is injected into an oil reservoir, it can be miscible (i.e., mixable in all proportions at specific conditions) with residual crude oil, so light hydrocarbons dissolve in the CO_2 and CO_2 dissolves in the oil. This causes the interfacial tension to disappear and enables the CO_2 to displace the oil towards a producing well. CO_2 also reduces the viscosity of the oil by causing it to swell as it dissolves, which also improves the efficiency of displacement. Usually CO_2 injections are alternated with water injections in a process called water alternating gas or WAG floods and this helps to prevent CO_2 from breaking through the producing well ahead of the oil (National Energy Technology Laboratory, 2010) (Figure 1.1). Unlike many other EOR processes, the CO_2 used during CO_2 EOR is produced along with the

crude oil and then can be collected and reinjected back into the reservoir. This process is called CO_2 recycling and is another one of the advantages of using CO_2 EOR over other methods. The process has some unintended by products, however. Along with the CO_2, other gases are typically present in the reservoir, such as hydrocarbon gases like methane and butane but also hydrogen sulfide and nitrogen (Petrowiki, 2018). In some projects, like in the Permian Basin, methane is separated from the CO_2, which increases capital and energy costs and is then sold (Melzer, 2012). If no separation processing is performed with each recycling of the CO_2 gas, the concentration of these contaminants increases and some can change the effectiveness of the CO_2 EOR process.

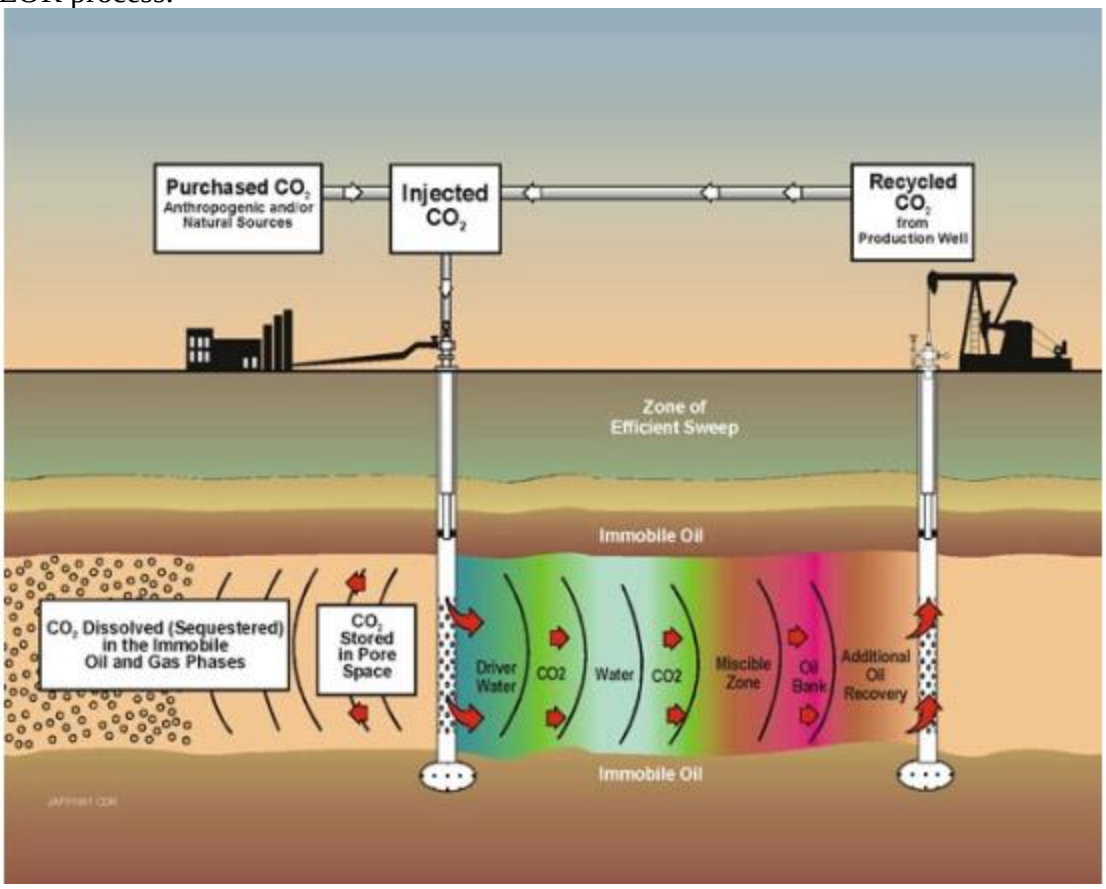

Figure 1.1: Depiction of WAG flood process (From National Energy Technology Laboratory, 2010)

CO_2 is a favorable process to utilize during EOR, not only because it is less expensive than many other similarly miscible fluids, but also because of its potential to help mitigate the production of greenhouse gases from anthropogenic sources (National Energy Technology Laboratory, 2010). Over the years, there has been concern from many over the change in climate caused by the emissions of greenhouse gases from anthropogenic sources. In 2017, the global average CO_2 was 405 parts per million (Lindsey, 2018). While CO_2 does not absorb the most heat per molecule among the greenhouse gasses, it is the most abundant besides water vapor and can remain in the atmosphere for thousands of years. CO_2 also contributes two thirds of the total energy imbalance causing Earth's temperature to rise (Lindsey, 2018). One of the solutions developed to help reduce these emissions is fitting carbon capture systems on large volume anthropogenic CO_2 facilities, which captures the CO_2 produced instead of releasing it into the atmosphere. After capture, the CO_2 can be disposed of by injecting it underground for storage or used for a variety of purposes such as CO_2 EOR. During project development, CO_2 EOR stores more CO_2 than the incremental oil it recovers ultimately produces, so the process is carbon negative making it potentially more environmentally friendly than other EOR methods (Nuñez-López et al., 2017).

The Gulf Coast is an important site for carbon sequestration because it has sites with large potential storage, many anthropogenic CO_2 sources, and existing infrastructure networks. Potential anthropogenic sources for CO_2 are from the production of electricity, cement production, biomass conversion, iron and steel, chemical plants, and refineries. The cost of capture from these sources varies widely along with transportation options to ideal sites. Models, such as the one created by Tutton (2018), optimize these options to determine the most economical and utilized path for sequestration.

The Gulf Coast also has a total of 810 MMBbl of economically recoverable oil with an oil price of $90 a barrel via CO_2 enhanced oil recovery and an additional bonus of 310 MMmt of CO_2 storage as a result. At the $90 a barrel oil price, this would make the oil recovered worth

$72.9 billion U.S. dollars. This makes the Gulf Coast the region with the largest amount of economically recoverable oil with CO_2 enhanced oil recovery in the offshore United States (Malone, 2014).

1.2 Potential Economic Effects of Legislation

Citizens of the United States have become increasingly concerned with the potential effects of climate change and have begun to push more for their elected representatives to pass legislation to combat it. In the 2018 congressional election, 48 percent of Americans said climate change should be a top priority for the president and Congress, and 40 percent of respondents said their position on global warming would be very important on deciding whom to vote for in the 2018 congressional election (Leiserowitz et al, 2018). As such, many legislators have begun to push for an agenda aimed at helping to mitigate climate change, which can sometimes greatly affect the economics of CO_2 enhanced oil recovery.

On February 9th 2018, Congress passed the Bipartisan Budget Act of 2018 containing a revamping of an existing tax credit called 45Q. The previous tax credit allowed for $20 per ton for stored CO_2 sequestration projects and $10 per ton for CO_2 stored as part of CO_2 enhanced oil recovery. The reauthorized tax credit allows for $50 per ton of CO_2 stored via sequestration projects and $35 per ton of CO_2 stored during CO_2 enhanced oil recovery projects with the limitation that constructions begin by 2024. This more than tripling of the tax credit for CO_2 enhanced oil recovery has since stimulated interest in starting new enhanced oil recovery projects.

Americans for Carbon Dividends, a 501(c)(4) organization created to support a carbon tax-and-dividend plan, has proposed a tax that would equal $40 per ton of carbon dioxide produced. This plan is supported by ExxonMobil (donating $1 million) and also by Exelon, BP, First Solar, General Motors, Shell, Total and PepsiCo (Mufson, 2018). However, no serious legislation containing a tax has come through the U.S. Congress. Such a tax would have a huge

impact on carbon sequestration and CO_2 enhanced oil recovery because sources of CO_2 would go from selling CO_2 to possibly having to pay to get rid of it. CO_2 enhanced oil recovery would depend on the price of oil being able to outpace the cost of the new tax or for the enhanced oil recovery job to be carbon negative.

1.3 Methane Caused Immiscibility

Miscibility is a function of many parameters including fluid composition and fluid properties, such as density, temperature, and pressure. The minimum pressure at which a crude oil will be miscible with carbon dioxide at reservoir temperature is called the minimum miscibility pressure. Changes in fluid composition or a drop-in pressure below minimum miscibility pressure can result in an immiscible CO_2 flood. Various gases in the reservoir can either raise or lower the minimum miscibility pressure. Whether an impurity raises or lowers the minimum miscibility pressure is dependent on whether it improves the solvency of CO_2. Solvency improves when the solvent is diluted with an impurity with a lower critical temperature (Lake, 2014). Methane, for example, increases the minimum pressure needed for miscibility, but other gases, such as ethane and H_2S, decrease the minimum miscibility pressure (Figure 1.2). Immiscible CO_2 flooding can also help recover additional oil by reducing oil viscosity and by reducing interfacial tension. However, it has been found in studies, such as the one conducted by Perera et al. (2016), that immiscible CO_2 flooding is less efficient than miscible CO_2 flooding and, therefore, miscible flooding is more widely utilized.

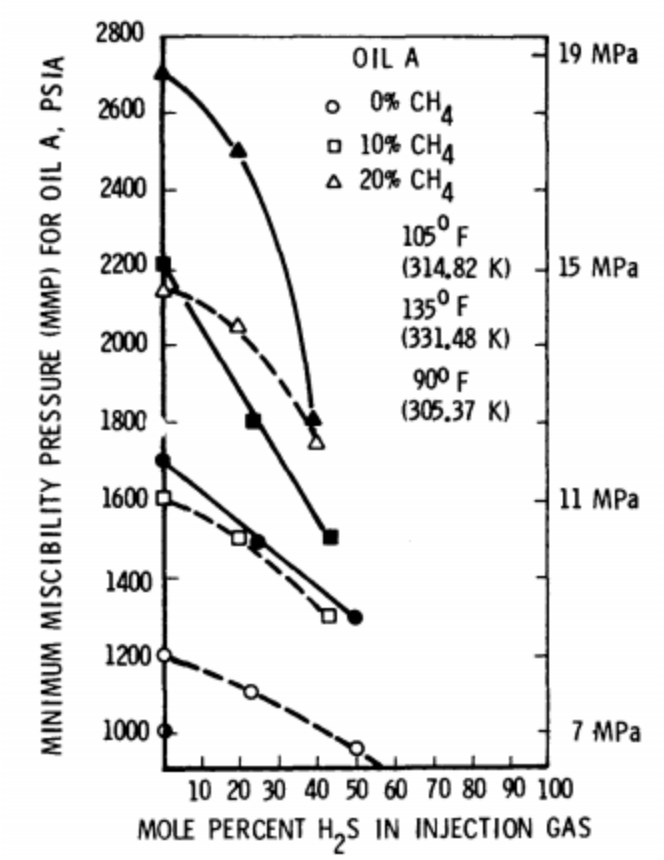

Figure 1.2: Effect of increasing H_2S and methane gas on minimum miscibility pressure (From Metcalfe, 1986).

A study by Ogbuabuo (2015) on the feasibility of CO_2 enhanced oil recovery used data from 3,598 offshore Gulf of Mexico oil reservoirs and, via a model, put them through several screening methods. The first screening used the guidelines depicted in Figure 1.3. The model assumed only CO_2 and methane was produced. Reservoirs that had a pressure difference between reservoir pressure and minimum miscibility pressure greater than 100 were immiscible. The model found that 28 percent of reservoirs would be rendered immiscible by 18 mole percent of methane in the recycled fluids. The problem was found to be worse in shallow water reservoirs, or reservoirs with less than 1,000 feet of water depth, with an increasing percent of reservoirs immiscible at 18 mole percent methane contamination with decreasing total depth (Figure 1.4) (Ogbuabuo, 2015).

Technical Screening Guides		
	Recommended	Range of Current Projects
Crude Oil		
Gravity, °API	>22	27 to 44
Viscosity, cp	<10	0.3 to 6
Composition	High percentage of intermediate hydrocarbons (especially C_5 to C_{12})	
Reservoir		
Oil saturation, % PV	>20	15 to 70
Type of formation	Sandstone or carbonate and relatively thin unless dipping.	
Average permeability	Not critical if sufficient injection rates can be maintained.	
Depth and temperature	For miscible displacement, depth must be great enough to allow injection pressures greater than the MMP, which increases with temperature (see Fig. 7 of Ref. 1) and for heavier oils. Recommended depths for CO_2 floods of typical Permian Basin oils follow.	
	Oil Gravity, °API	Depth must be greater than (ft)
For CO_2-miscible flooding	>40	2,500
	32 to 39.9	2,800
	28 to 31.9	3,300
	22 to 27.9	4,000
	<22	Fails miscible, screen for immiscible*
For immiscible CO_2 flooding (lower oil recovery)	13 to 21.9	1,800
	<13	All oil reservoirs fail at any depth
At <1,800 ft, all reservoirs fail screening criteria for either miscible or immiscible flooding with supercritical CO_2.		

Figure 1.3: Screening guidelines for CO_2 EOR (From Taber et al., 1997).

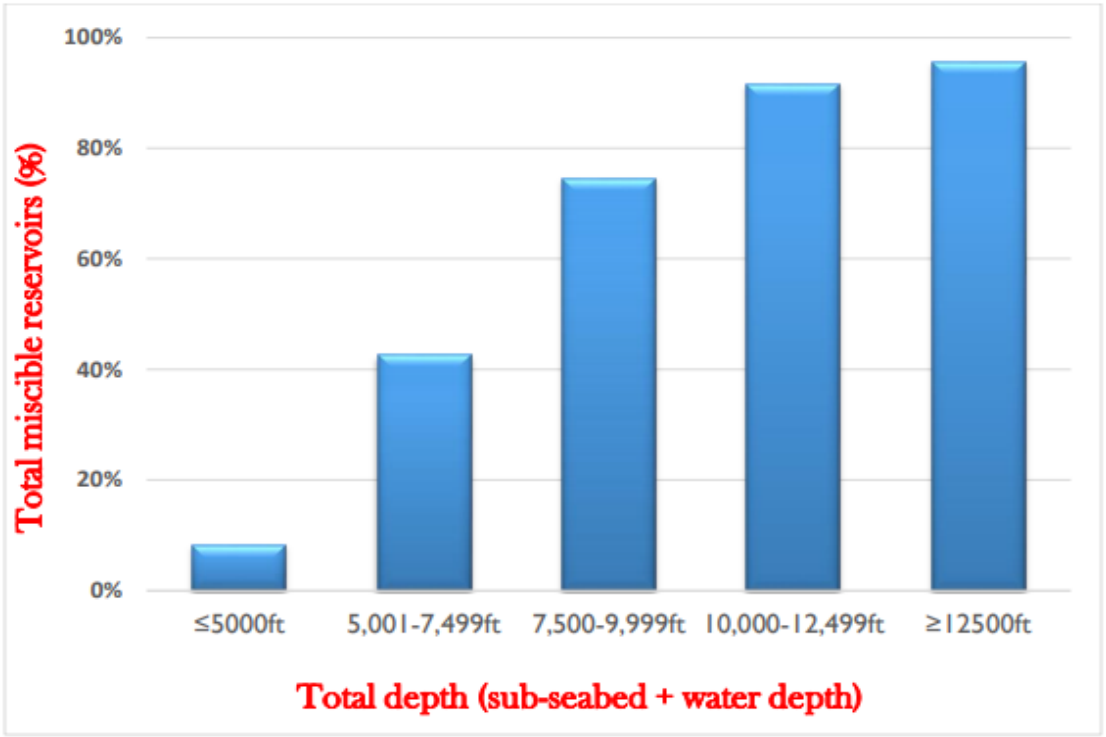

Figure 1.4: Percentage of 3,598 Gulf of Mexico oil reservoirs miscible at 18 mole percent methane contamination at varying total depths (From Ogbuabuo, 2015).

Most reservoirs are more oil prone or have lower gas to oil ratios (GOR) in deep water and more gas prone, or higher gas to oil ratios, in shallow water in the Texas Gulf Coast, meaning these sites may be more likely to experience methane contamination (Figure 1.4). Immiscibility as a result of methane contamination could render CO_2 enhanced oil recovery in many of these reservoirs uneconomical unless a way to isolate methane and oil production can be identified.

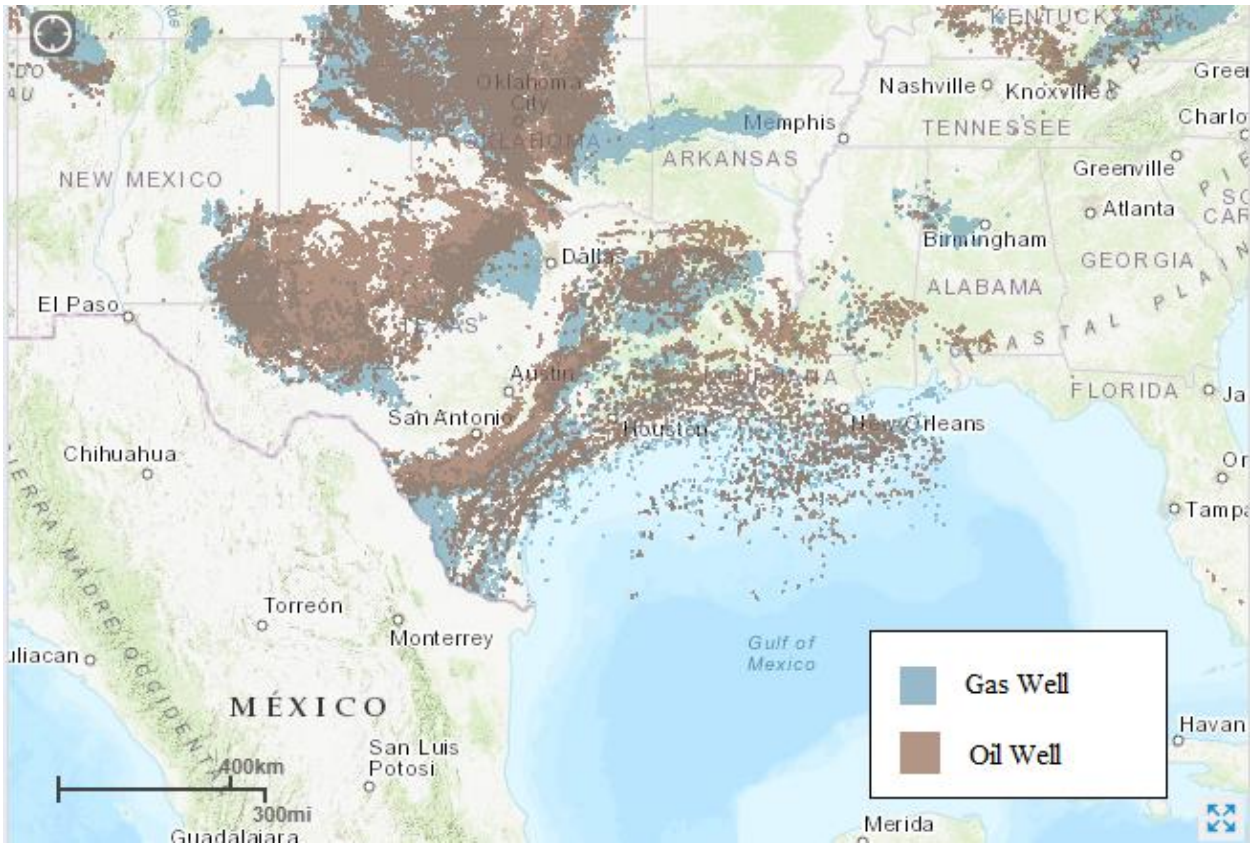

Figure 1.5: Map of oil and gas wells in Gulf Coast (Modified from EIA, 2019).

For this study, I classified reservoirs into the three scenarios depicted in Figure 1.6. In scenario one and two, the gas can, for the most part, be avoided by a strategic well completion design, and contamination of CO_2 by methane during EOR would be reduced. In scenario three, which is controlled by solution gas drive, gas and oil are mixed, and methane contamination would be unavoidable. In order to know how many of the Gulf Coast oil reservoirs that are

potential enhanced oil recovery candidates would be affected by the methane separation cost or miscibility loss, the geometry of their oil and gas within the reservoir must be determined.

Figure 1.6: Three common scenarios for hydrocarbon geometry. Green denotes oil molecules and red denotes gas molecules.

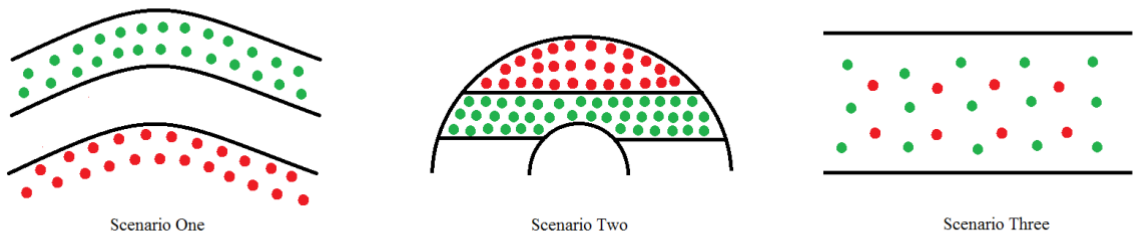

A preliminary search for literature containing structure data showing the geometry of fluids of the reservoirs in the gulf coast was made and did not find any substantial data sources. Therefore, I selected High Island 24L, High Island 10L, and ST TR 60S to use as a case study because there was suitable structure data from 3D Seismic interpretation done by DeAngelo (2019), Beckham (2018), Ruiz (2019), Fifariz (2019), and Ramirez-Garcia (2019). A suite of well logs were interpreted for hydrocarbons and paired with the structure data to determine the fluid geometry.

Chapter 2: Regional Geology of the Gulf of Mexico Basin

2.1 Basin History

Development of the Gulf of Mexico Basin began during the Late Triassic and Early Jurassic as the North American tectonic plate separated from the South American and African plates causing basin subsidence and continental crust thinning as rifting progressed to the Middle Jurassic (Salvador, 1987). During the Late Jurassic, a narrow connection between the Gulf of Mexico and the Atlantic Ocean developed from the southward drift of the Yucatan block, causing salt deposition and low sediment supply, which resulted in carbonate deposition.

During the Cenozoic, the main fluvial axes for the Gulf of Mexico Basin, from the westernmost to easternmost, was the Rio Bravo, Rio Grande, Guadalupe, Colorado, Houston-Brazos, Red, Mississippi, and Tennessee, with the High Island area lying between the Houston-Brazos and Red (Figure 2.1).

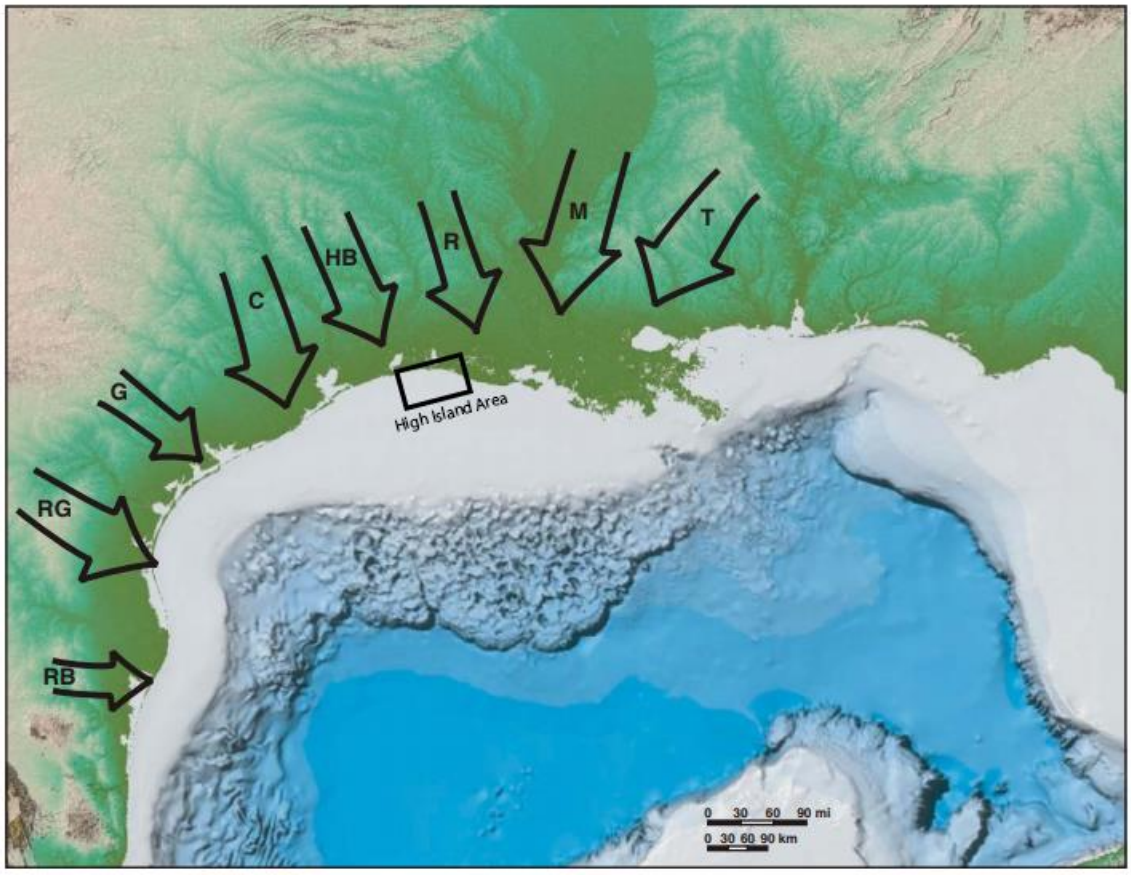

Figure 2.1: Fluvial Input Axes of the Gulf Coast during the Cenozoic (From Galloway et al., 2011).

Starting in the Early Cretaceous and through the early Paleocene, the Laramide orogeny resulted in high sediment yields of mixed carbonates and siliclastics at rates greater than 100,000 km^3/m.y (Galloway et al., 2011). During the late Paleocene through early Eocene, there was a high influx of sediments via newly established river systems, which allowed for massive, fluvial-dominated deltaic deposition of siliclastics in the northwestern part of the basin and caused progradation of the continental margin by tens of kilometers (Galloway et al., 2000). Delta systems' sediment-input volume decreased during the latest Eocene but increased again to approximately 55,000 km^3/m.y of clastic sediments in the Norias/Rio Grande delta systems during the Oligocene, which culminated in a significant transgression and subsequent regression (Galloway et al., 2001, 2011).

Galloway et al. (2000) categorized three primary depositional tracts during the Cenozoic as deep basin, coastal, and plain (Figure 2.2). The deep basin depositional sequence is the fluvial to delta to delta-fed apron; the coastal depositional sequence is the coastal plain to shore zone to shelf to shelf fed apron; and the plain is the delta flank to submarine fan. The deep basin systems tract extended from mid-Louisiana to about Houston, Texas, and this is the location of the High Island area.

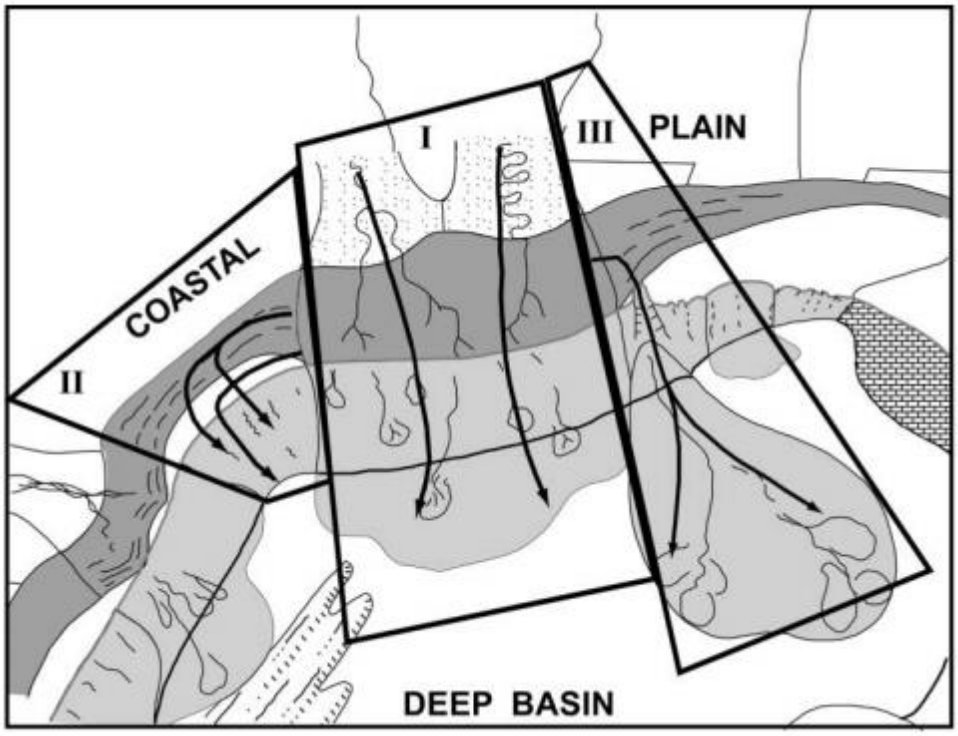

Figure 2.2: Three principal depositional systems tracts in the Gulf of Mexico during the Cenozoic (From Galloway et al., 2000).

2.2 MIOCENE REGIONAL GEOLOGY

The lower Miocene of the northwestern Gulf of Mexico Basin experienced an eastward shift of depositional axes that was caused by a shift from a Paleogene pattern of sediment supply dominated by northwestern fluvial systems to a Neogene pattern dominated by fluvial systems entering from the north of the basin (Galloway, 2005). The early- to mid-Miocene's sedimentation patterns were affected by the glaciation of Antarctica, which caused eustatic fluctuations in sea level (Lewis and others, 2007). During the middle Miocene, the eastward shift of the depositional axes continued with establishment of the Tennessee River axis east of the Mississippi River axis with the two merging by the late Miocene to produce the dominant depocenter of the basin (Combellas-Bigott and Galloway, 2006). The Corsair axis, which is

located on the middle Texas Coastal plain, also contributed to sediment influx during this time period (Galloway, 2005; Galloway et al., 2011).

2.3 MIOCENE STRATIGRAPHY AND STRUCTURE

The Miocene is defined by four basin-margin "genetic stratigraphic sequences" (Galloway, 1989) using "bounding marine flooding horizons" along the basin margins, which are comprised of the first lower Miocene (LM1), the second lower Miocene (LM2), the middle Miocene (MM) and the upper Miocene (UM) (Figure 2.3) (Galloway et al., 2000). The two confining zones of most significance are the *Marginulina ascensionesis* (Marg A) and *Amphistegina chipolensis* (Amph B) biochronozones, which comprise the genetic sequence boundaries of LM1 and LM2. Within the lower to middle Miocene, maximum regressive lower maximum flooding surfaces have been interpreted from Seismic Data, including MFS08, MFS09, MFS10, and MFS11. MFS09 is also known as the Amph B biochronozone.

The significant fault zones that affected the Miocene succession in the Texas shoreline are the lower Miocene Clemente-Tomas growth fault zone and the Corsair and Wanda systems (Figure 2.4) (Galloway, 1989; Bradshaw and Watkins, 1994; McDonnell et al., 2009). During the deposition of the LM1 and LM2, the strike-parallel Clemente-Tomas growth fault displaced strata by over 4,000 feet as a result of sediment loading and salt evacuation (Winker and Edwards, 1983; McDonnell and others, 2009; Nicholson, 2012). Along the Texas coast, faults developed as deltas loaded the shelf edge above mobile fine-grained facies of the Anahauc Formation in the south and above mobile allochthonous salt in the north, causing the shelf edge to founder (Winker and Edwards, 1983; McDonnell and others, 2009). In some areas, shale and salt evacuation along the Clemente-Tomas growth fault caused a greater-than-three-fold increase of thickness of the LMI. By LM2, growth faulting ceased, and progradation of the shelf margin farther to the southeast occurred into the Corsair growth fault trend (Bradshaw and Watkins, 1994). Corsair system growth faulting lasted from the middle to the late Miocene (Vogler and Robison, 1987). The Wanda fault system occurred during the same time as the Corsair system growth

faulting as a result of salt evacuation. Twofold thickening of the upper Miocene section occurred across the Wanda fault system, and salt diapirs associated with the secondary salt withdrawal penetrated Miocene strata (Bradshaw and Watkins, 1994).

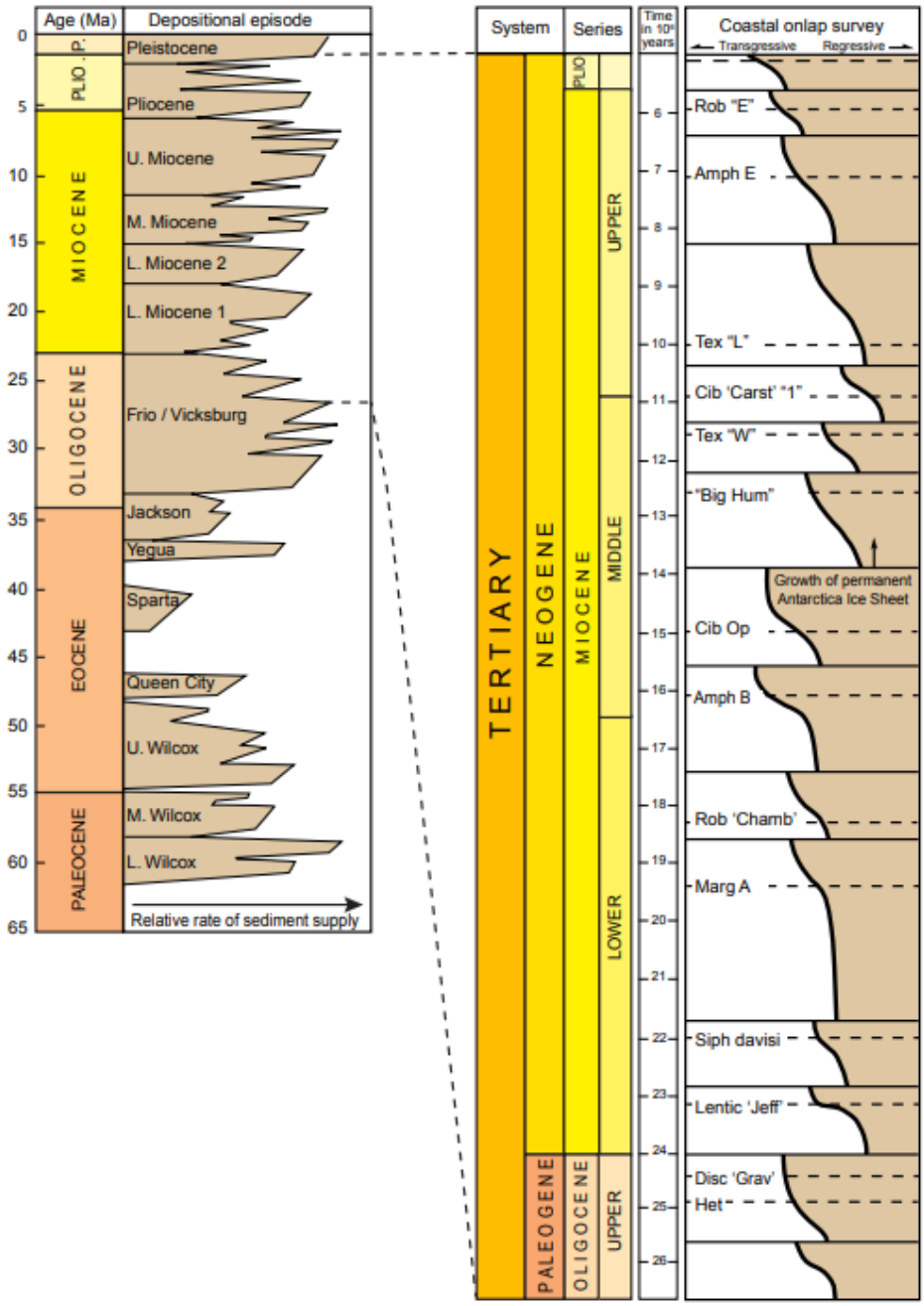

Figure 2.3 Stratigraphic column of major Tertiary depositional episodes with detailed Miocene costal-on lap curve with benthic foraminiferal biochronozones abbreviations (From Trevino, 2017).

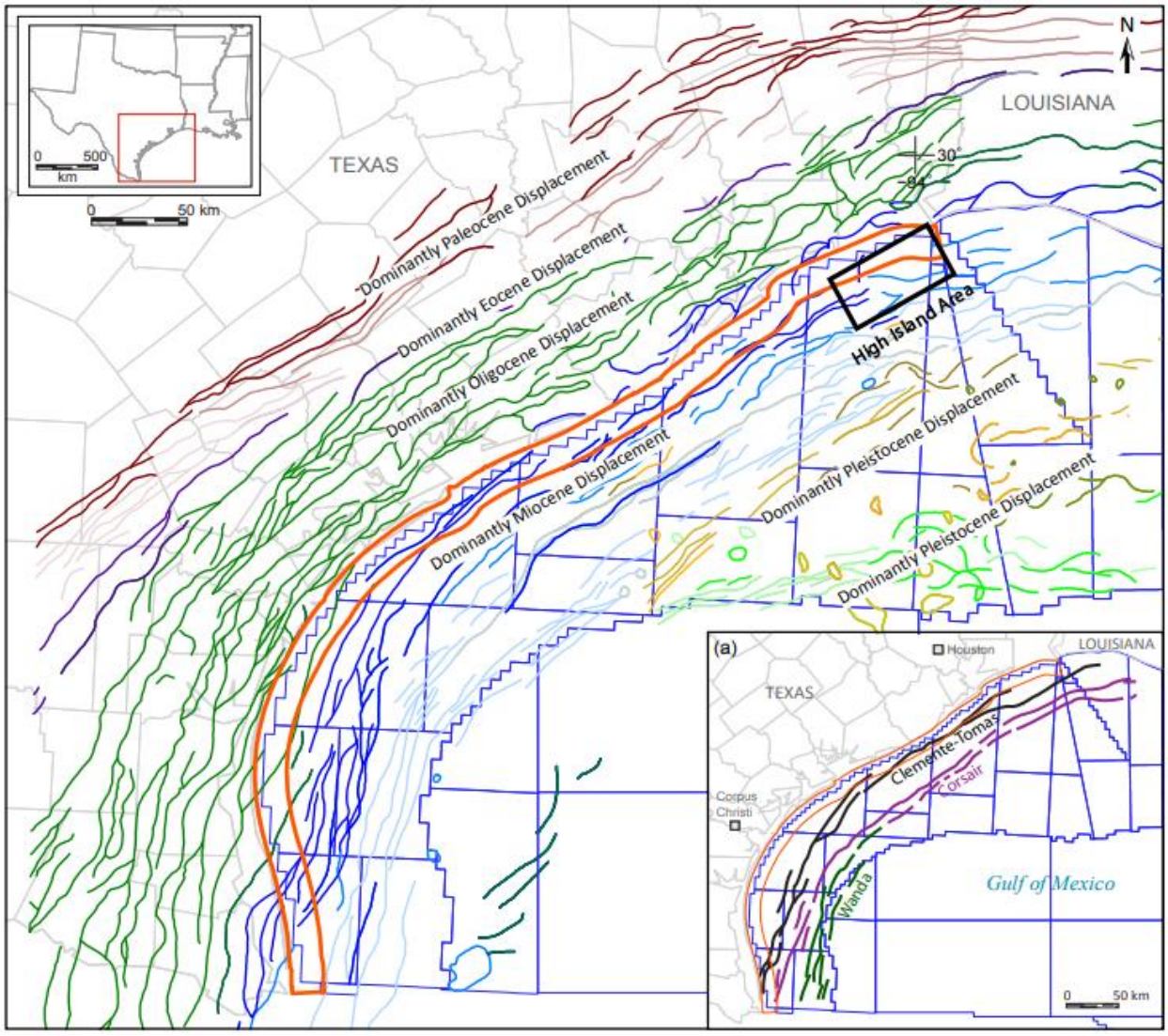

Figure 2.4: Map of Texas Coast showing major Cenozoic fault zones with inset map highlighting Miocene-age fault zones (From Trevino et al., 2017). Black box indicates study area.

2.4 HIGH ISLAND 10-L

High Island 10-L field, discovered in 1955, is located 13.5 miles southwest of Sabine Pass, Texas. High Island 10-L field is a small faulted anticline downthrown along a major northeast-southwest striking growth fault (Seni, 1997; Fowler, 1986). There is a 600-foot succession of aggradational and retrogradational sandstone overlain by a regional regressive

shale seal interval of 400 feet. Beneath the seal are sands with porosities up to 30 percent and permeability of approximately 460 millidarcies. This setting has retained one million barrels of oil and 25 billion cubic feet of gas (Fowler et al, 1987).

2.5 HIGH ISLAND 24-L

High Island 24-L field, discovered in 1967, is located approximately 20 miles southwest of Sabine Pass, Texas. The field is highly faulted with anticlinal fault traps and 10 Miocene age sandstones capable of production. The largest single productive sandstone has a porosity of 29 to 35 percent porosity, 50-2500 MD permeability, and 182 BCF original gas in place (Fowler et al, 1987).

2.6 ST TR 60S

ST TR 60S field, discovered in 1988, is located approximately 13 miles west of Sabine Pass, Texas and 2 miles off the Gulf Coast of Mexico shore line in Jefferson County, Texas. The ST TR 60S field has at least ten Lower Miocene sands containing oil and gas, which are deposited over a gently formed salt or shale ridge. This feature contains an anticlinal shaped structure that is bounded by north and south trending faults giving the appearance of a horst and graben system. Most of the hydrocarbons are located on the east and west up-thrown horst blocks (Richards, 1998).

Chapter 3: Data Acquisition and Analysis

3.1 Hydrocarbon Analysis

Figure 3.1 illustrates the process applied to log interpretation. A high gamma ray response indicates shale; whereas, a low gamma ray response indicates sand. Within the sand formation, a high resistivity indicates where hydrocarbons are present, and a low resistivity reading indicates a brine. Neutron porosity and bulk density are plotted on the same track and, when scaled correctly for lithology, indicate hydrocarbon type. A wide separation of the curves indicates the presence of gas; a smaller separation indicates the presence oil; and, if the resistivity is low and the separation small, this indicates the presence of a brine. In order to obtain estimates on hydrocarbon volumes, the effective porosity of the formation must be calculated and then the amount of water saturation. These values can be calculated through the previously listed logs and the formation water resistivity (RW) or through an SP log and the mud filtrate resistivity (RMF) and max temperature of a well.

The wells used in this study were selected on the basis of data availability. Data on the wells and well logs were acquired from TGS, IHS, and the Bureau of Ocean Energy

Management (table 3.1). Wells that did not have the full suite of necessary logs for hydrocarbon interpretation were used for comparison and correlations.

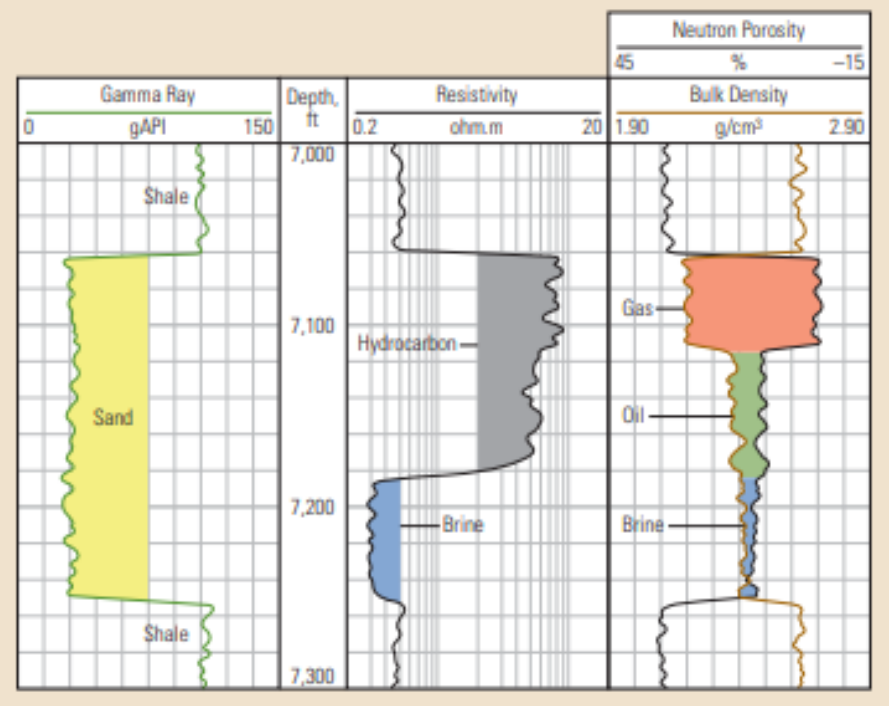

Figure 3.1: Idealized well log showing fluid interpretation (From Varhaug, 2016)

Table 3.1 Location and cumulative production from wells used in study.

	Well Number	Year Drilled	TD	Perferations	Longitude	Latitude	Average Production Oil BBL per day	Average Gas Production MCF per day
10L								
42708302880000**	1	1983	7800		-93.99955	29.555		
42708303580000**	2	1997	12355		-93.98969	29.55708		
42708302400000*	3	1979	8444	5850-5872	-94.00341	29.54986	367.74	18146.37
24L								
42708303470000*	4	1996	9639	9496-9526	-94.11115	29.52457	58.76	45606.38
42708303420000	5	1996	13552	13262-13297, 13330-13338, 13372-13410, 13415-31471, 13498-13508	-94.1197484	29.5275674	1071.53	321119.45
42708303400000	6	1996	12545	11362-11382, 11664-11764	-94.11975	29.52726	132.55	109529
42708303290000	7	1990	8740	7680-7685, 8220-8235, 8310-8325, 8383-8394, 8402-8418	-94.14586	29.5447	1012.73	12350.59
42708302280000	8	1979	9400	7543-7547, 7938-7950	-94.1312	29.54761	238.6	66105.75
42708303270000	9	1990	8956	8271-8276, 8872-8877	-94.12305	29.5408	603.19	6445.59
42708303220000*	10	1989	8100	7635-7639, 7936-7946, 7972-7980	-94.13505	29.55063	620.38	87542
STTR 60S								
42606301720000*	11	1991	8780	7809-7815, 8672-8688	-94.12463	29.62227	2175.78	3093.06
42606301700000	12	1990	9027	8440-8446, 8450-8567, 8582-8610, 8740-8755, 8740-8755, 8917-8928	-94.1195916	29.61935	1512.08	1037.82
42606301650000	13	1989	8725	8122-8127, 8194-8216	-94.12466	29.62224	1073.34	721.62
42606301620000**	14	1989	8550		-94.12147	29.62161		
42606301570000**	15	1986	8498		-94.1148	29.62285		
42606301490000**	16	1983	8540		-94.11651	29.6148		
42606301450000**	17	1982	8580		-94.11779	29.62143		
*Converted to gas well								
**abandonded								

I assumed that perforations are reliable indicators of hydrocarbon zones. If information on depth of perforations was not available, then hydrocarbon zones were interpreted based on where perforations were found among other wells in the field and the year it was drilled (Table 3.2). Most wells drilled within the same area produced from the same interval and had similar depths if drilled within the same time frame, so it was concluded to be likely the well was producing from the same target (Figures 3.2, 3.3, 3.4, and 3.5). If no hydrocarbons were located in a possible perforation range, then it was ignored.

Table 3.2 Perforation Assumptions.

	Well Number	Perforations	Assumed Possible Perforation Range
10L			
42708302880000	1		5750-5900
42708303580000	2		5750-5901
42708302400000*	3	5850-5872	
24L			
42708303470000	4	9496-9526	
42708303420000	5	13262-13297, 13330-13338, 13372-13410, 13415-31471, 13498-13508	7500-8400, 9400-9500
42708303400000	6	11362-11382, 11664-11764	7500-8400, 9400-9501
42708303290000	7	7680-7685, 8220-8235, 8310-8325, 8383-8394, 8402-8418	
42708302280000	8	7543-7547, 7938-7950	
42708303270000	9	8271-8276, 8872-8877	
42708303220000	10	7635-7639, 7936-7946, 7972-7980	
STTR 60S			
42606301720000	11	7809-7815, 8672-8688	
42606301700000	12	8440-8446, 8450-8567, 8582-8610, 8740-8755, 8740-8755, 8917-8928	
42606301650000	13	8122-8127, 8194-8216	
42606301620000	14		7750-7850, 8100-8200, 8400-9000
42606301570000	15		7750-7850, 8100-8200, 8400-9000
42606301490000	16		7750-7850, 8100-8200, 8400-9000
42606301450000	17		7750-7850, 8100-8200, 8400-9000

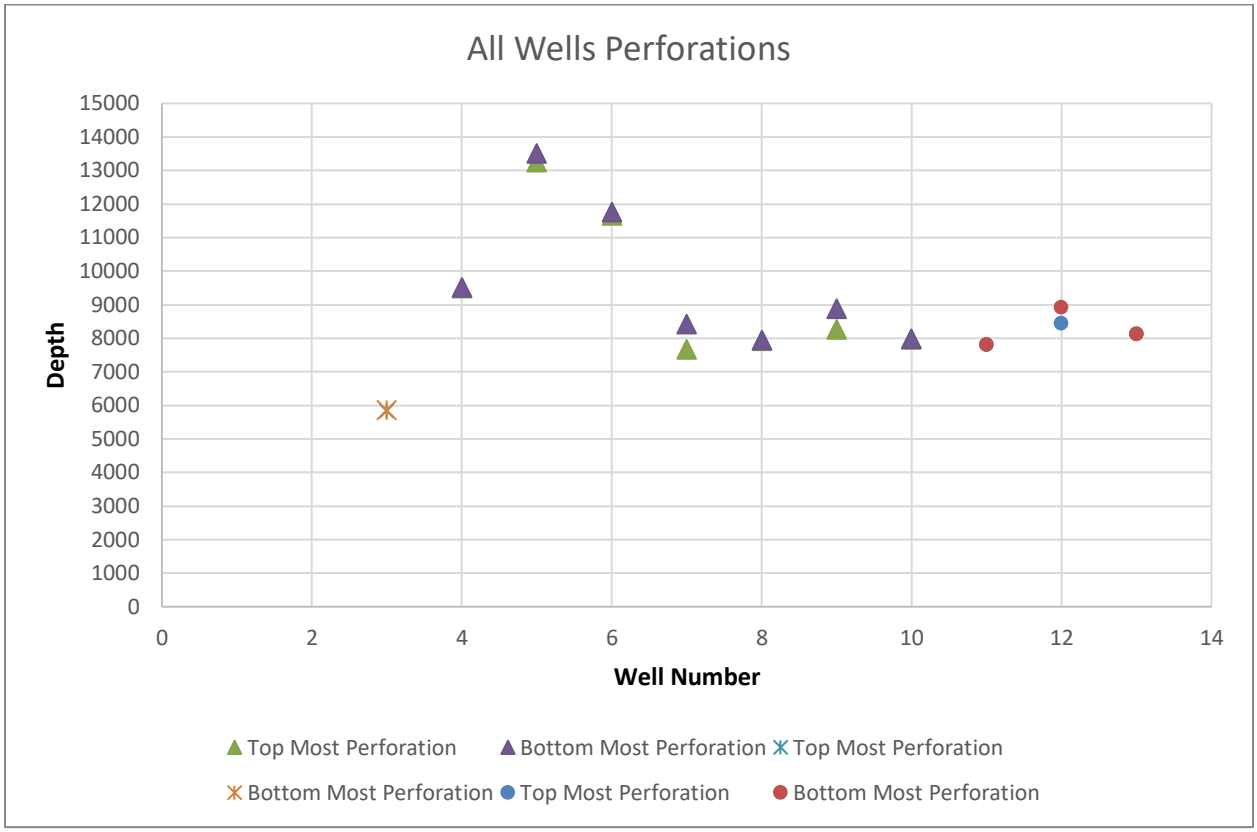

Figure 3.2: Perforation interval range for all wells.

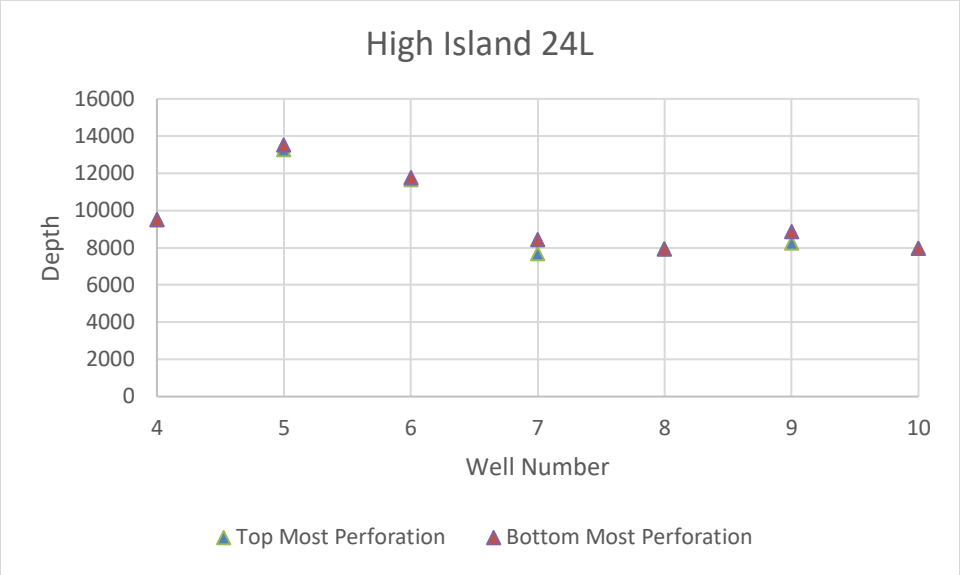

Figure 3.3: Perforation interval range for High Island 24L

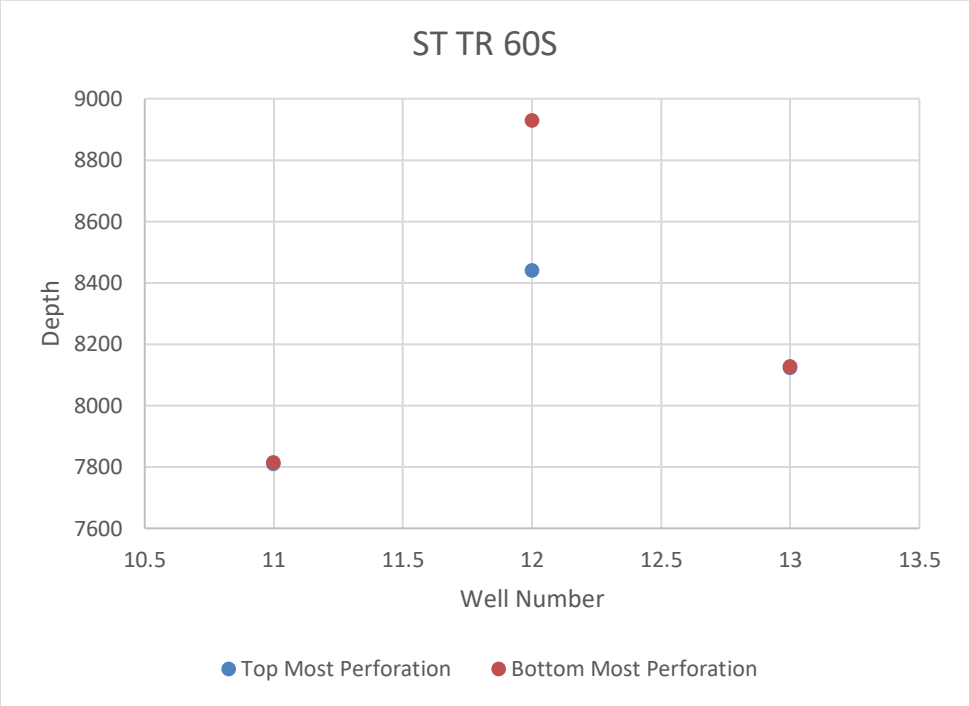

Figure 3.4: Perforation interval range for ST TR 60S

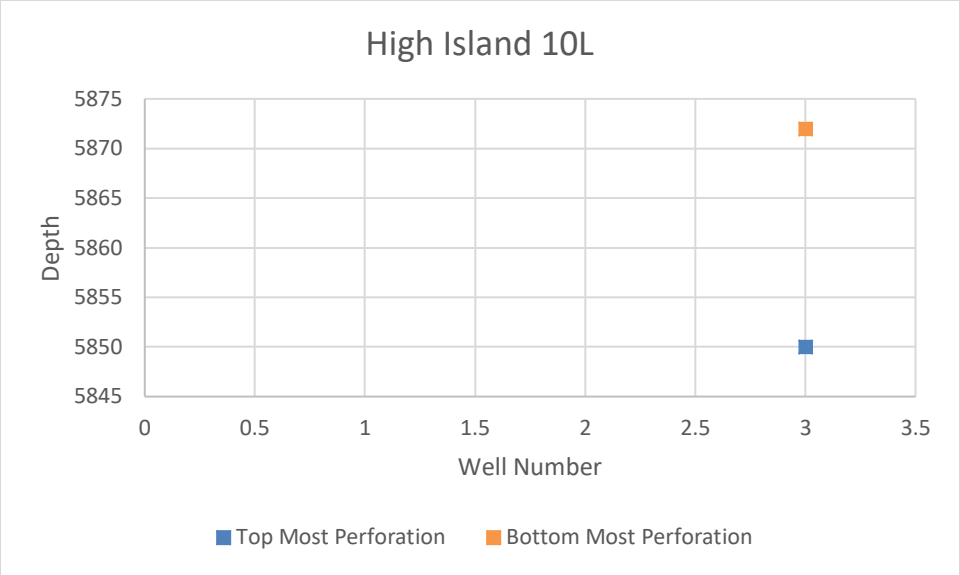

Figure 3.5: Perforation interval range for High Island 10L.

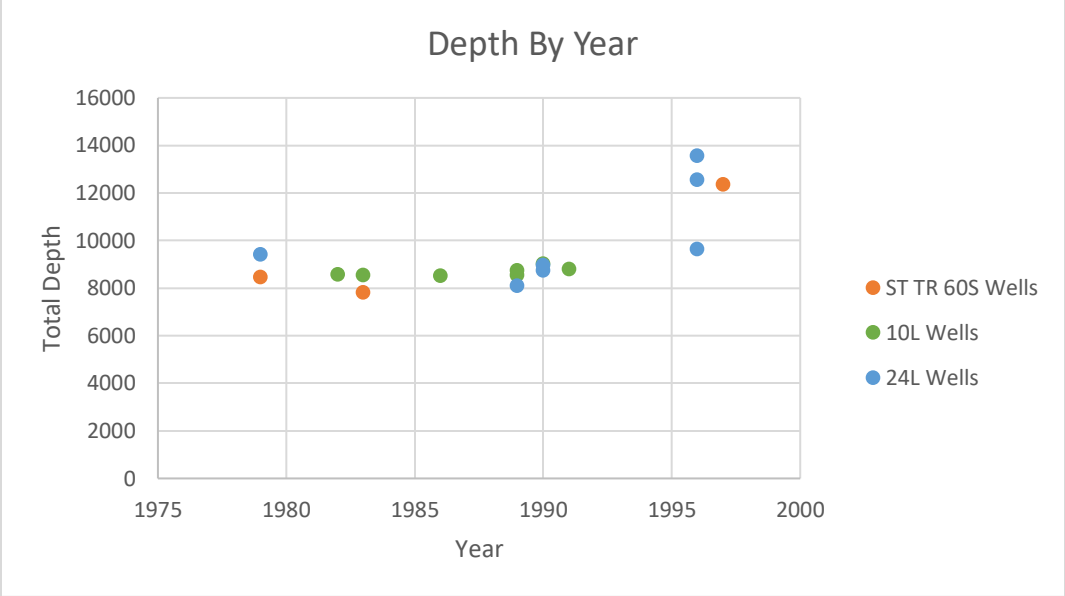

Figure 3.6: Depth of wells by year.

Well logs were purchased as images and then digitized using Neuralog. Digitized well logs were all categorized by well logs as shaly sands, and I used Schlumberger's Techlog for the interpretation of the logs. Most curves used were density porosity (DPHI), neutron porosity (NPHI), gamma ray (GR), resistivity (SLFU), and SP. Some wells had bulk density (RHOB) instead of density porosity, so it was converted to density porosity using Equation 1 (as shown

below). Shale content (Csh) was calculated using Vsh and gamma ray or neutron porosity if gamma ray wasn't available. Total porosity was calculated with Equation 2, and effective porosity was calculated by doing corrections to neutron porosity and density porosity, which were obtained via Equations 3 and 4 and then Equation 5. All wells, except for one, did not have the Rw listed, so it was calculated using points from a shale free interval and the equations 6, 7, and 8 and a RWE to RW chart, such as pictured in Fgure 3.8. After obtaining the RW, it was used in Dual-Water, and the water saturation and bulk water saturation was calculated. The m value used in Dual Water was the default 2, the a value was the deafult 1, and the n value was 2. Hydrocarbon saturation was calculated simply by Equation 9. Figure 3.7 is a flow chart that

illustrates the process of interpretation. Details on the equations used can be found in the paper by Asquith et al. (2004).

$$DPHI = \frac{(RHOB-2.65)}{(1-2.65)} \quad (1)$$

$$Total\ Porosity = \sqrt{\frac{NPHI^2+DPHI^2}{2}} \quad (2)$$

$$DPHIc = DPHI - \text{Csh(DPHI)sh} \quad (3)$$

$$NPHI = NPHI - Csh(NPHI)sh \quad (4)$$

$$Effective\ Porosity = \sqrt{\frac{NPHI^2+DPHI^2}{2}} \quad (5)$$

$$SP = -Ksp * log\frac{Rmfe}{Rwe} \quad (6)$$

$$Tf = Ts + \left(\frac{Tmax-Ts}{Dmax}\right) * D \quad (7)$$

$$RMF2 = RMF1(\frac{T1+6.77}{T2+6.77}) \quad (8)$$

$$1 - Water\ Saturation = Hydrocarbon\ Saturation \quad (9)$$

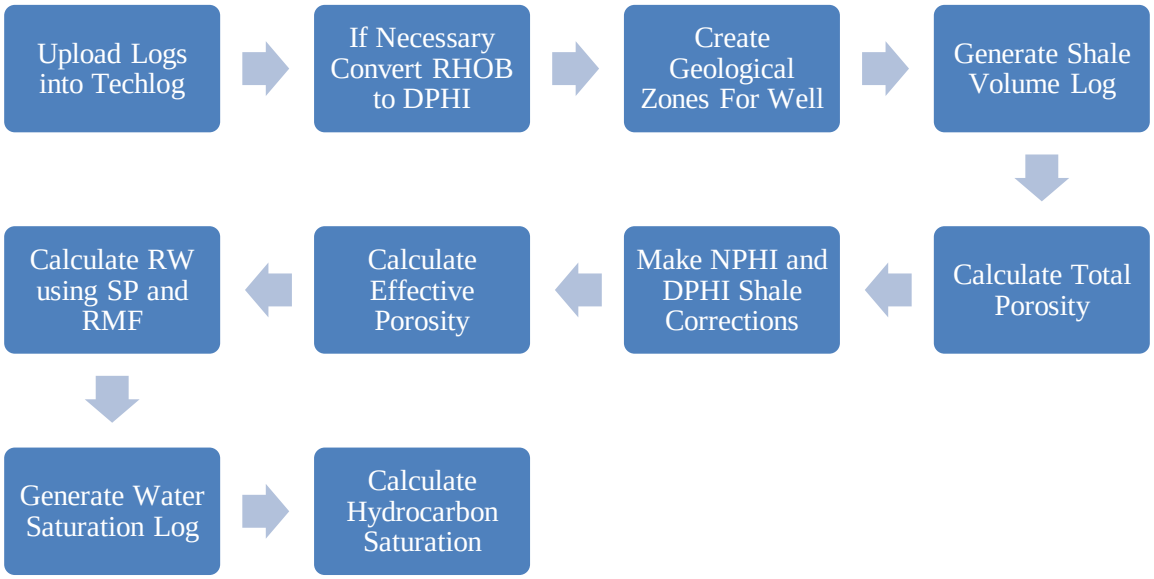

Figure 3.7: Well log intepretation flowchart.

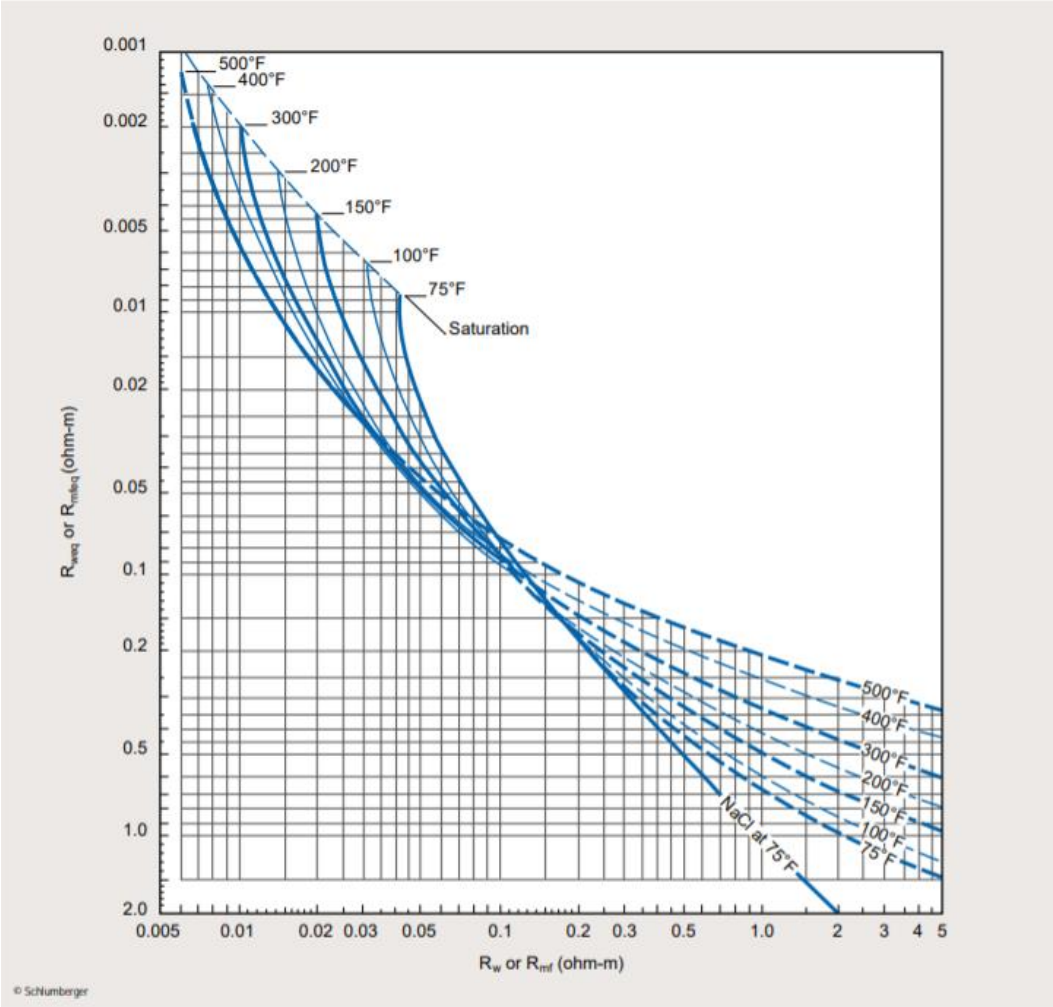

Figure 3.8: Rweq v Rw and formation temperature (From Schlumberger, 2009).

3.2 STRUCTURE DATA

3D seismic data was leased from Seismic Exchange, Inc. The data are from ten different 3D seismic surveys and encompass a 1,013 square mile area. The depth imaged in the volume is between 0-30,000 ft (Beckham, 2018).

The key horizons within the seismic, MFS04, MFS05, MFS07, SB_M08, MFS09, SB_M09, MFS 10, and MFS12, were converted from time scale into depth scale by DeAngelo (2016) via three different methods. The first method was to apply a two-way time conversion factor derived from the sonic logs of well 427084001600. The conversions were MF05: 3.10, for SB-M08: 3.53, and SB_M09 was 3.71. The second method, aka TDQ, involved building an internal velocity model from wells, which has synthetic seismograms generated and matching that to adjacent seismic trace. The values were measured in depth (ft) and from the Kelly Bushing level (KB), and this method is considered to be the most robust. The third method used a time-based average (RMS) velocity cube provided by the data processing contractor. Depending on the horizon, there could be large differences between the methods (Figure 3.9 and Figure 3.10). Time and depth versions of the faults and surfaces in the seismic were interpreted by DeAngelo (2019), Ruiz (2019), Beckham (2018), Fifariz (2019), and Ramirez Garcia (2019).

To place the logs interpreted in this study into appropriate context, DecisionSpace was used to plot the wells on the interpreted surfaces and to view seismic data. Three seismic cross section lines were drawn: 1) High Island 24L to High Island 10L, 2) High Island 24L to ST TR 60S, and 3) High Island 10L to ST TR 60S. Petra was used to create cross-sections of wells, and correlations were partially based on interpretations done by Olariu et al. (2019) and drawn in manually.

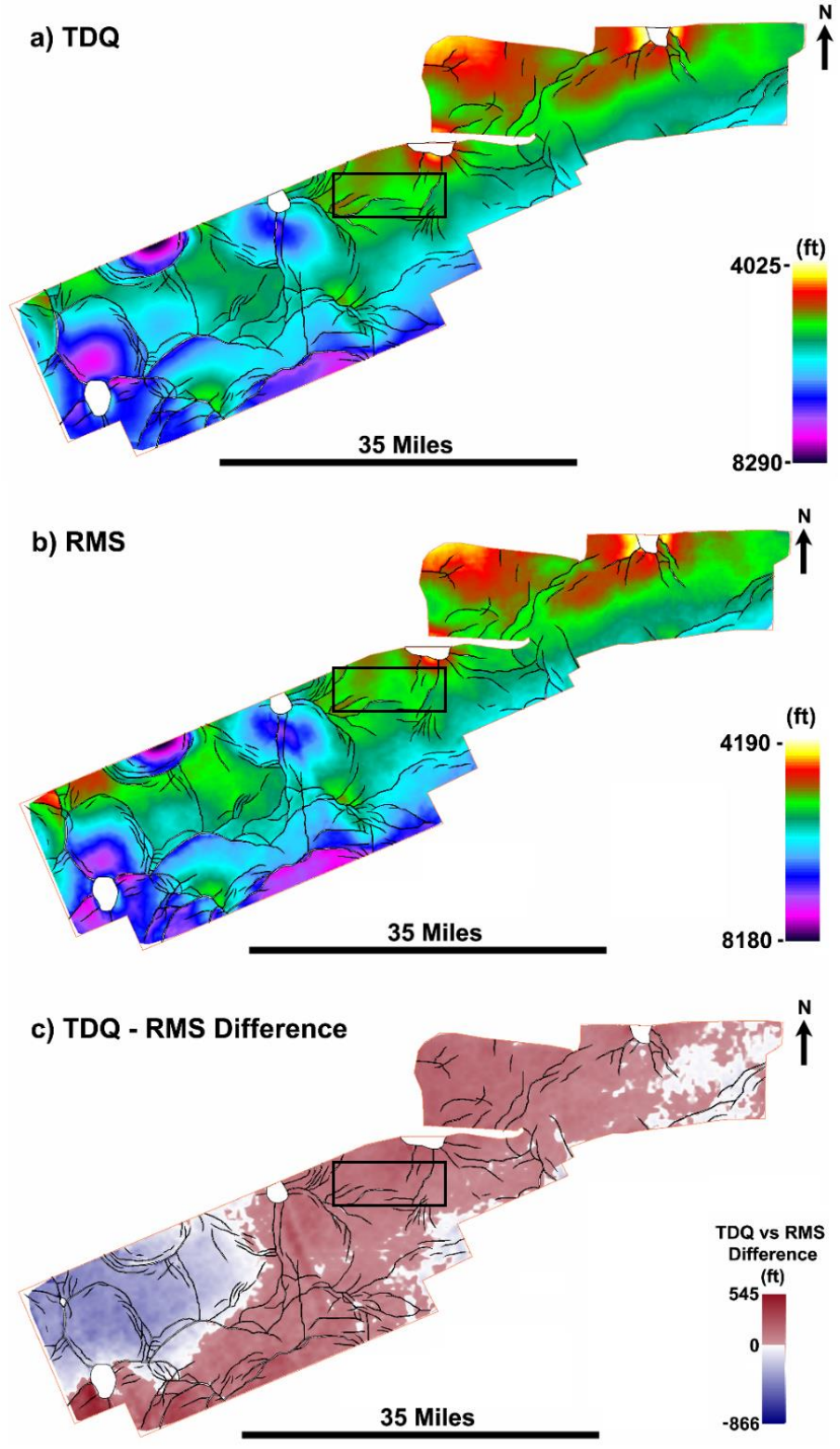

Figure 3.9: MFS10 depth models; a) TDQ method, b) RMS method, and c) difference between TDQ and RMS (From DeAngelo, 2016).

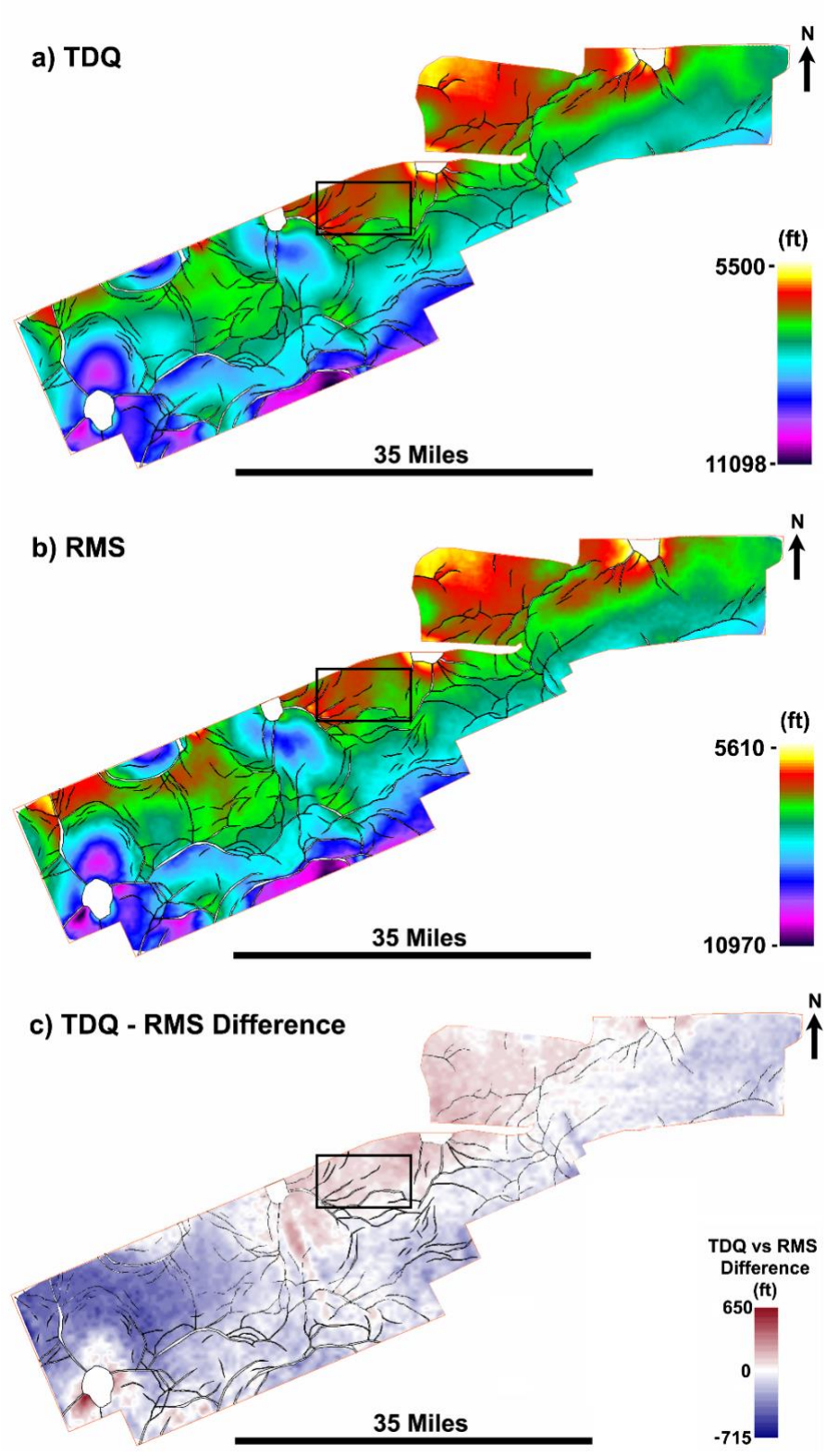

Figure 3.10: MFS11 depth models; a) TDQ method, b) RMS method, and c) difference between TDQ and RMS (From DeAngelo, 2016).

3.3 MECHANISM

Drive mechanism was interpreted for wells that had available production histories. Knowing whether a reservior is controlled by at least partially solution gas drive aids in interpretation of dissolved gas in oil because it is required by the drive mechanism. The drive mechanism can be interpreted from a well's production history. If the reservior has an increasing ratio of gas to oil over time or a logarithmic production decline, then it is likely controlled by solution gas drive (Figure 3.11 and Figure 3.12). Some production data had a gap where there was no data for a year or more. Data to the right of the gap was ignored since it was either from water injection, which can be distinguished by a sudden increase in production or from well recompletion for the purpose of being converted to a gas well. Some wells had no gap but had water injected for additional oil recovery, only data before the water injection was used.

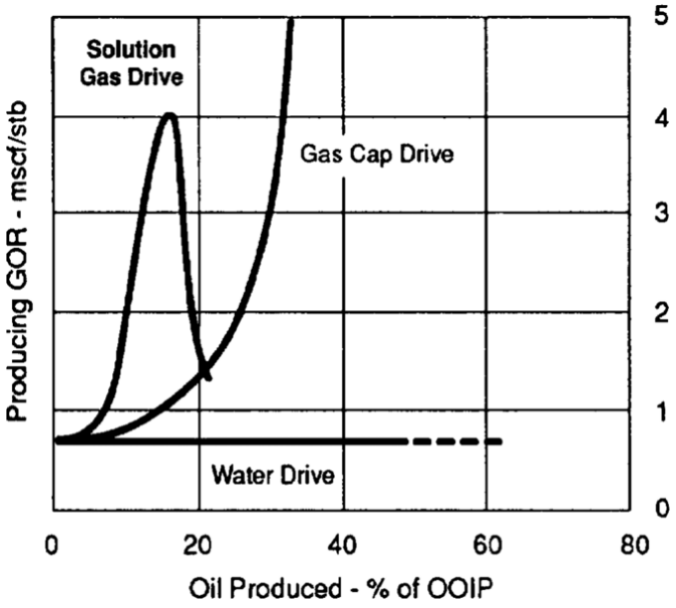

Figure 3.11: Producing gas to oil ratio v oil produced (From AAPG, 2016).

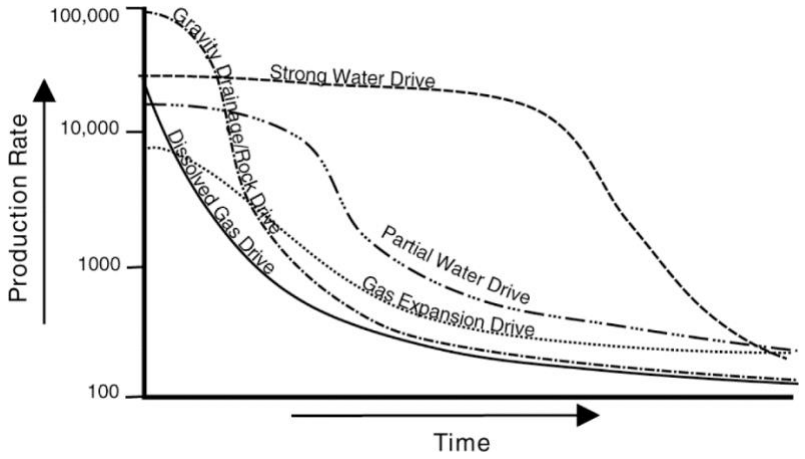

Figure 3.12: Production rate v time (From AAPG, 2016).

Chapter 4: Results

4.1 Log and Drive Interpretation Results

Images of all well log interpretations can be found in the appendices. Based on well log interpretation, only one well appeared to not have methane dissolved in oil, Well 1, which is currently abandoned, appeared to have gas possibly geologically separated from oil in the interval that was produced in Well 3 in the same field (Figure 4.2). Well 1 was interpreted to have geologically separate hydrocarbons because there were gaps between hydrocarbon shows coordinating with an increase in shale content. All other wells appeared to have methane dissolved in the oil (Figure 4.1).

Six wells had enough available production history data to interpret drive mechanism. Production graphs of all can be found in the appendix. Four were interpreted to have solution gas drive, and two were interpreted to have combination drive, which appeared to be a combination of water drive and solution gas drive (Table 4.2).

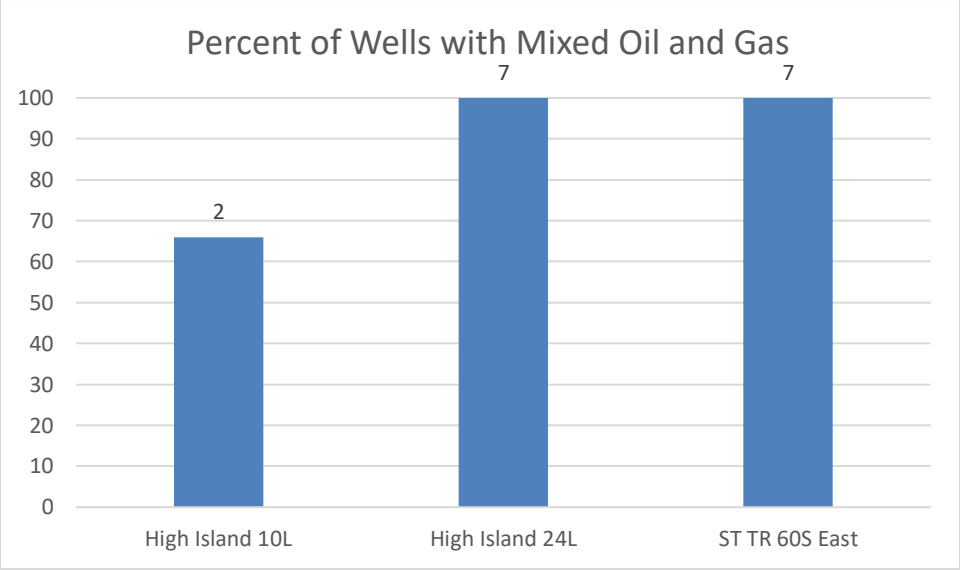

Figure 4.1: Percent of wells interpreted that had solution gas drive by field.

Table 4.1 Well and hydrocarbon interpretation.

Well Number	Log Interpretation
1	Geologically Separate Hydrocarbons
2	Gas Dissolved in Oil
3	Gas Dissolved in Oil
4	Gas Dissolved in Oil
5	Gas Dissolved in Oil
6	Gas Dissolved in Oil
7	Gas Dissolved in Oil
8	Gas Dissolved in Oil
9	Gas Dissolved in Oil
10	Gas Dissolved in Oil
11	Gas Dissolved in Oil
12	Gas Dissolved in Oil
13	Gas Dissolved in Oil
14	Gas Dissolved in Oil
15	Gas Dissolved in Oil
16	Gas Dissolved in Oil
17	Gas Dissolved in Oil

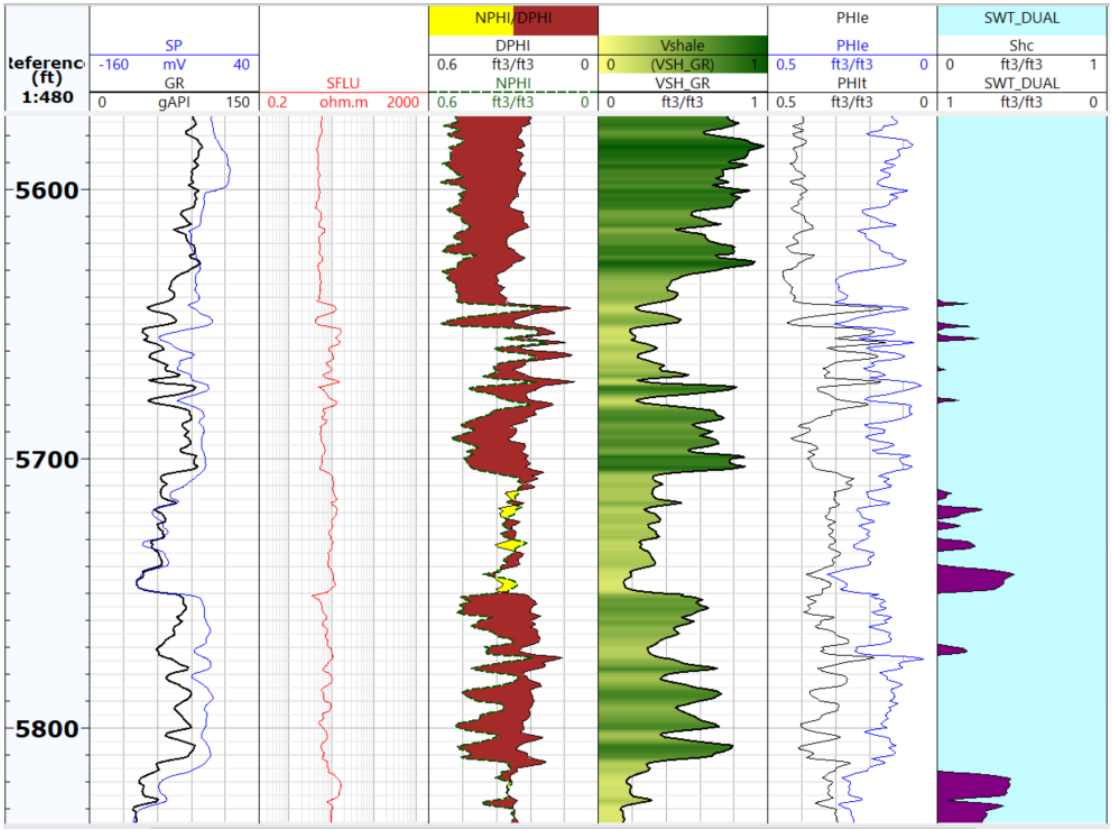

Figure 4.2 Well 1 evaluated at perforation interval that Well 3 was produced.

Table 4.2: Interpreted Drive of Wells.

Well Number	Perforations	G/O Ratio (MCF/Bbl)	Drive Type
4	9496-9526	1686	Gas
5	13262-13297, 13330-13338, 13372-13410, 13415-31471, 13498-13508	299	Gas
7	7680-7685, 8220-8235, 8310-8325, 8383-8394, 8402-8418	64	Gas
11	7809-7815, 8672-8688	0.66	Combination
12	8440-8446, 8450-8567, 8582-8610, 8740-8755, 8740-8755, 8917-8928	0.68	Gas
13	8122-8127, 8194-8216	0.81	Combination

4.2 STRUCTURE INTERPRETATION

The seismic line presented from ST TR 60S and High Island 24L is located along a strike (Figure 4.3). The well seen on the far left is that of ST TR 60S, and the wells on the right are from High Island 24L. The area is faulted, mostly normal faults, giving a horst and graben like appearance in the center. Despite the faulting, two anticlines can be seen on both the left and right sides with wells drilled on the tops of the anticlines (Figure 4.4) The seismic line from High Island 24L to High Island 10L is somewhat along dip (Figure 4.5) The wells seen on the left side are from High Island 24L and the wells on the right side are from High Island 10L. From this seismic image a significant amount of deformation along the paths of the wells can be seen. There are also many mostly normal faults, including what appears to be a growth fault, near the well paths (Figure 4.6). The seismic line from High Island 10L to ST TR 60S is somewhat along dip (Figure 4.7). The wells on the left of the seismic are from ST TR 60S, and no wells can be seen from High Island 10L in the current frame. The significant deformation near High Island 10L can also be seen in this image as well as the extensive faulting. ST TR 60S has some faulting visible, but it is mostly below the well paths and there is not as significant deformation as High Island 10 L (Figure 4.8).

For the well correlations in High Island 10L, only one well had perforation data, so the rest of the wells were assumed to have produced from the same regressive interval above a large aggradational sequence between MFS9 and MFS10 (Figure 4.9 and Figure 4.10). Hydrocarbons were indicated on the well logs of the other wells, so it is likely these were, indeed, at least one of the produced intervals of the wells. The large shifts in surface depth despite the wells being close together is likely due to the faulting observed in the seismic. High Island 10L is an anticline, and it appears from the perforations and locations of the wells they were all sourcing the top of the anticline as opposed to the flanks.

High Island 24L wells had perforations in both MFS10 and MFS11, though most were concentrated in MFS10 and in a transgressive sequence (Figure 4.11 and Figure 4.12). There is

deformation creating a couple of small anticlines within the larger anticlines, where a few wells have perforations at the top. High Island 24L is an anticline, and it appears from the perforations and locations of the wells that they are producing from the top of the larger anticline or the tops of the smaller anticlines, which themselves are on the top of the larger anticline.

ST TR 60S wells had all perforations in MFS11 in a primarily transgressive sequence (Figure 4.13). The perforations are within short sequences of sandstone intervals in a primarily shaly zone. ST TR 60S is an anticline and its wells are all producing from the top of an anticline.

All three sites were anticline structures with faulting and wells with paths located through the tops of the anticline and were found to have solution gas drive. Using this information from the seismic, well correlations, and well log interpretations, a depiction of the basic fluid geometry interpretation was created (Figure 4.14). As can be seen in the figure, the oil is primarily within a single zone and has gas dissolved within it. There would be no way to complete well design to avoid production of methane along with the oil.

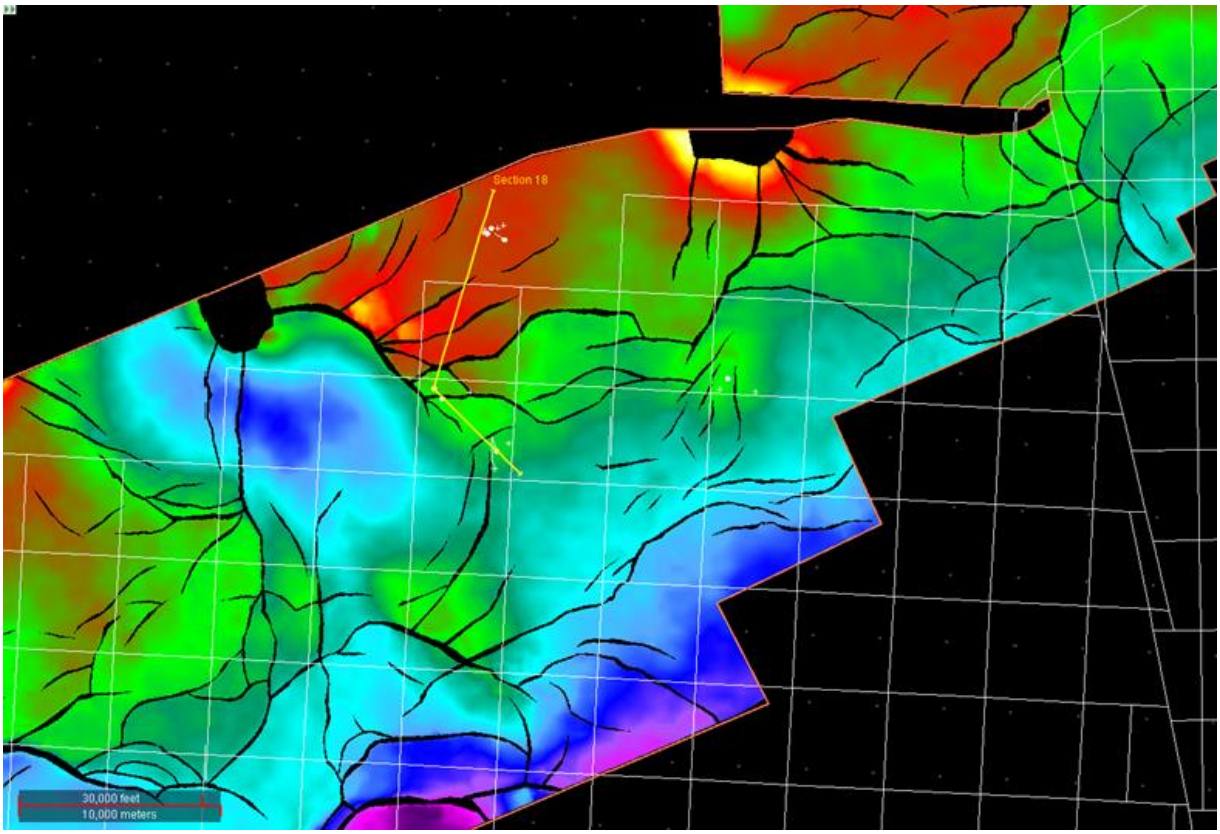

Figure 4.3: Seismic cross section line from High Island 24L to ST TR 60S.

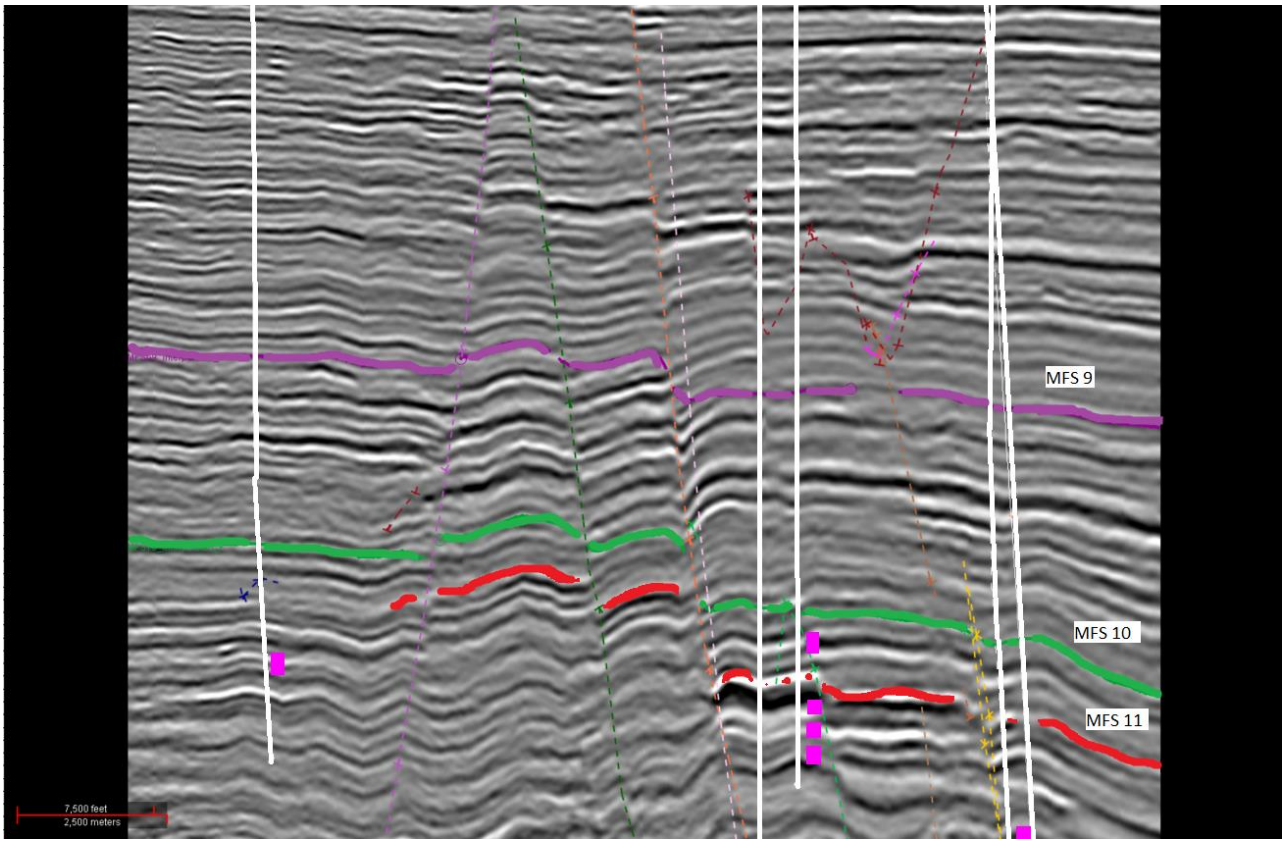

Figure 4.4**:** Seismic from High Island 24L to ST TR 60S. White vertical lines are well paths and dotted colored lines are faults. Pink blocks indicate approximate perforations and are not to scale**.** Seismic data owned or controlled by Seismic Exchange, Inc.; interpretation is that of Sarah Prentice.

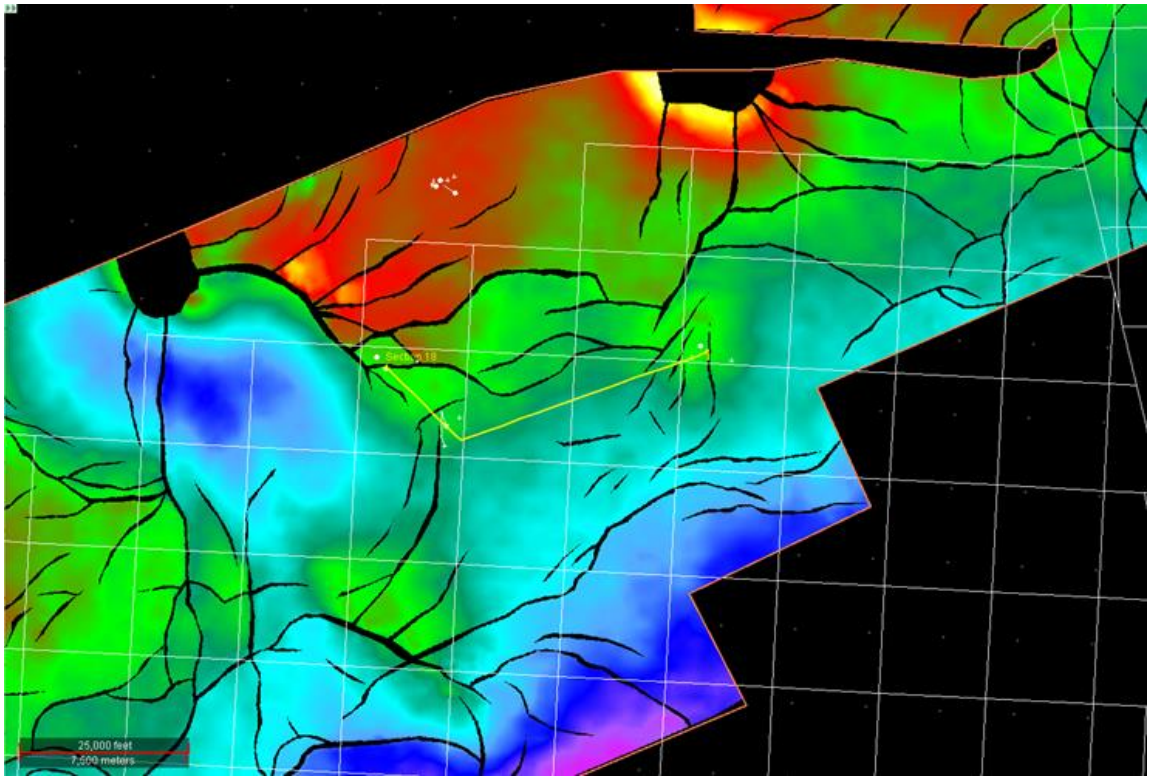

Figure 4.5: Seismic cross section line from High Island 24L to High Island 10L.

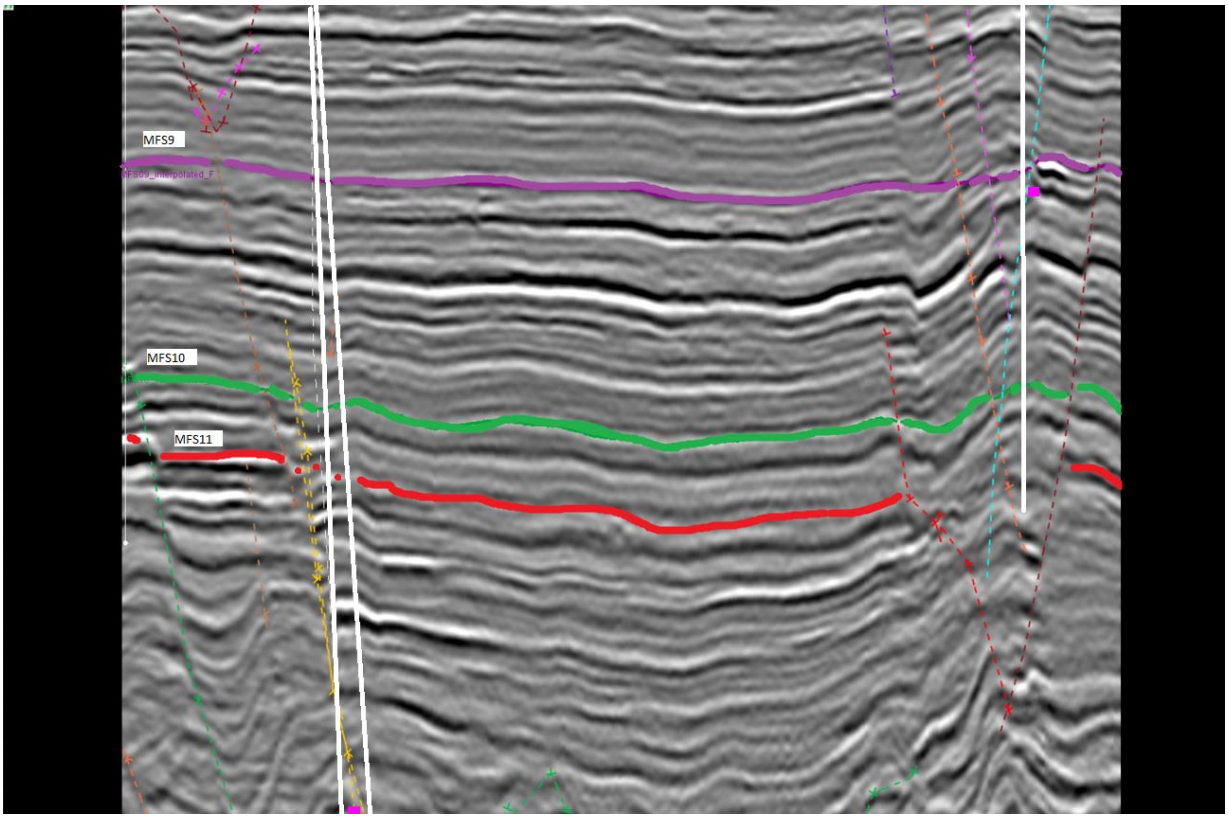

Figure 4.6: Seismic from High Island 24L to High Island 10L. White vertical lines are well paths and dotted colored lines are faults. Pink blocks indicate approximate perforations and are not to scale. Seismic data owned or controlled by Seismic Exchange, Inc.; interpretation is that of Sarah Prentice.

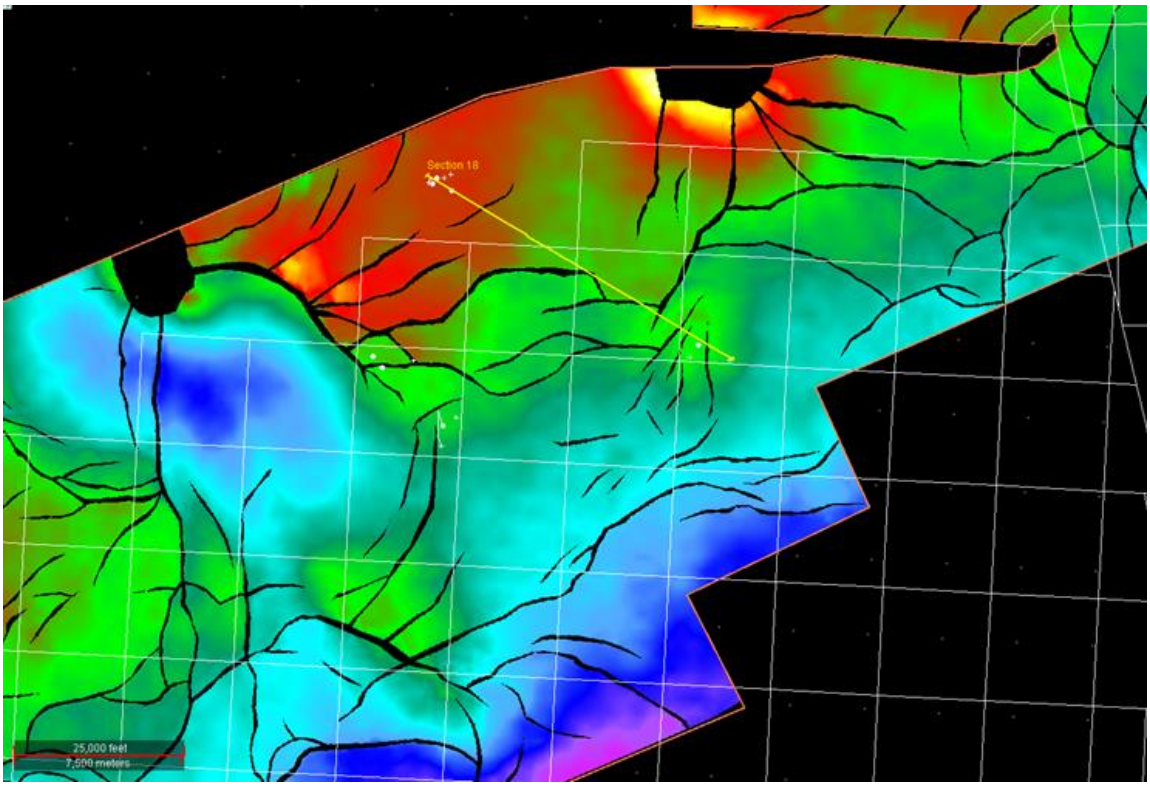

Figure 4.7: Seismic cross section line from High Island 10L to ST TR 60s.

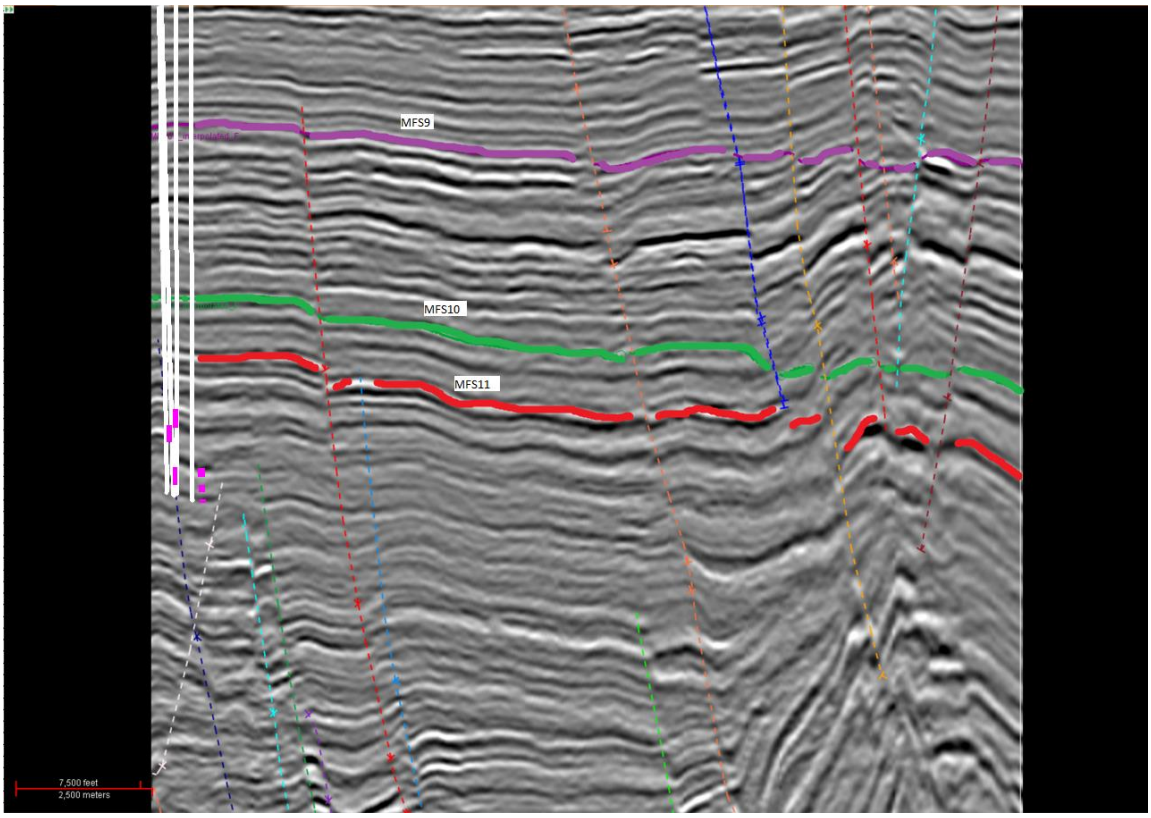

Figure 4.8: Seismic from High Island 10L to ST TR 60S. White vertical lines are well paths and dotted colored lines are faults. Pink blocks indicate approximate perforations and are not to scale. Seismic data owned or controlled by Seismic Exchange, Inc.; interpretation is that of Sarah Prentice

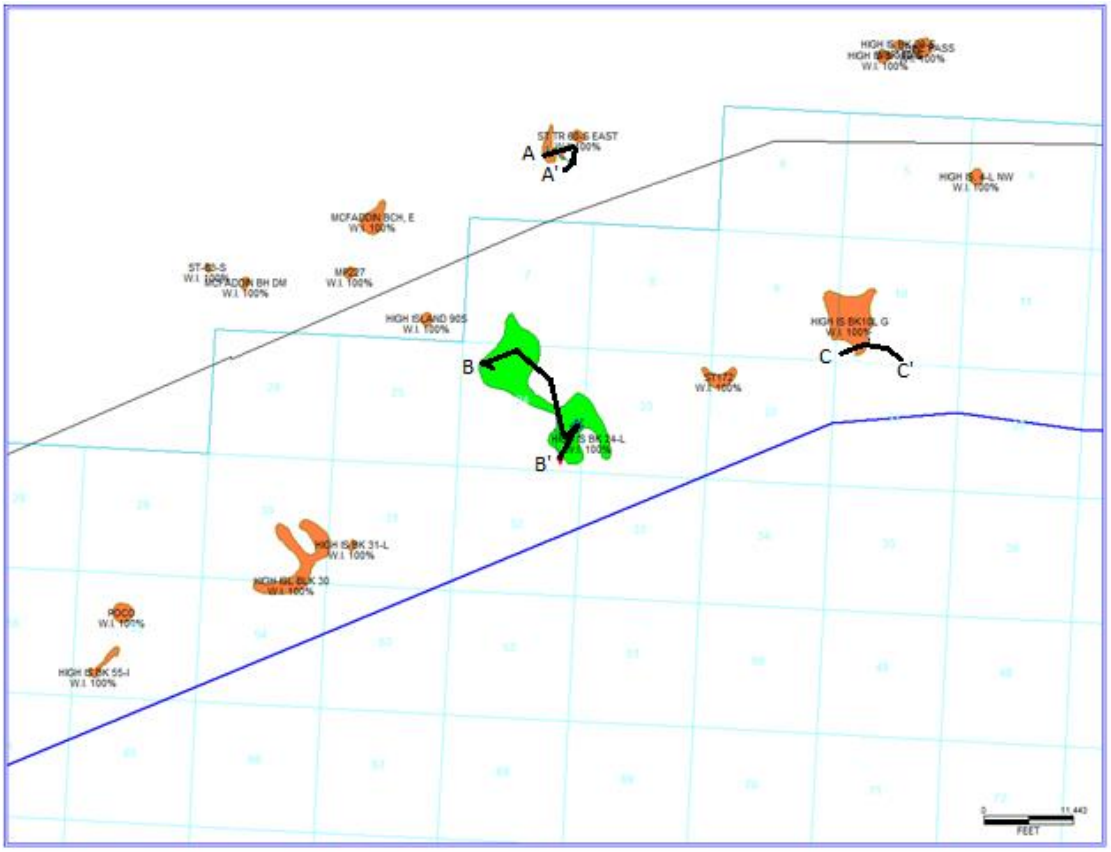

Figure 4.9: Well correlation crosslines.

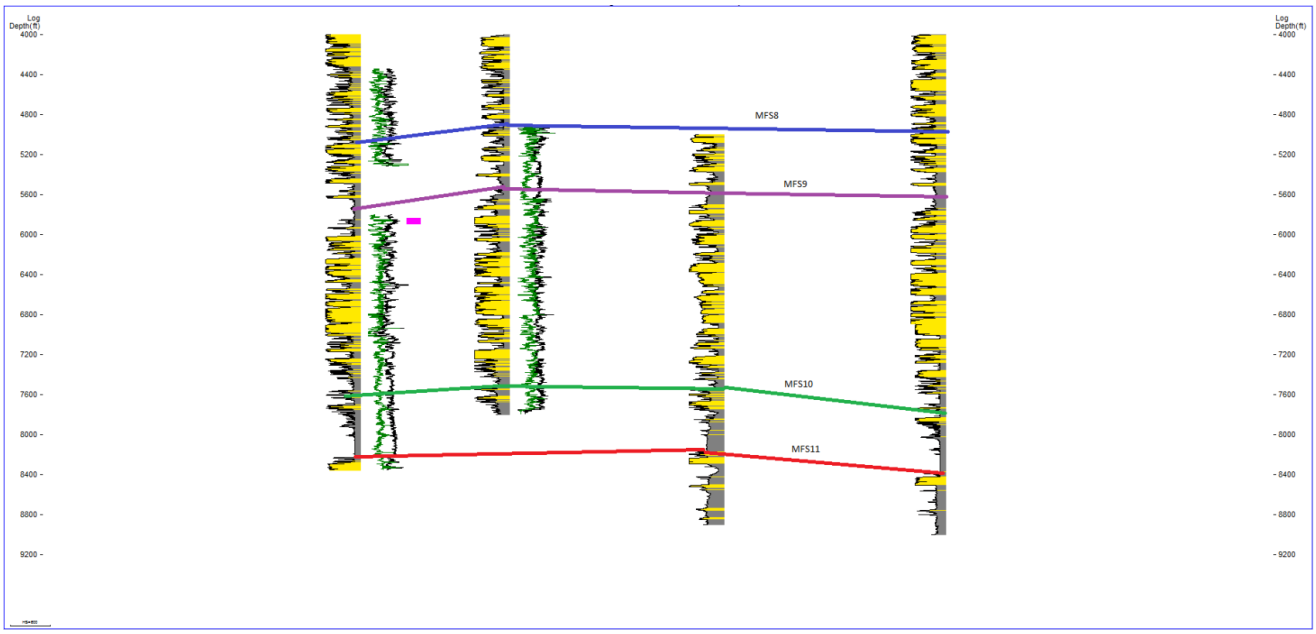

Figure 4.10: Well correlation for High Island 10L. Green line is neutron porosity, black is density porosity, lithology from SP curves grey is mud and yellow is sand. Pink blocks indicate approximate perforations and are not to scale

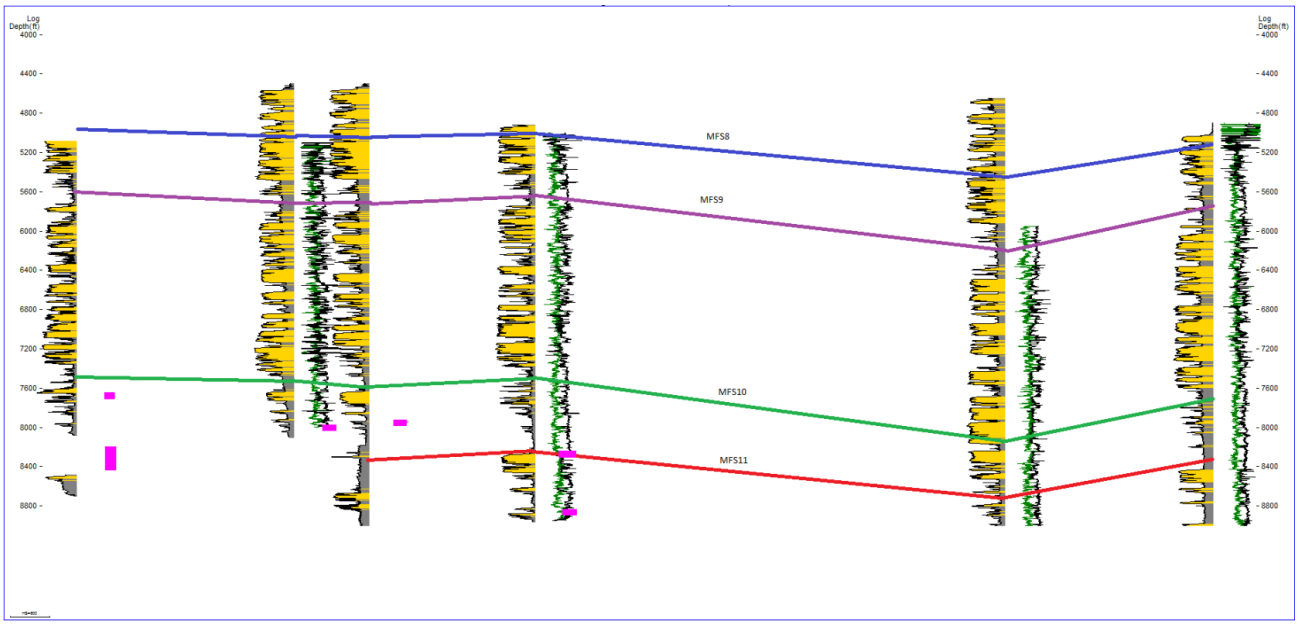

Figure 4.11: Well correlation for High Island 24L. Green line is neutron porosity, black is density porosity, lithology from SP curves grey is mud and yellow is sand. Pink blocks indicate approximate perforations and are not to scale.

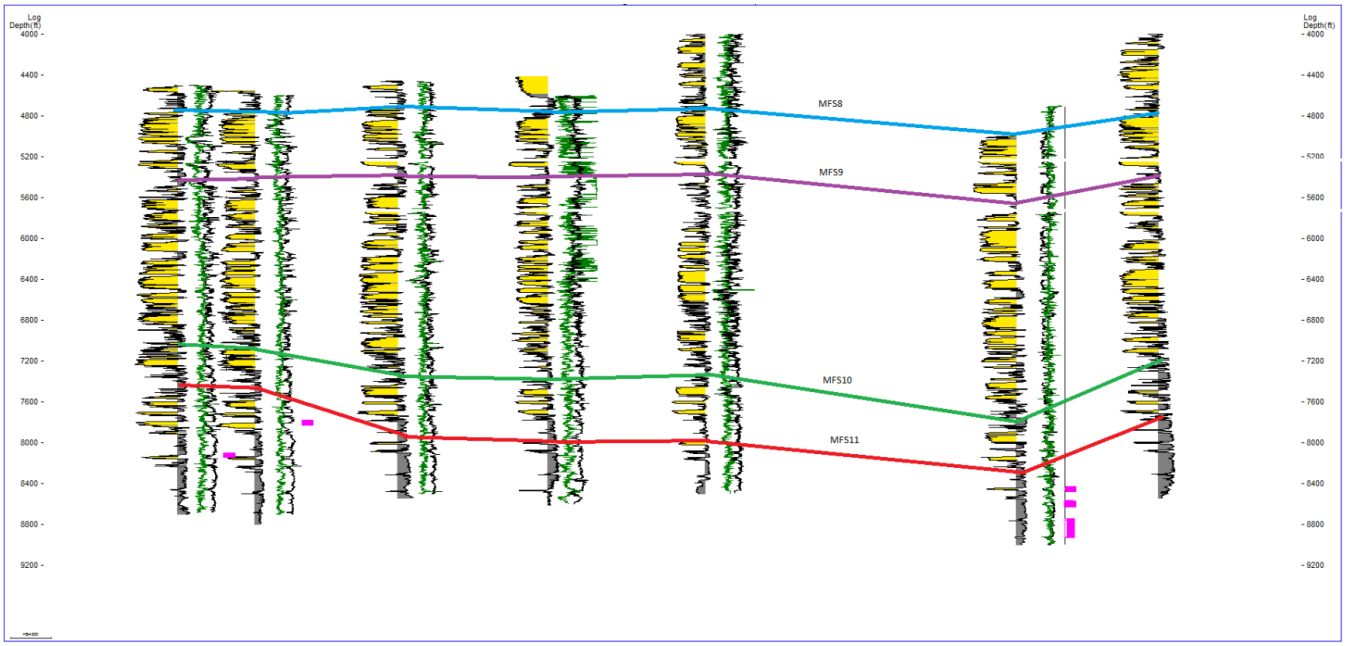

Figure 4.12: Well correlation for ST TR 60S. Green line is neutron porosity, black is density porosity, lithology from SP curves grey is mud and yellow is sand. Pink blocks indicate approximate perforations and are not to scale.

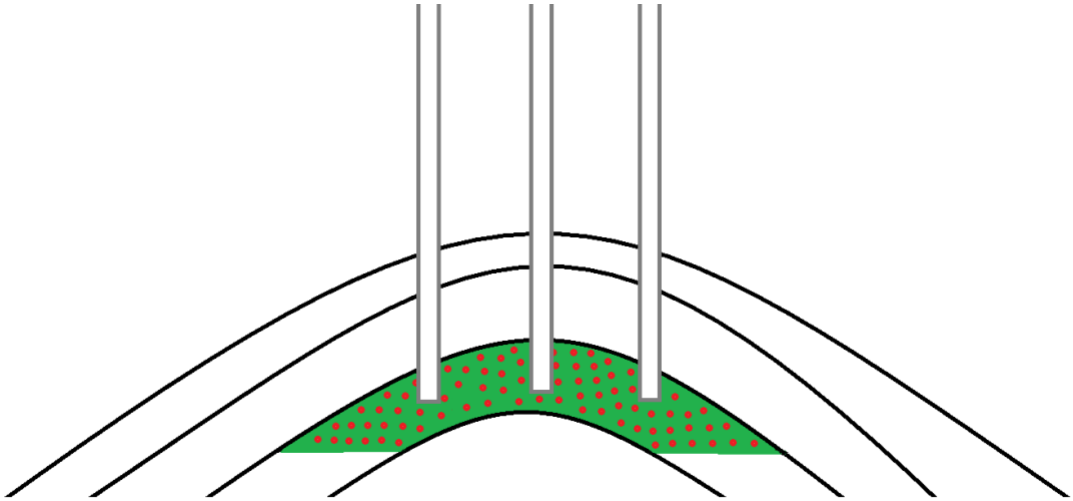

Figure 4.13: Simple interpretation of struture for fields. Grey Lines are example well, green indicates oil and red indicates gas molecules.

Chapter 5: Uncertainty

Data used for these analyses was sparse due to the age of the wells in the area (Figure 5.1). Median ages were 1978 for High Island 10L, 1984 for High Island 24L and ST TR 60S was 1990. Many of the wells within the study area did not have the full suite of logs necessary for fluid interpretation because some well drillers only collected gamma ray or SP logs during that time period. This creates a bias in that of the few wells drilled, only newer wells could be used for interpretation. The well data was acquired in the form of scanned well logs and some of the scans were poor in quality and were crooked in multiple directions down the whole log (Figure 5.2 and 5.3). Therefore, there may be room for some error in the digitization of the data. Not all wells logs had the same type of well logs, but they were all interpreted using the same methods, which is a potential source of error. Only one well had an RW log. For others, I assumed the RW was the same value throughout the well which was used to calculate hydrocarbon content. Data on produced hydrocarbon composition that confirms that the overlap of density porosity and neutron porosity was oil were not available. If densities of the produced hydrocarbons were available it could be used to check the porosities in the hydrocarbon zones and interpret the hydrocarbon present.

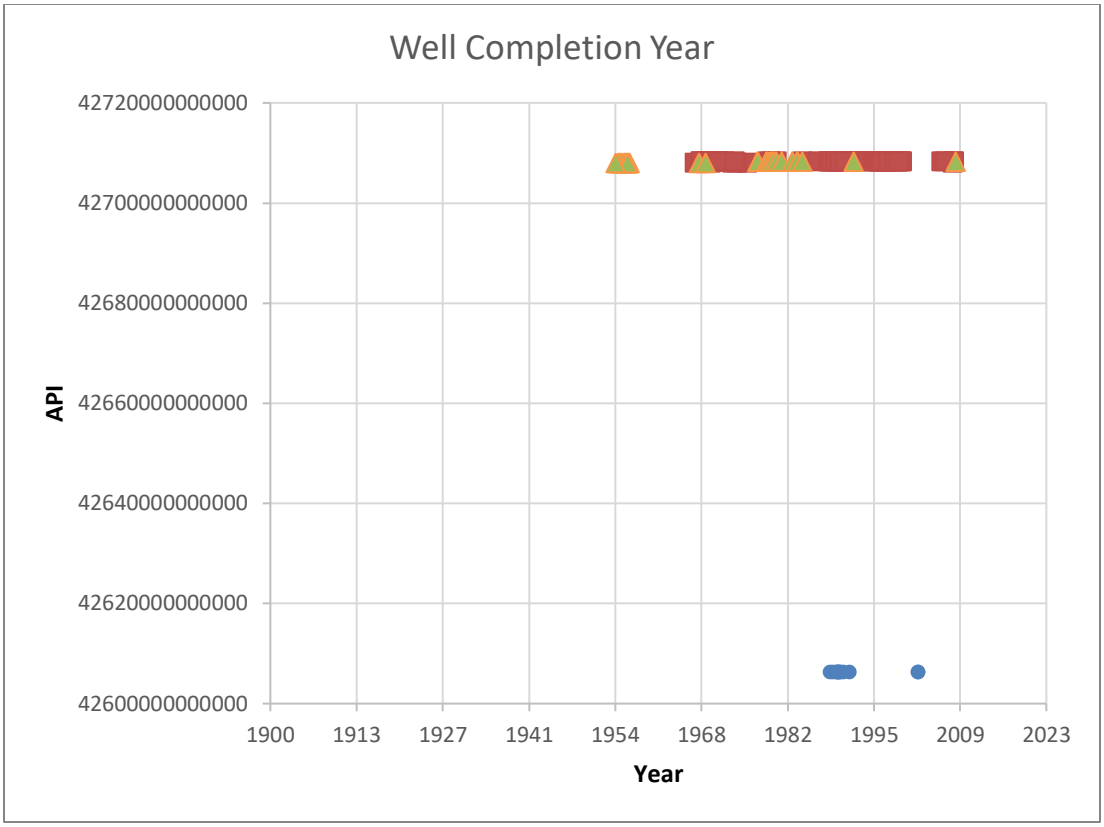

Figure 5.1: Median age of all wells in database of each field.

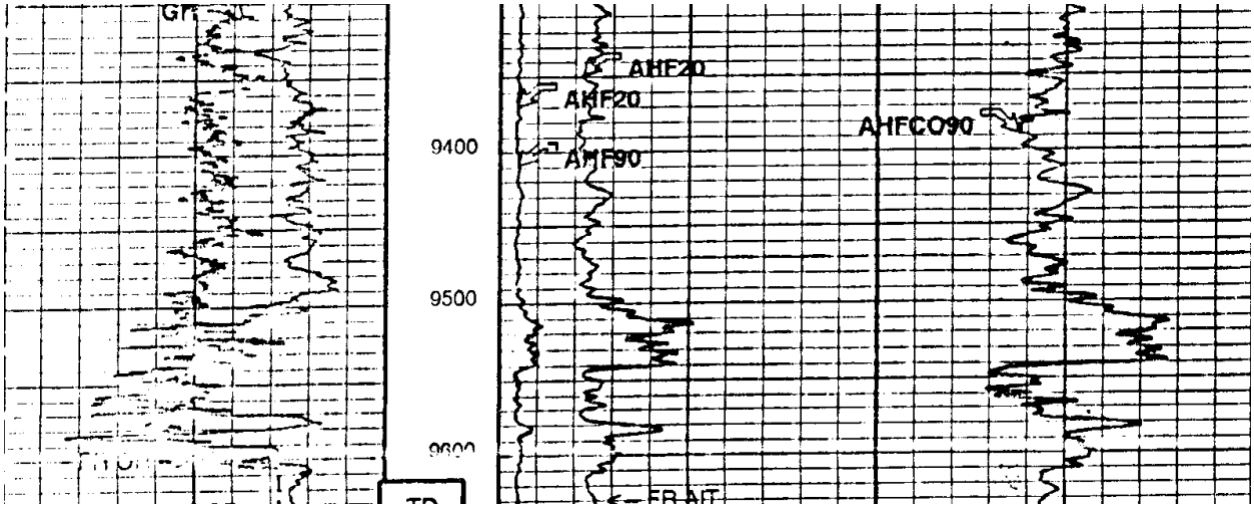

Figure 5.2: Well log used showing spot poor scan quality.

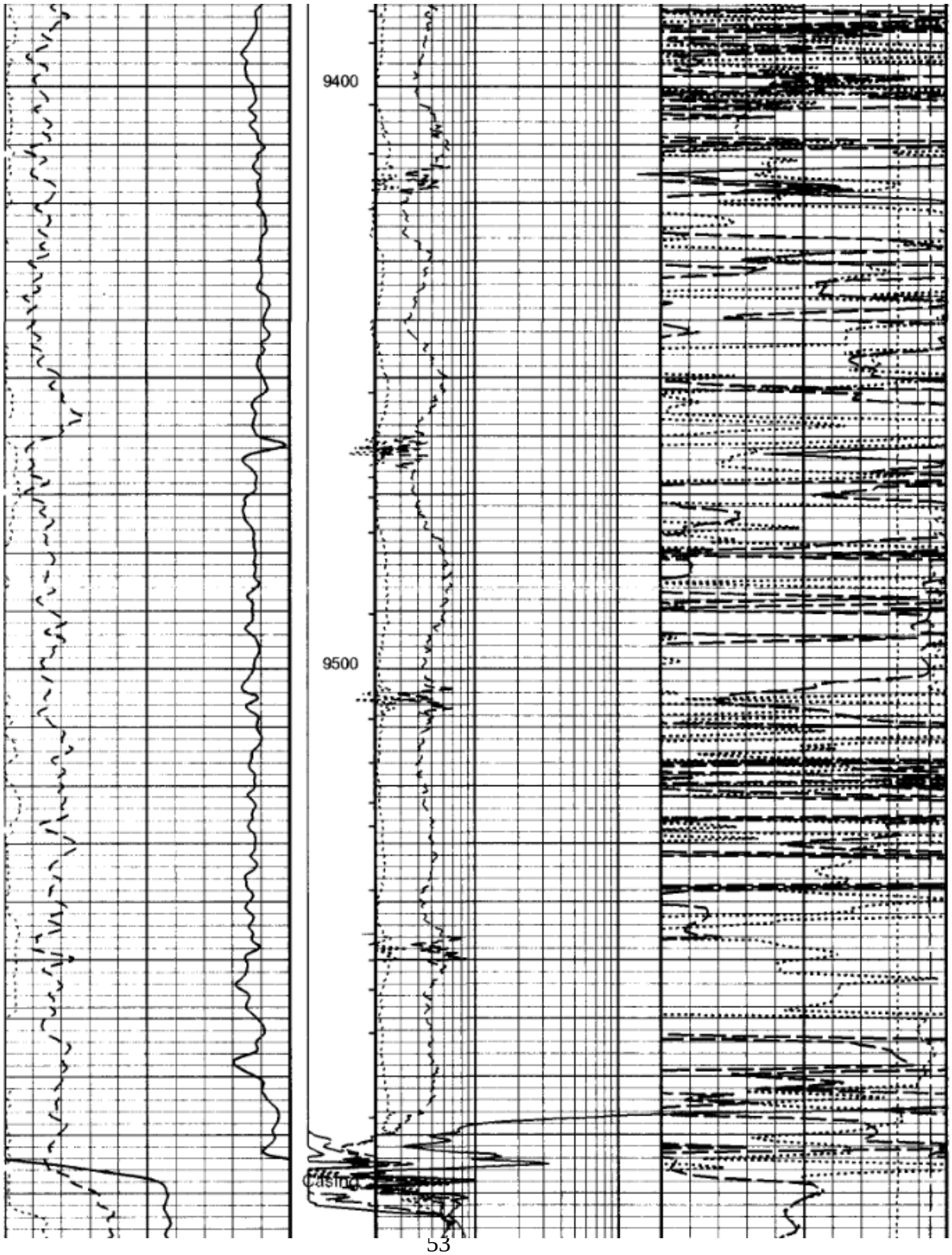
9400
9500
Casing

Figure 5.3: Well log used showing poor data quality and difficulty of reading log.

Depth uncertainty based on time-depth corrections leads to some uncertainty in which zones are produced. The depth correction created for the seismic using the TDQ method had few faults whereas the study area had many which can cause incorrect depths. This and distance created up to 500-foot errors within an area though most were only 100-250-foot errors. While this is not a significant error for most structural work it is an issue for wells which have perforations near two different zones. A 100-foot error could mean for those wells that it is producing from a different zone than interpreted.

Chapter 6: Discussion

6.1 Well Log Interpretation

All wells except for well 1 had similar results for hydrocarbons. For most wells there was thin overlap of neutron density over density porosity, and the overlap was about the same width throughout the hydrocarbon intervals (Figure 6.1) This space has been interpreted to be a reading for oil with no gas like intervals. For some wells there is production data and perforation intervals so the exact interval that was produced and the subsequent hydrocarbons produced is known. In these wells the space between the bulk density and neutron porosity overlap appeared to be that of oil and no gas cap however there was a large amount of gas produced from the interval. It was therefore concluded if the well logs were only showing oil and gas was being produced then there must be gas dissolved in the oil.

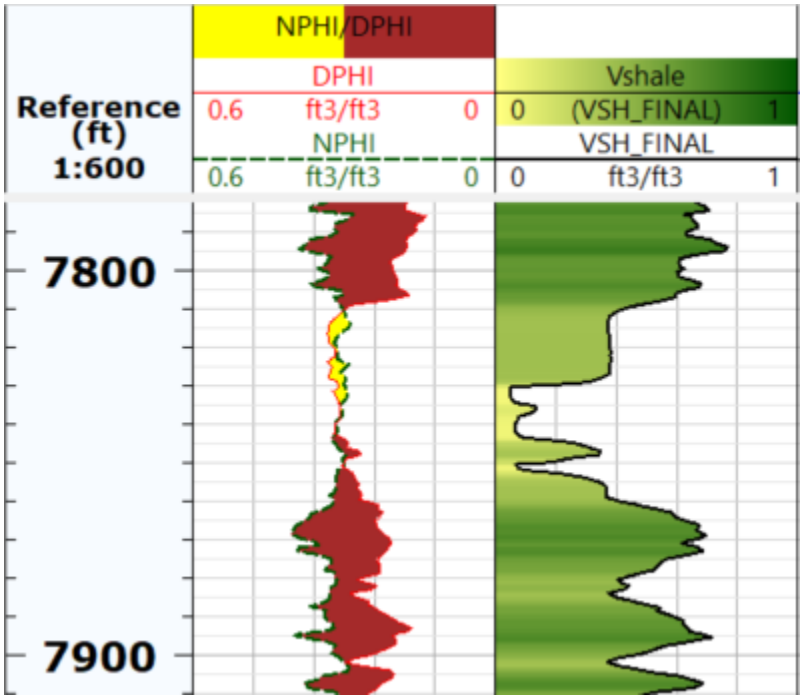

Figure 6.1: Well 11 at perforation interval 7809-7815 ft.

6.3 Drive Interpretation

Only six wells had sufficient reservoir data to make an interpretation, there were others with production data but it was either too short or too choppy to make a reasonable interpretation. For most of the wells interpreted to have solution gas drive there was both logarithmic decline in oil and an increasing gas to oil ratio such as depicted in Figure 6.2.

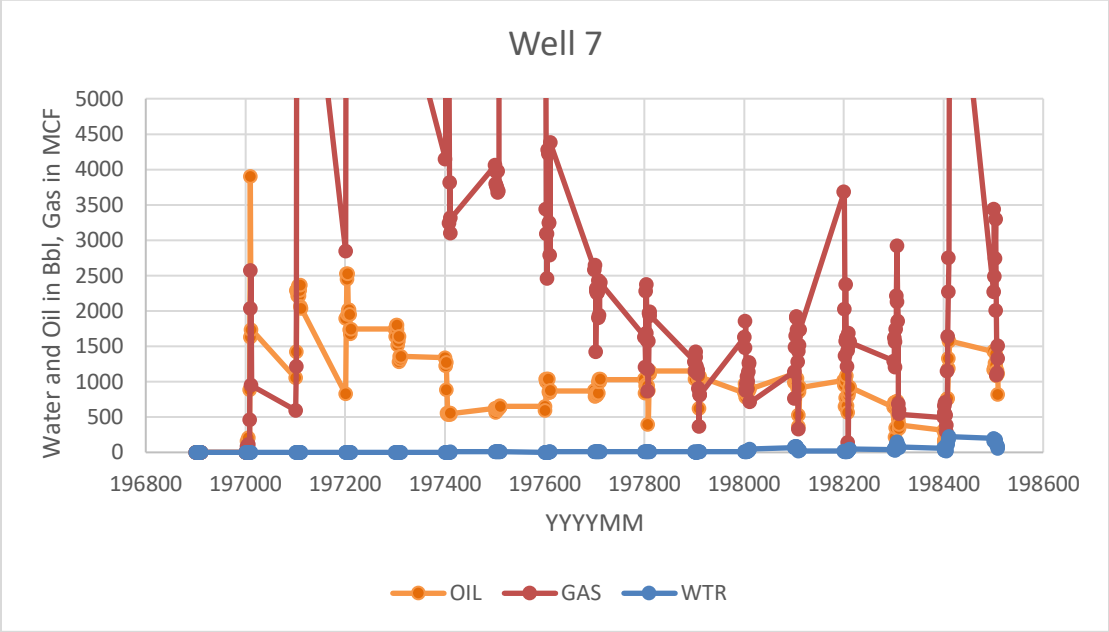

Figure 6.2: Well 7 production Oil is green in bbl, red is gas in MCF, and water is blue in bbl.

For wells 11 and 13 there was a decline indicative of water drive but increasing gas to oil ratio such as depicted in Figure 6.3. This was interpreted to mean that there was

both water drive and solution gas drive in the wells.

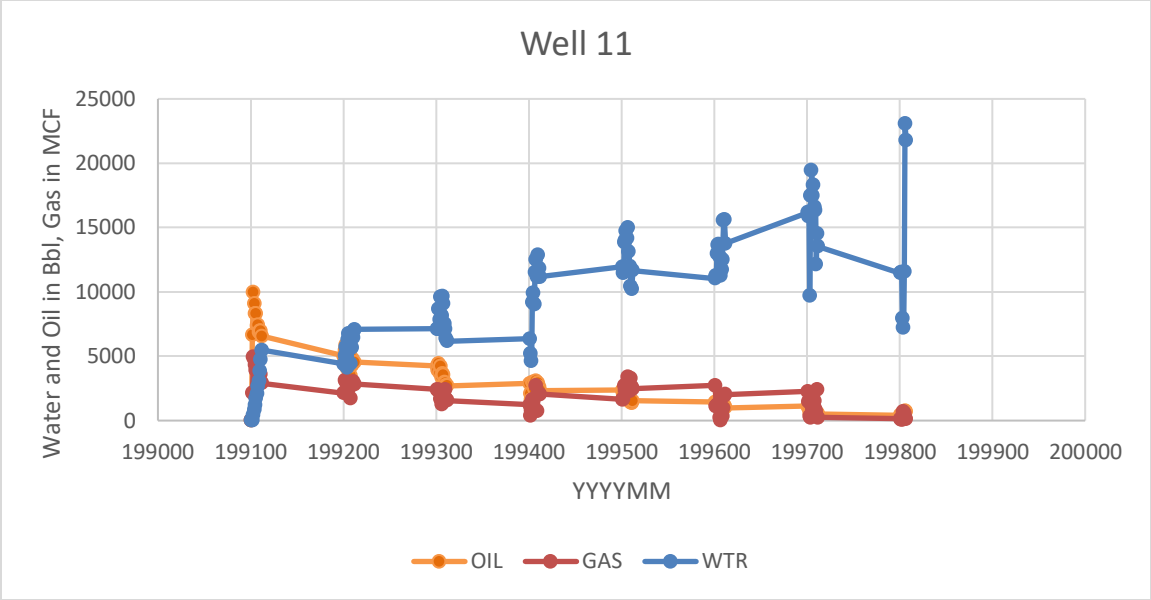

Figure 6.3 Well 11 production. Oil is green in bbl, red is gas in MCF, and water is blue in bbl.

Although I was able to interpret drive mechanisms only for approximately 35% of the wells it confirms the interpretation of solution gas drive being present in the six is an accurate and correct interpretation. Since half of the wells in each field are producing from the same zone then it is highly likely that if three wells in the field have solution gas drive then they all do because they are nearby each other and hydrocarbon forming conditions are likely similar across short distances within the sandstone unit. Similarities in fields GORs and structure also supports this argument. This production data allows for high confidence in solution gas drive being largely present in High Island 24L and ST TR 60S.

6.4 Similarity of Geology Across the Gulf Coast

Fields that had the same fluvial input and same principal depositional systems tract are geologically similar and the fields that lie within the just same principal depositional systems tract are geologically similar. Using High Island 10L as an example a list was compiled of fields that were as similar as possible on the basis of being Lower Miocene eastern progradational sandstone fields and having a similar overall structural geology (Table 6.1). 21 fields were identified as being highly similar to High Island 10L meaning they may also have the geological seals necessary to support solution gas drive.

An area of nearby fields was selected and GORs calculated from total cumulative gas and oil production (Figure 6.4 and Table 6.2) The wells were sorted by GOR and then selected depending on being within + plus or minus 20 MCF/Bbl of the GOR of High Island 10L, 81.46 MCF/Bbl. Seven fields in the area were found to have wells with GORs within the limits. Six of the seven are also on the list of geologically similar fields to High Island 10L. If the islands have similar GORs this means they likely had similar hydrocarbon formation and history and if they also have the same geology this means they likely have solution gas drive as well.

Since 6 fields alone are very similar in geology to High Island 10-L and have similar GORs it is likely more fields are similar enough to High Island 10L, High Island 24L and ST TR 60S that a significant proportion of fields in the deep basin depositional system have solution gas drive. The deep basin is also where the most nearshore oilfields are with increasing concentration in the eastward direction, so it is the area of the most interest for enhanced oil recovery.

Table 6.1: List of fields geologically similar to High Island 10L

Field Name	Structure
Block 176-S	rollover anticline into growth fault
GOM 27-L	faulted anticline
Galveston 175-S	rollover anticline into growth fault
Shipwreck	rollover anticline into growth fault
ST. TR. 60-S Central	faulted anticline
ST. TR. 60-S East	faulted anticline
ST. TR. 60-S West	faulted anticline
Freeport	faulted anticline
Galveston 102-L	faulted anticline
GOM-ST-214-L	faulted anticline
Lafittes Gold	faulted anticline
Block 98-L	faulted anticline
High Island Blk. 55-L	rollover anticline into growth fault
High Island Blk 30	rollover anticline into growth fault
Poco	rollover anticline into growth fault
High Island Block 31-L	rollover anticline into growth fault
High Island Blk 24L	rollover anticline into growth fault
Blk 87-S	faulted anticline
McFaddin Beach, E.	faulted anticline
Sabine Pass	faulted anticline
High Island 4-L NW-4	faulted anticline

Table 6.2: Fields with GORS similar to High Island 10L. Multiple wells for same field have been deleted and only one representative well displayed.

API	Field	Gas in MCF	Oil in Bbl	GOR
4.2606E+13	MCFADDIN BEACH E	816166	8116	100.5625924
4.27083E+13	HIGH ISL BK 98L	4731494	47055	100.5524174
4.26053E+13	BLOCK 0176-S	130690	1374	95.11644833
4.2708E+11	HIGH ISL BK 52	12579478	136619	92.07707566
4.27083E+13	HIGH ISL BK 30	2547205	27817	91.57008304
4.2708E+13	HIGH ISL BK 24L	2580311	28398	90.86241989
4.27154E+11	SABINE PASS BK 17	360844	4009	90.00848092

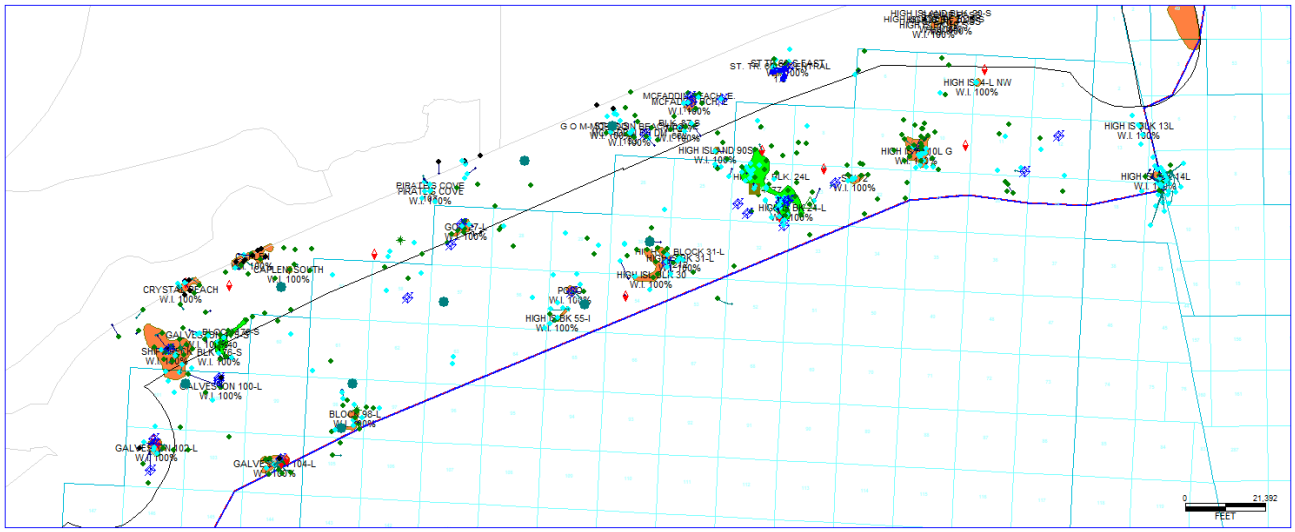

Figure 6.4: Selected wells for GOR comparison.

6.5 High Gas Content of High Island

Gas production in High Island 10L, High Island 24L, and ST TR 60S was high and many wells were converted to gas wells later in life (Figure 6.5, Figure 6.6, Figure 6.7, and Figure 6.8). In Ogbuauo's model the percent miscible reservoirs rapidly decline with increasing methane impurity (Figure 6.9). The high gas content in the fields means both the 18-mole percent of methane would be achieved more quickly than fields with lower gas content and that all fields would likely become immiscible if CO_2 recycling was operated normally. While the concentration of oil fields to gas fields increases eastwardly, gas production, which translates to higher GORs on average, is high within the deep basin depositional sequence tract (Figure 6.10). It is, therefore, likely that all the fields with solution gas drive would also have accelerated methane impurity during production.

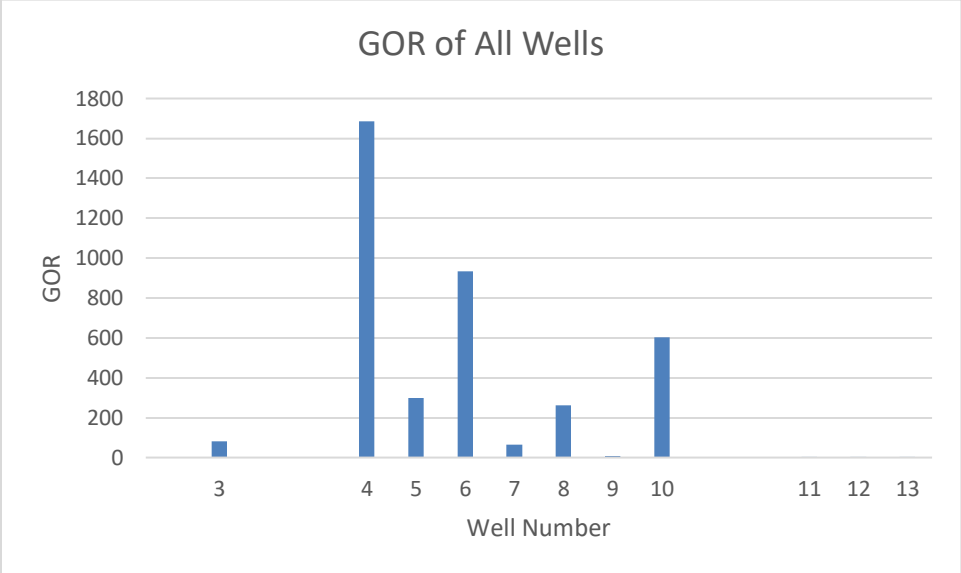

Figure 6.5: Cumulative GOR (MCF/Bbl) for all wells in database.

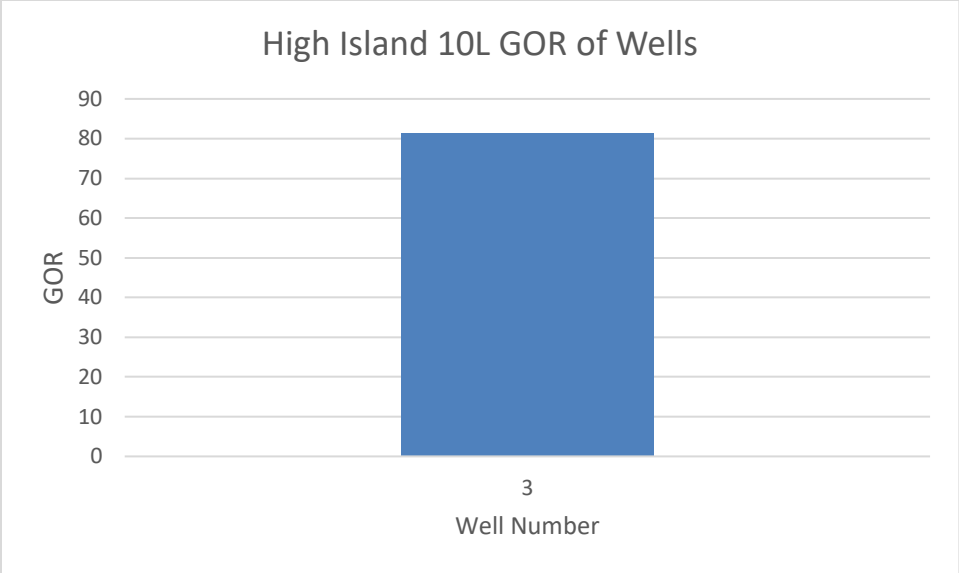

Figure 6.6: Cumulative GOR (MCF/Bbl) for High Island 10L.

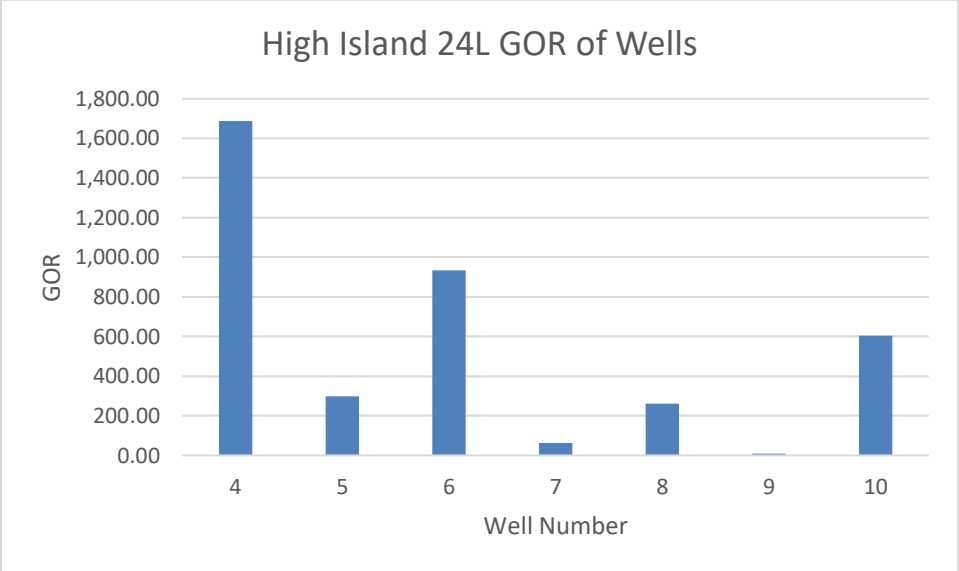

Figure 6.7: Cumulative GOR (MCF/Bbl) for High Island 24L.

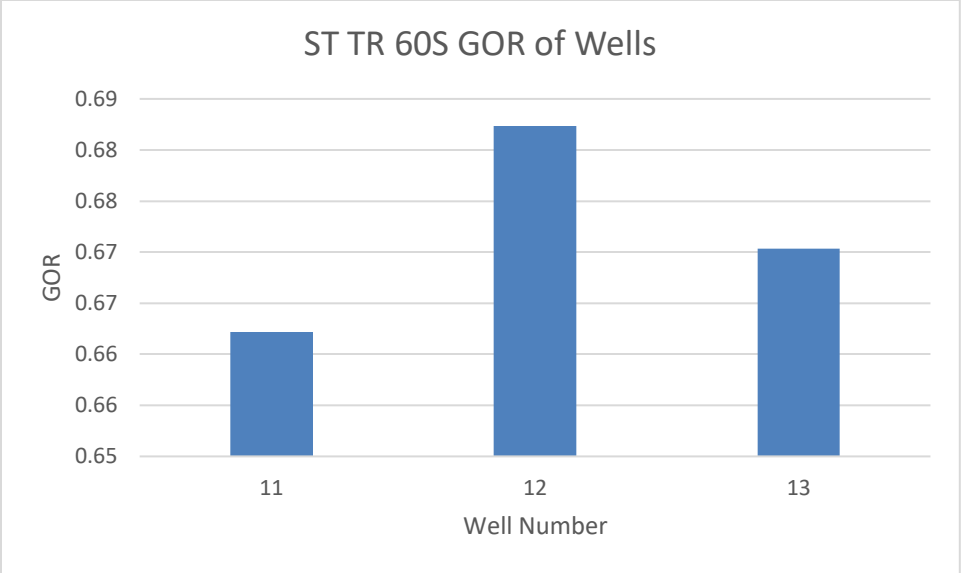

Figure 6.8: Cumulative GOR (MCF/Bbl) for ST TR 60S.

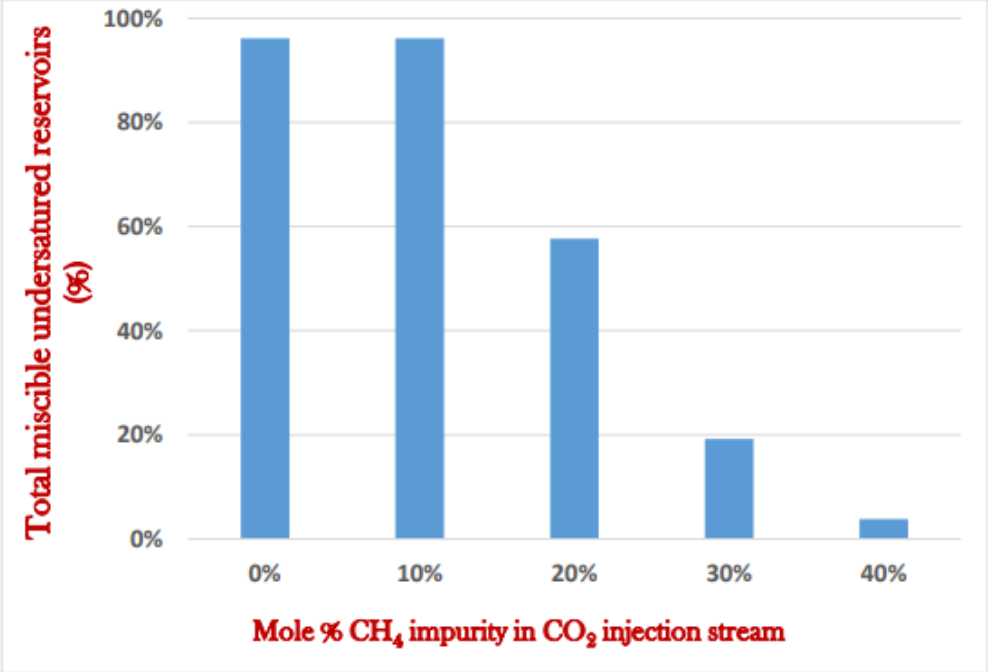

Figure 6.9: Total miscible undersaturated (pressure below bubble point) reservoirs at increasing mole percent methane impurity (From Ogbuabuo, 2015).

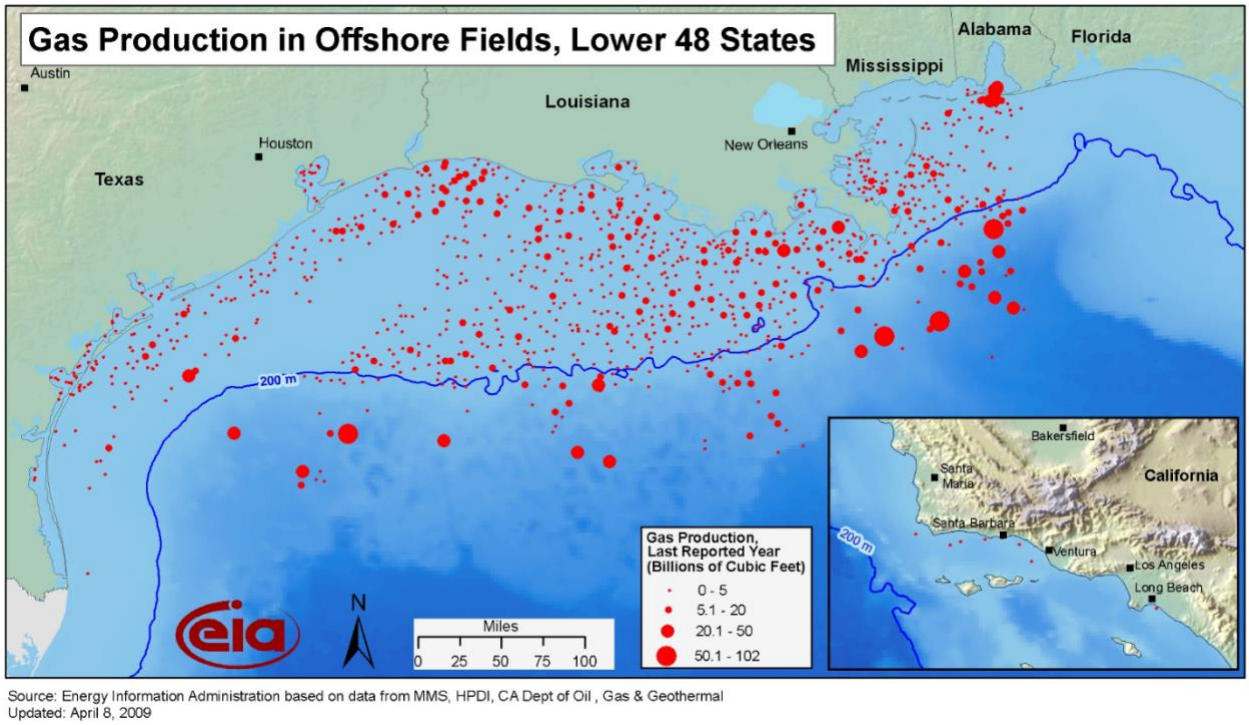

Figure 6.10: Gas Production in Gulf Coast (From EIA, 2009).

6.6 Economics of Offshore CO_2 EOR

Without the complications of miscibility, offshore CO_2 EOR already costs more than onshore. OPEX and maintenance costs are higher, if the field is old CAPEX required for the modification of existing wells and equipment are higher than onshore, and transportation of the CO_2 either by ship or pipeline is more expensive on shore. Shallow water fields are mature fields and many are near abandonment and having their platforms removed, which would increase the cost of CO_2 EOR significantly if they were to be brought into production again.

The economic viability of CO_2 EOR is dependent on three main things: the cost of oil, the cost of CO_2, and the efficiency of EOR. A study done by NETL (2014) found that CO_2 costs over \$60/mt with current CO_2 EOR technology would make CO_2 EOR in the Gulf of Mexico uneconomic with a \$90 per bbl oil price and economic recoverability was highly sensitive to CO_2 costs (Table 6.3) .

Table 6.3: Economically recoverable offshore oil based on a varying CO_2 cost and a \$90/B oil price (DOE/NETL, 2014).

($90/B Oil Price; Current CO_2-EOR Technology)

CO_2-Sale Price plus Transportation ($/mt)						
	$20	**$30**	**$40**	**$50**	**$60**	**$70**
Shallow Water	1,080	860	700	390	290	40
Deep Water	260	220	220	80	50	20
Undiscovered	1,180	1,000	1,000	340	230	90
Total	**2,520**	**2,080**	**1,920**	**810**	**570**	**150**

If CO_2 EOR is to be done in these areas and many are affected by the methane induced immiscibility problem, then a cost-effective solution must be developed. There are several options that are available to deal with the problem. The first has to do with using a plant to separate the methane from the produced CO_2 for reinjection.

6.6.1 Plant Separation Facility

It is assumed that the shallow water fields that will be using CO_2 EOR are mature fields and therefore have an existing design, so adding a plant could be unachievable, or

impractical due to weight limits or due to safety impact and equipment damage from corrosion from the process systems (Salim et al, 2012; Ruhe and Griffin, 1970). The options for a plant separation facility then is to either build a new facility with a bridged link to the platform for separation, to make a subsea facility, or to pipe the produced gas to an onshore facility and send back to the offshore platform for reinjection.

Lula field in offshore Brazil does above sea gas separation for CO_2 EOR using a floating production storage and offloading vessel separate from the platform and designed to do such from the beginning, so they did not have to make modifications to the existing equipment ,and they are trying to develop methods to deal with the corrosion problems from CO_2 and water (IEAGHG, 2017; Henriques et al., 2012). A bridge-linked facility solution is used by the Sleipner CCS project, which separates CO_2 and methane on the Sleipner T platform (CCS Network, 2019). Subsea facilities have been posited by several papers, such as Dalane et al (2017), but no application of subsea processing has been used to date. The Snøhvit project in offshore Norway produces natural gas and CO_2, transporting the gases to an onshore separation facility and sending the CO_2 back to near the offshore gas field to be sequestered (Heiskanen, 2006).

It seems for mature fields that are going to go the route of separation, the best two options of the plant separation facility solutions would be to build a bridge linked facility for separation or to pipe on shore for separation. Which of these two things would be more economical depends on the circumstances of the project. Creating the bridge linked facility would have a high upfront cost, but if it was designed to be transportable it can be moved to other fields once EOR is completed in another. For transporting back onshore via pipeline, the cost is dependent on the location of the field. If the field is near existing pipes, and gas is transported to an existing facility, then costs are low. If the field is not

near pipelines for transportation, they would have to be built, and that cost would only serve the immediate areas around the new pipeline.

6.6.2 Avoid CO_2 Recycling

Recycling the CO_2 used during enhanced oil recovery is what causes an increase in methane content, so logically reducing this process would help with the immiscibility problem. Producers could vent and flare the methane-contaminated CO_2 and replace it with new CO_2. This can be very costly at current prices of CO_2, but, if the price of CO_2 were lower, it could be a valid option. A con of this process though would be a loss of CO_2 storage tax credits that CO_2 EOR projects may receive if they are from an anthropogenic source and a loss of value in greenhouse gas reduction. Alternatively, instead of replacing all of the CO_2 and venting and flaring, the producer could continuously add new CO_2 to keep the percentage of methane down. This has been done at sites onshore, such as Cranfield in Mississippi (Choi et al., 2013). This becomes costlier with higher gas content but is likely more economic than complete replacement since there is not a loss of tax credits.

6.6.3 Immiscible Flooding

Incremental oil recovery can be achieved using immiscible CO_2 flooding. In immiscible flooding, instead of mixing with the oil, the CO_2 causes the oil to swell and for its density to decrease and improving mobility. In very heavy oils (i.e, >30°API) or very light oils (i.e., <22°API), if the reservoir is kept just below the minimum miscibility pressure, immiscible flooding can be more effective than miscible. Most of the reservoirs

are not within this API range and keeping the reservoir pressure just below minimum miscibility can be difficult. For most fields, miscible CO_2 flooding is about twice as effective as immiscible CO_2 flooding (Lake, 2014; Perera et al., 2016). Assuming that the fields in the Gulf Coast are typical, using immiscible CO_2 EOR flooding could only hope to yield half the revenue that miscible flooding could achieve. In order for it to be economical, the cost of doing immiscible CO_2 EOR would have to be half the cost of miscible CO_2 EOR.

6.6.4 Cutting CO_2 With Another Gas

It is possible that another gas could be blended with the CO_2 to help lower the minimum miscibility pressure within the reservoir, thus avoiding a loss of miscibility from the methane impurity. A possible gas to do this with is ethane, which is a gas produced from most reservoirs and is therefore abundant. Ethane is also very effective at lowering minimum miscibility pressure, up to twice as effective as CO_2. There has not been much published research on this process; however, scientists at Energy and Environmental Research Center in North Dakota are currently using an unknown ratio of ethane and CO_2 to produce from the Bakken formation (Okuno et al., 2017).

6.6.5 Solution Cost Comparison

Due to the nature of the varying needs for CO_2 enhanced oil recovery from field to field, exact costs for the various options for recovery cannot be calculated without knowing exact parameters, which is beyond the scope of this thesis. However, in order to

illustrate how the various solutions might increase the cost of an enhanced oil recovery project, the following equation was developed.

$$\begin{aligned} &General\ Additional\ Costs\ of\ CO2\ Enhanced\ Oil\ Recovery \\ &\quad = (Cost\ of\ CO2\ Recycling\ Plant + Cost\ of\ Pipelines \\ &\quad + Cost\ of\ CO2\ to\ Offset\ Methane\ Immiscibility \\ &\quad + Transportation\ costs + O\&M\ costs + Pipeline\ Operation\ Costs) \\ &\quad - (Value\ of\ Storage\ Tax\ Credit) \end{aligned} \tag{10}$$

Where:

$$Cost\ of\ CO2\ to\ Offset\ Methane\ Immiscibility = \left(cost\ of\ \frac{CO2}{ton} * tons\ of\ CO2\ needed\ to\ offset\ Methane\right)$$

$$Cost\ of\ Pipelines = (cost\ of\ pipeline\ construction\ per\ mile * mumber\ of\ miles)$$

$$Value\ of\ Storage\ Tax\ Credit = (\frac{\$35}{ton} of\ CO2\ stored\ Tax\ Credit * tons\ of\ stored\ CO2)$$

The equation considers the general large costs that may be associated with a CO_2 enhanced oil recovery project and subtracts the storage credits that may be received for using anthropogenic CO_2. In order to look at the effect of the solutions for immiscibility on a project's cost, a table was developed showing what general trends may be expected using the components of the equation and assuming a use of anthropogenic CO_2 for recovery (Table 6.3).

In Table 6.3, changes in cost of CO_2 enhanced oil recovery were represented using a scale of 0-5. A zero indicates there is no change in cost, a 1 indicates a 10 percent or less change in total cost and 5 indicates a 50 percent or greater total change. A negative number indicates either a cost was reduced or an increase in tax credit was achieved. A positive number indicates either an increase in cost or loss of tax credit. It is important to note that the option of cutting the CO_2 with ethane does not include the cost

of ethane, which would be an added expense. The table also does not consider how many fields could be serviced by a certain option and what economic value that may have.

Table 6.3: Possible changes in cost from CO2 Enhanced Oil Recovery due to Immiscibility.

	Methane Separation Plant Options				Alterations to Recycling		Cutting With Another Gas
	Piped to Existing Onshore Separation Facility	Piped to Constructed Onshore Separation Facility	Transportable Attached Platform	Modify Existing Platform	Dilute Methane with more CO2	Don't Recycle CO2	Cutting With Ethane
Cost of CO2 Recycling Plant	0	5	5	5	0	0	0
Cost of Pipelines	5	5	0	5	0	0	0
Cost of CO2 needed to Offset Methane	0	0	0	0	3	5	-1
Transportation Costs	0	0	2	0	1	1	1
O&M Costs	0	0	0	1	0	0	0
Pipeline Operation Costs	1	1	0	1	0	0	0
Value of Storage Tax Credit	0	0	0	0	-1	4	2
Total Change:	6.00	11.00	7.00	12.00	3.00	10.00	2.00

6.8 Recommendation for Further Studies

Despite the uncertainties from the quality of available data, the current analysis results show that solution gas drive is likely significantly present in the study area. Due to the geological history of the area, the Miocene age fields surrounding the study area have similar geology, so there is a likelihood that a significant number of wells have solution gas drive. The rest of the Gulf Coast is somewhat similar geologically, which means a large number of wells in the rest of the Gulf Coast may be similarly affected.

Due to the limited scope and quality of data used in this study, more field testing is required to determine the extent of the problem of gas methane gas production during CO_2 EOR. I recommend for a larger scale look at the fields of the Gulf Coast and for production data of many more well sites be interpreted for drive mechanism since the appropriate well logs and structure data may be lacking in other areas in the nearshore.

I also recommend a study of the expected changes in project economics based on the method of miscibility solution used and get real numbers on how much each aspect of the equation created would cost. A model could then be devised to calculate the cost for all methods for any area and to help evaluate which is most economical for a CO_2 EOR project in that area.

Chapter 7: Conclusion

The upper Texas offshore GoM could be a tempting location for CO_2 enhanced oil recovery due to its large unrecovered oil resource and possible CO_2 sources. A small sample of reservoirs were studied using available sparse data, using wireline logs analysis to interpret fluid distribution in perforated zones, and examining production history. Approximately 93 percent of wells studied likely had solution gas drive and the fluid geometry was such that methane production during EOR could not be avoided. It is likely that high methane production of produced and recycled CO_2 would lead to reduced miscibility unless the methane was abated. Due to the similarity of geology within the Houston to Louisiana coast and similar GORs, it is possible that many fields also have solution gas drive, and methane production would be unavoidable. There are several methods to deal with the immiscibility problem of which the most economical is dependent on the equation

$$\begin{aligned} &General\ Additional\ Costs\ of\ CO2\ Enhanced\ Oil\ Recovery \\ &\quad = (Cost\ of\ CO2\ Recycling\ Plant + Cost\ of\ Pipelines \\ &\quad + Cost\ of\ CO2\ to\ Offset\ Methane\ Immiscibility \\ &\quad + Transportation\ costs + O\&M\ costs + Pipeline\ Operation\ Costs) \\ &\quad - (Value\ of\ Storage\ Tax\ Credit) \end{aligned}$$

$$\begin{aligned} &Cost\ of\ CO2\ to\ Offset\ Methane\ Immiscibility \\ &\quad = \left(cost\ of\ \frac{CO2}{ton} * tons\ of\ CO2\ needed\ to\ offset\ Methane\right) \\ &Cost\ of\ Pipelines = (cost\ of\ pipeline\ construction\ per\ mile * mumber\ of\ miles) \\ &Value\ of\ Storage\ Tax\ Credit \\ &\quad = (\frac{\$35}{ton} of\ CO2\ stored\ Tax\ Credit * tons\ of\ stored\ CO2) \end{aligned}$$

Due to the current price of oil and this miscibility issue, it seems likely that CO_2 enhanced oil recovery will not become widespread at any time soon. However, prices of oil could go up or the cost of CO_2 EOR could decrease as technology improves, so studies should be done now to further evaluate how the Gulf Coast might be affected by the methane immiscibility problem in the future.

Appendix

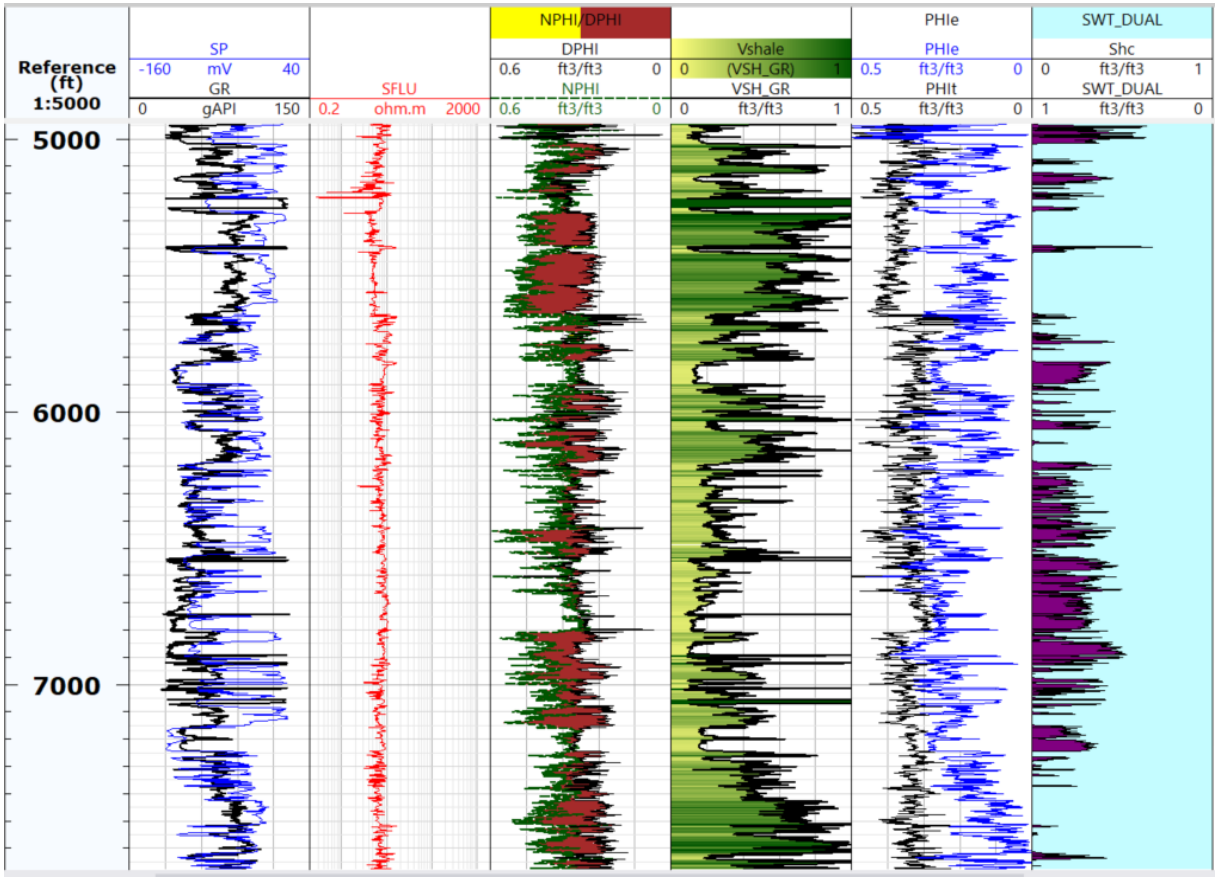

Appendix 1: Well 1 well log interpretation.

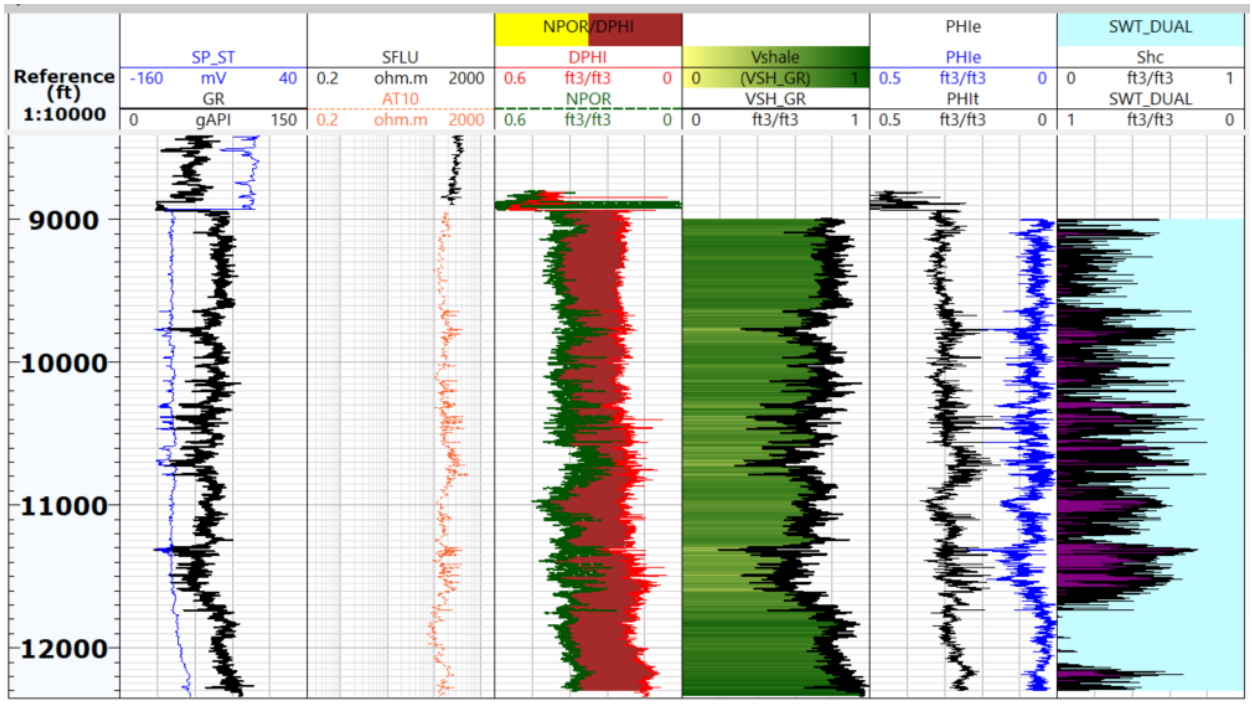

Appendix 2: Well 2 well log interpretation.

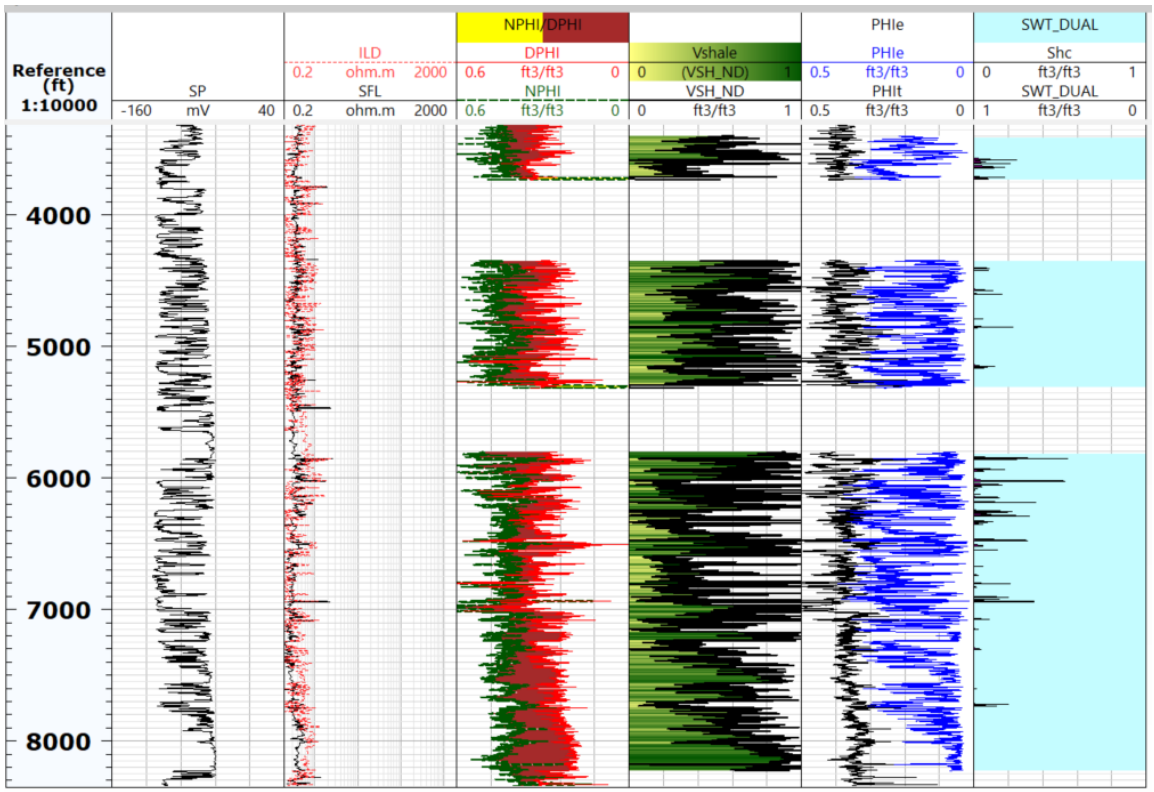

Appendix 3: Well 3 well log interpretation. Spaces in data were present in original well logs. Well 3 had no gamma ray data so neutron density was used for Vshale.

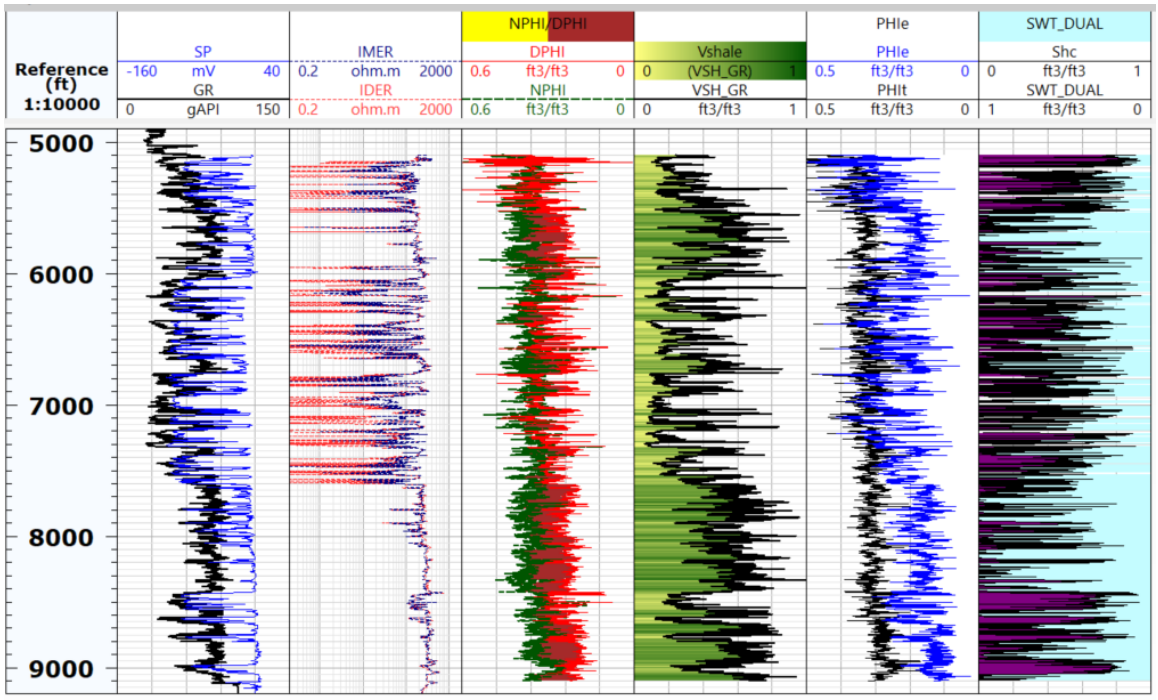

Appendix 4: Well 4 well log interpretation.

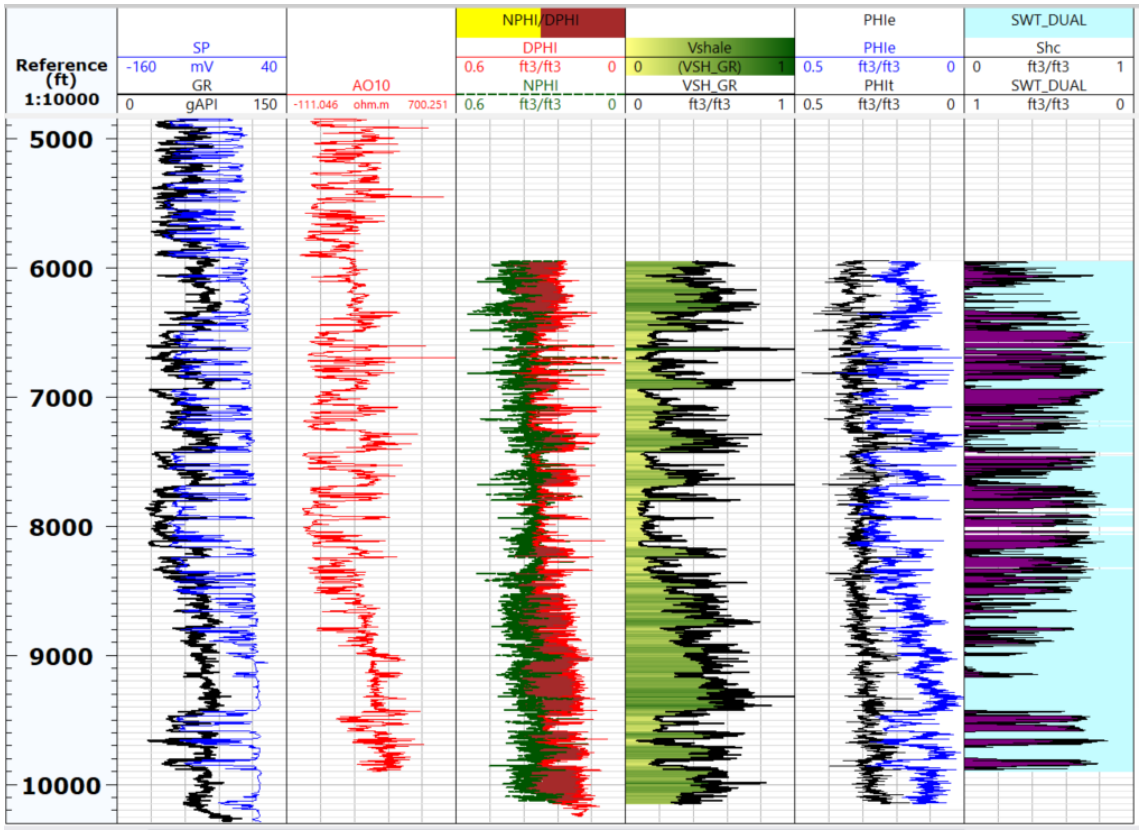

Appendix 5: Well 5 well log interpretation.

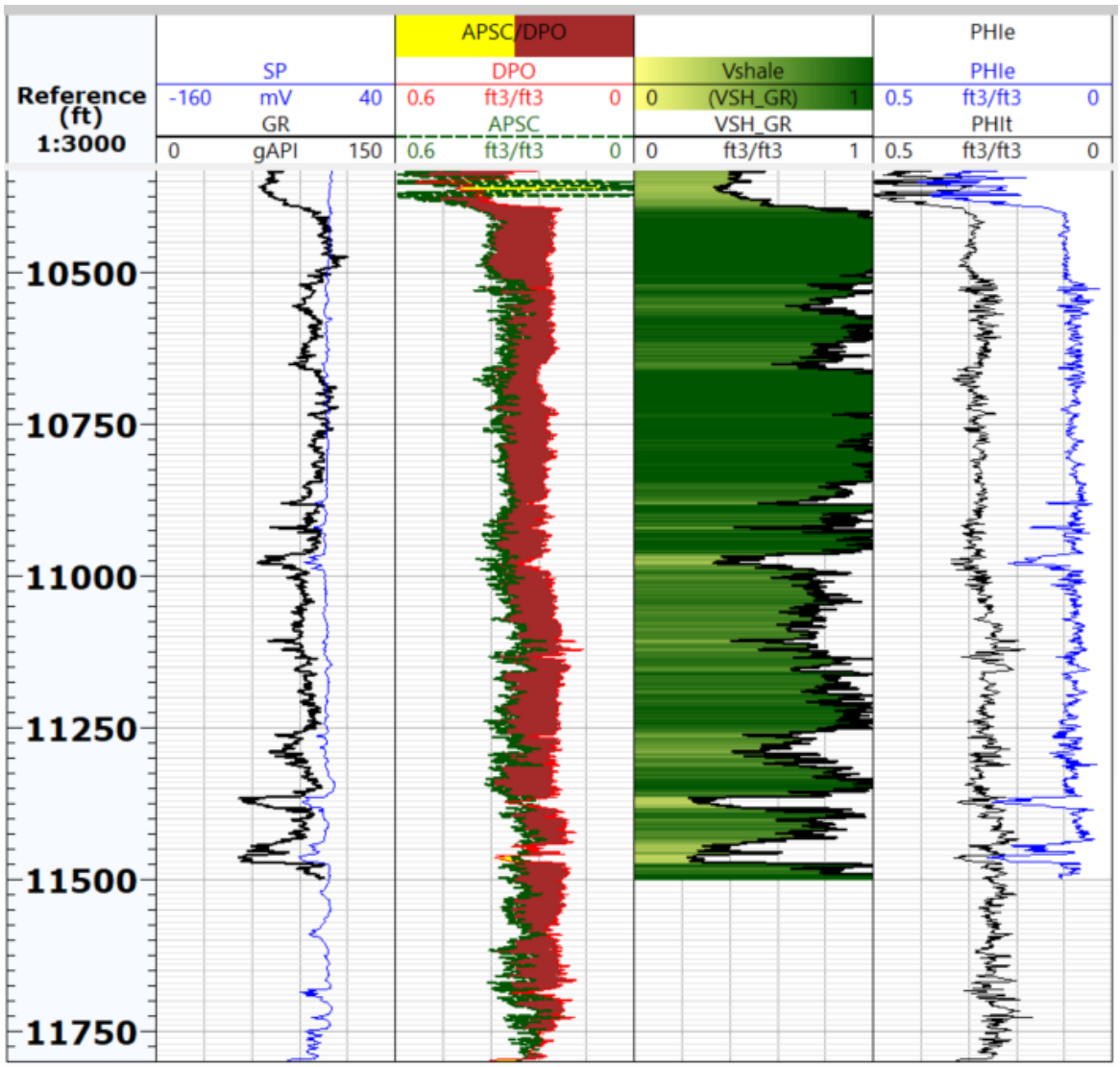

Appendix 6: Well 6 well log interpretation. Neutron Density overlap of density porosity is from error in original well log.

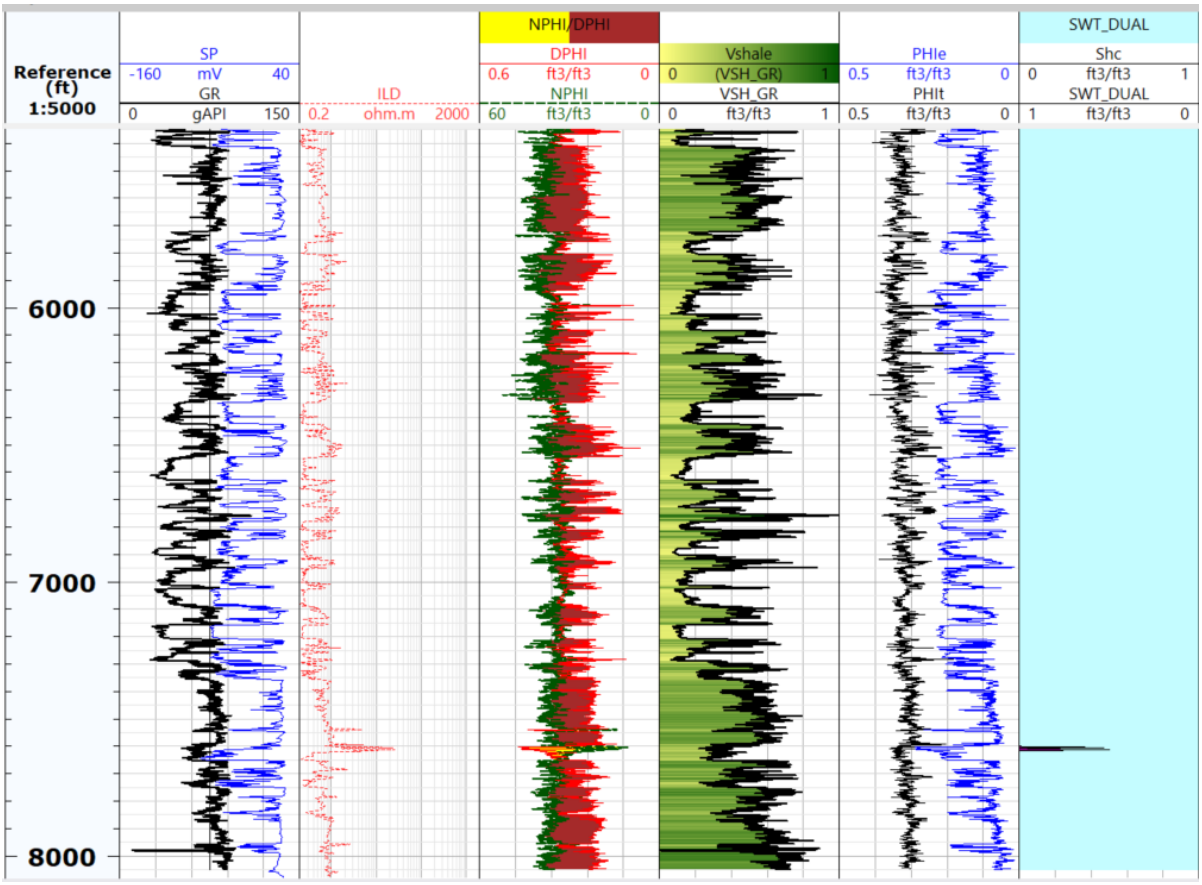

Appendix 7: Well 7 well log interpretation.

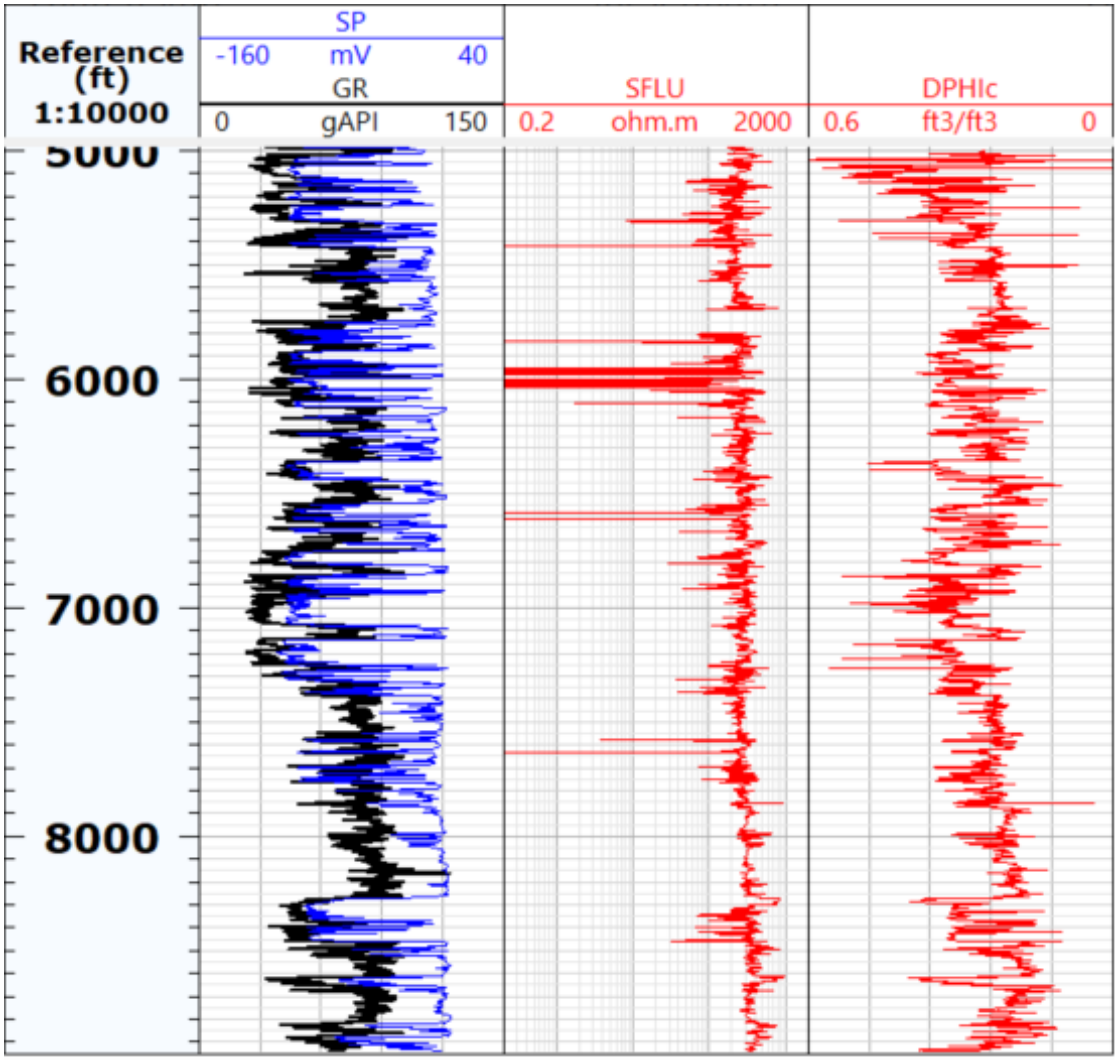

Appendix 8: Well 9 well log interpretation. Well 9 had no neutron porosity and was used for correlation. Only change from original data was bulk density was converted to density porosity.

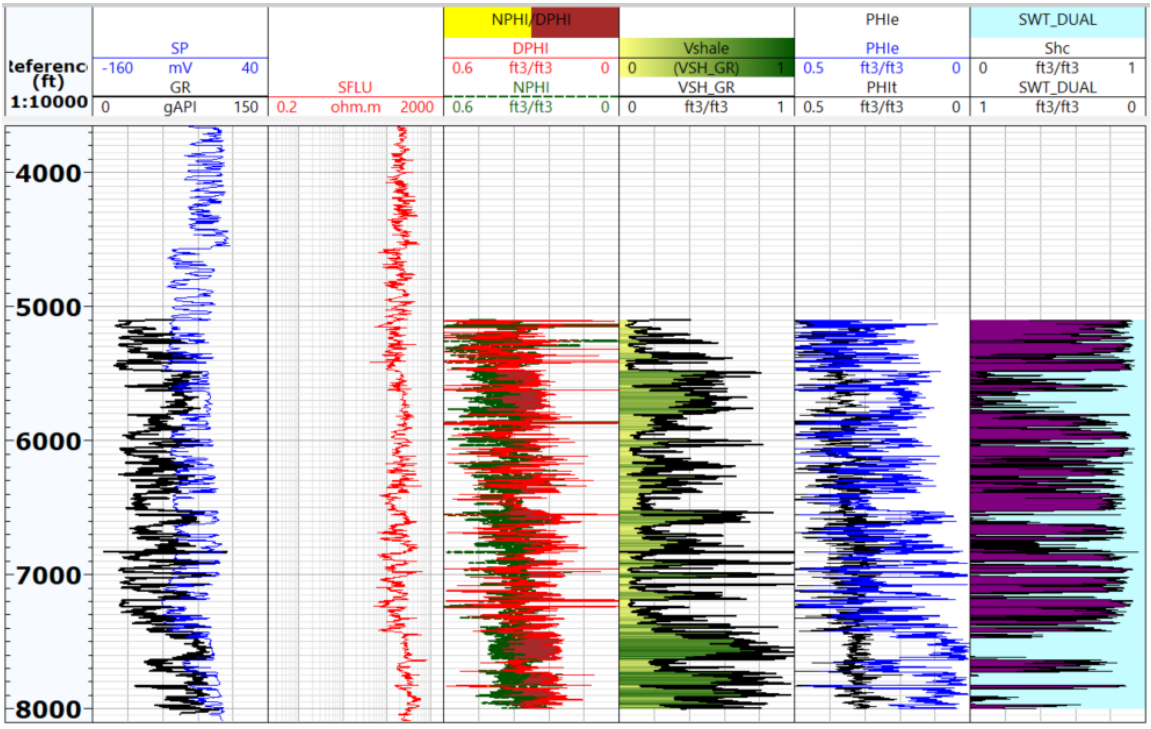

Appendix 9: Well 10 well log interpretation.

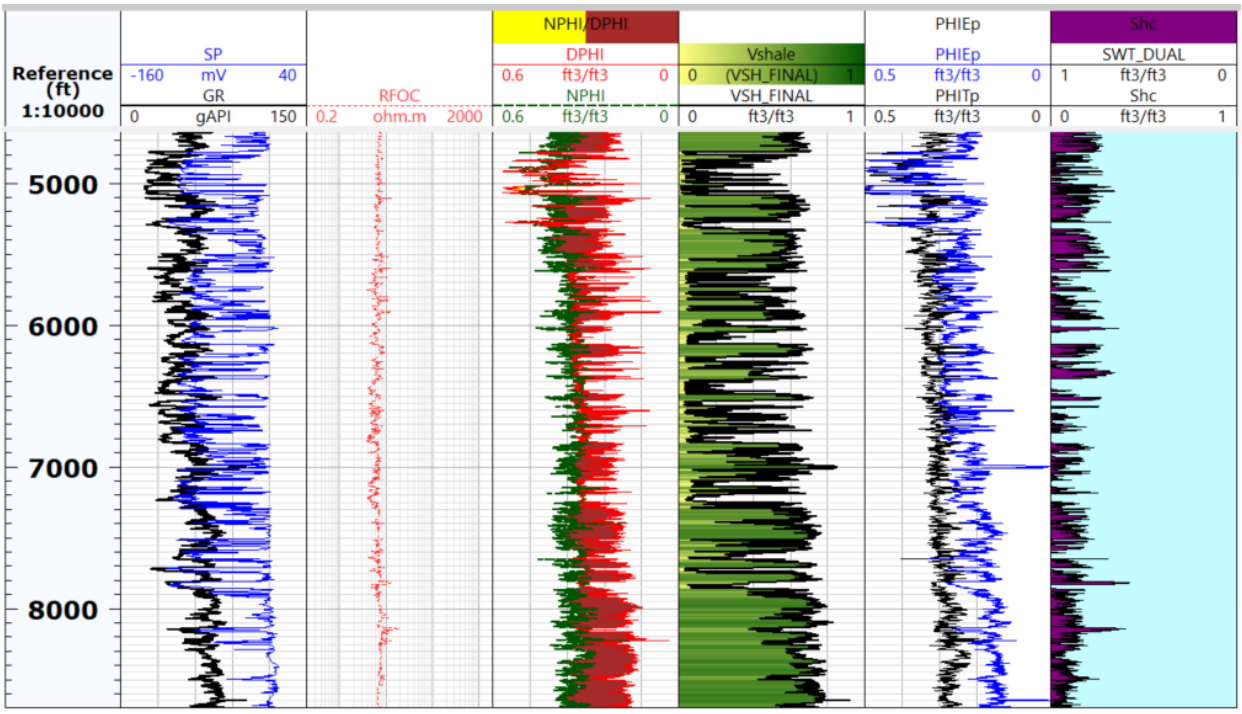

Appendix 10: Well 11 well log interpretation.

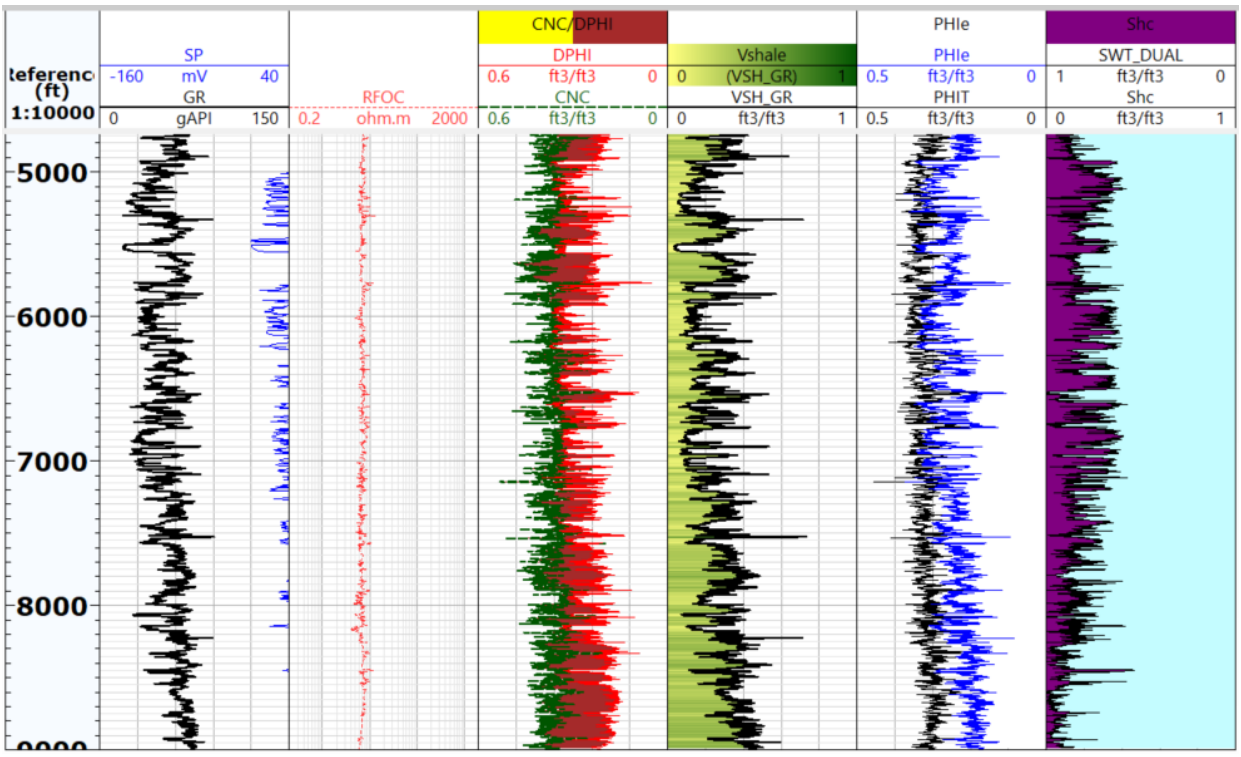

Appendix 11: Well 12 well log interpretation.

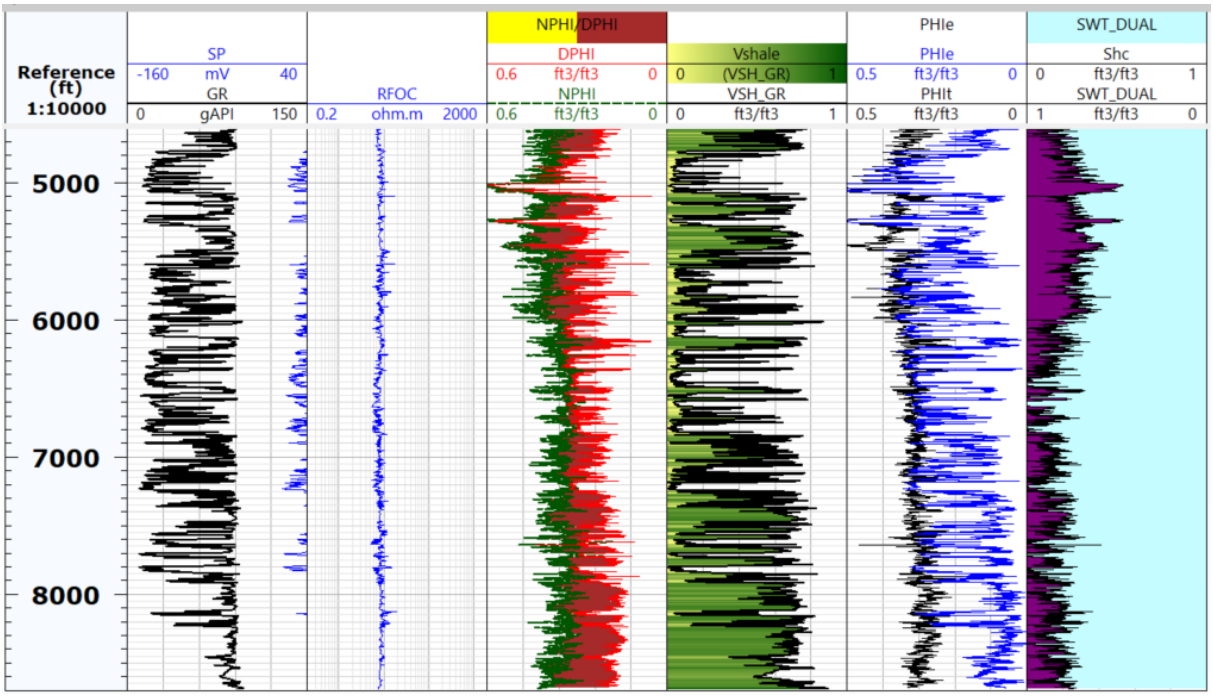

Appendix 12: Well 13 well log interpretation.

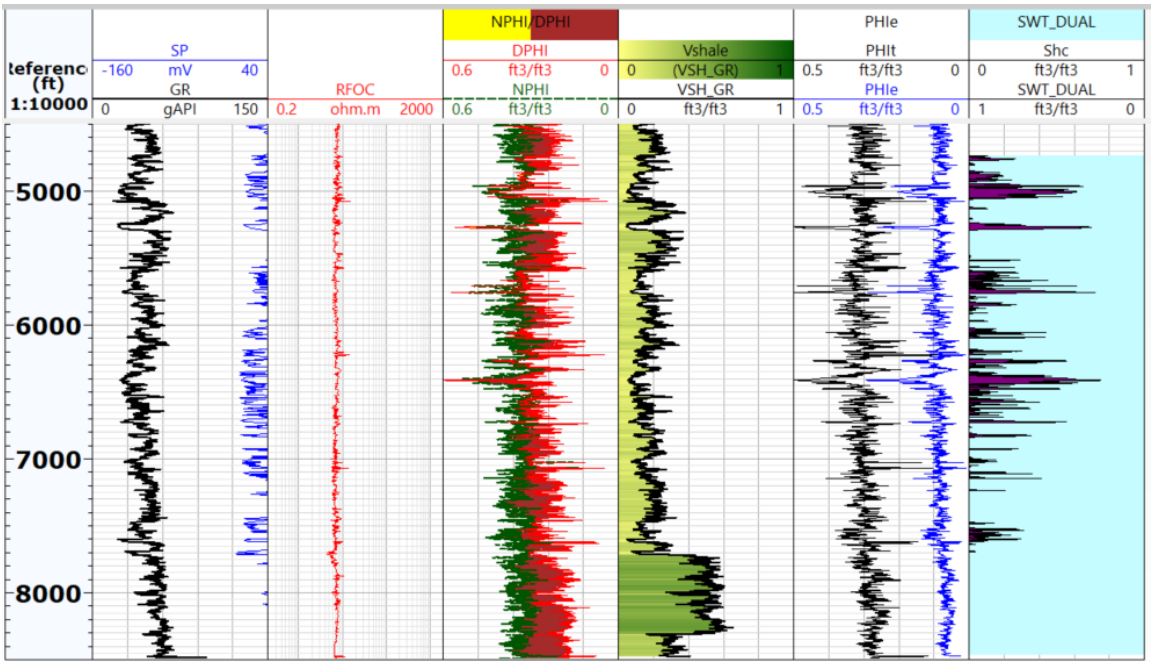

Appendix 13: Well 14 well log interpretation.

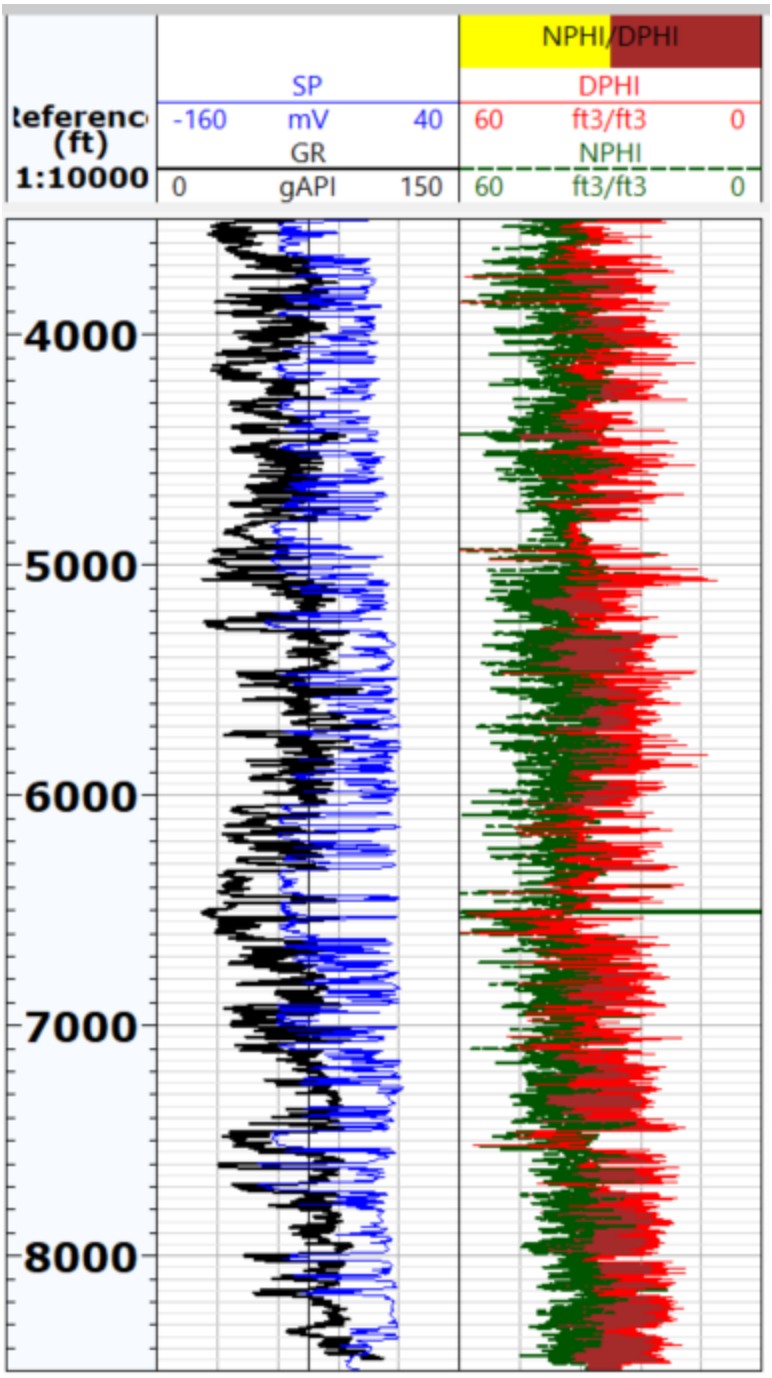

Appendix 14: Well 15 well log interpretation. Well 15 did not have resistivity so it was not fully interpreted.

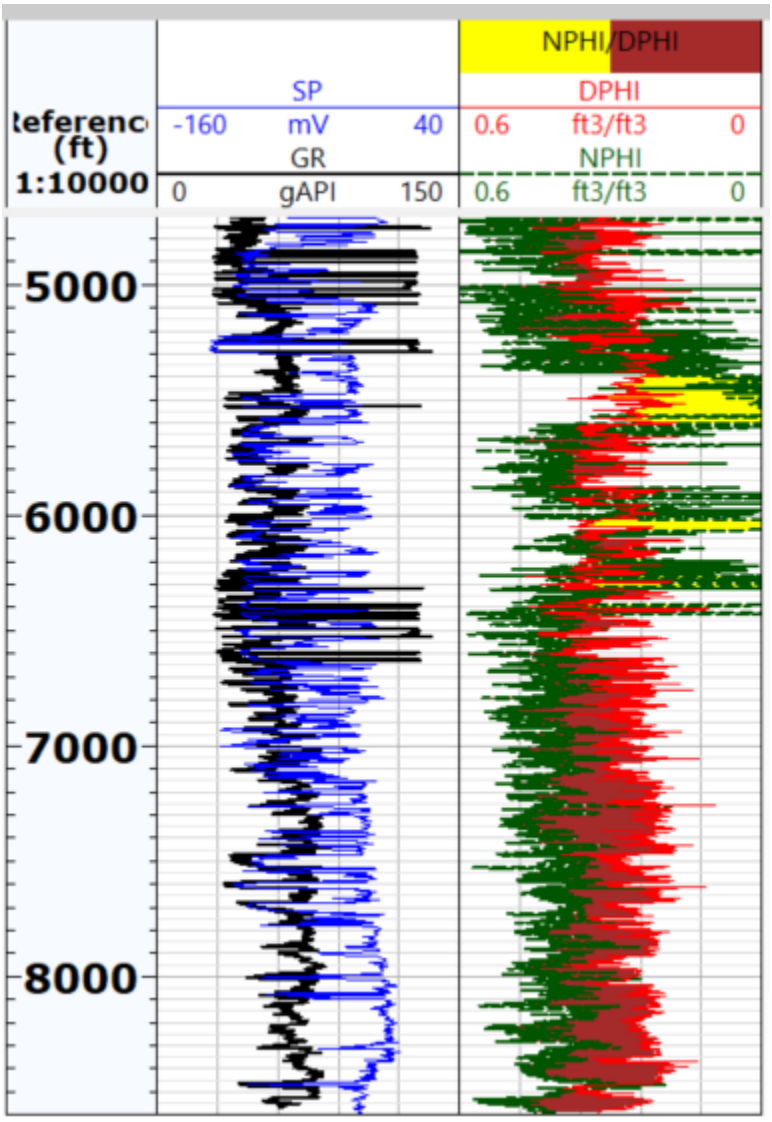

Appendix 15: Well 17 well log interpretation. Well 17 did not have resistivity so it was not fully interpreted. Large neutron density overlap of density porosity is result of error in original well log.

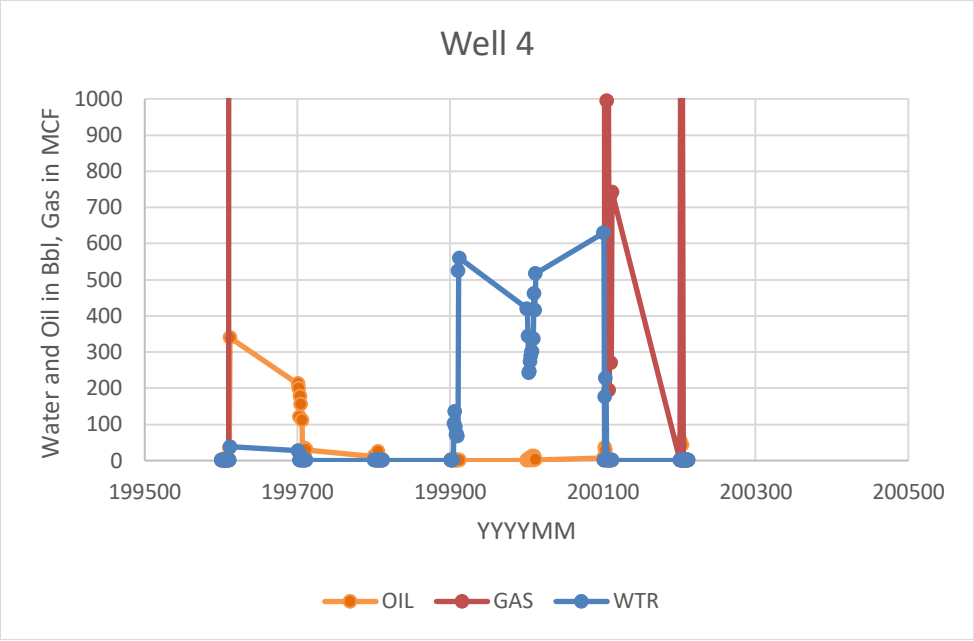

Appendix 16: Well 4 original primary production data. Gas production is out of range because it was too high to display oil trend

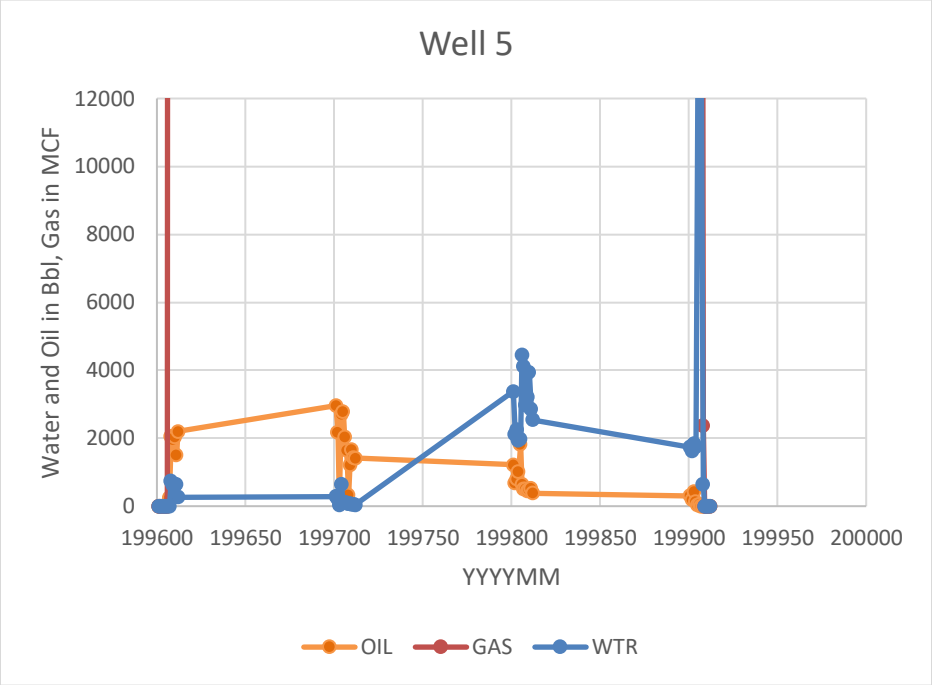

Appendix 17: Well 5 original primary production data. Gas production is out of range because it was too high to display oil trend

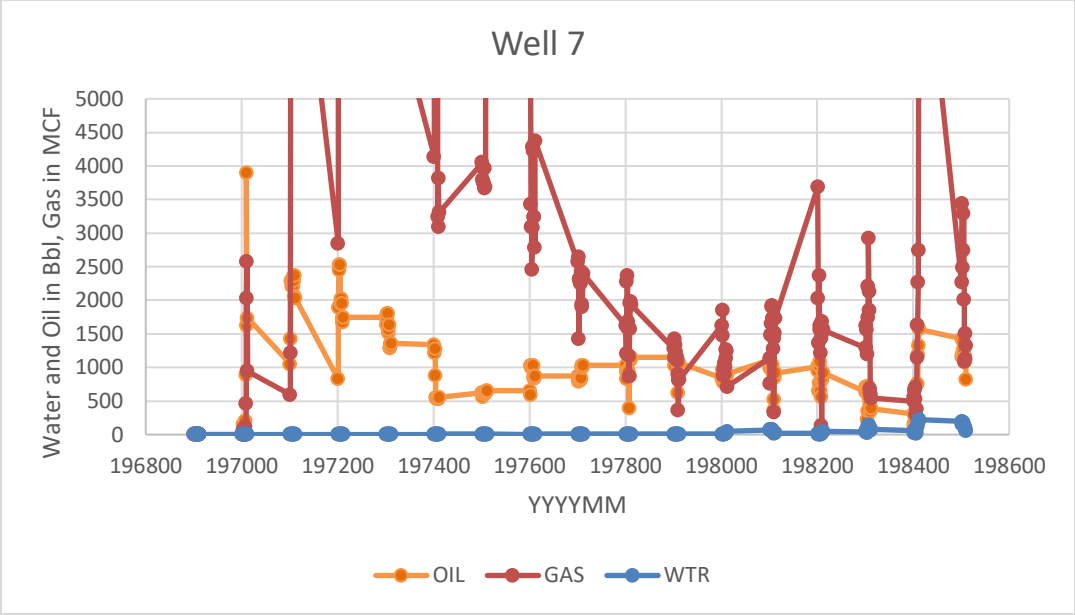

Appendix 18: Well 7 original primary production data. Part of Gas production is out of range because it was too high to display oil trend.

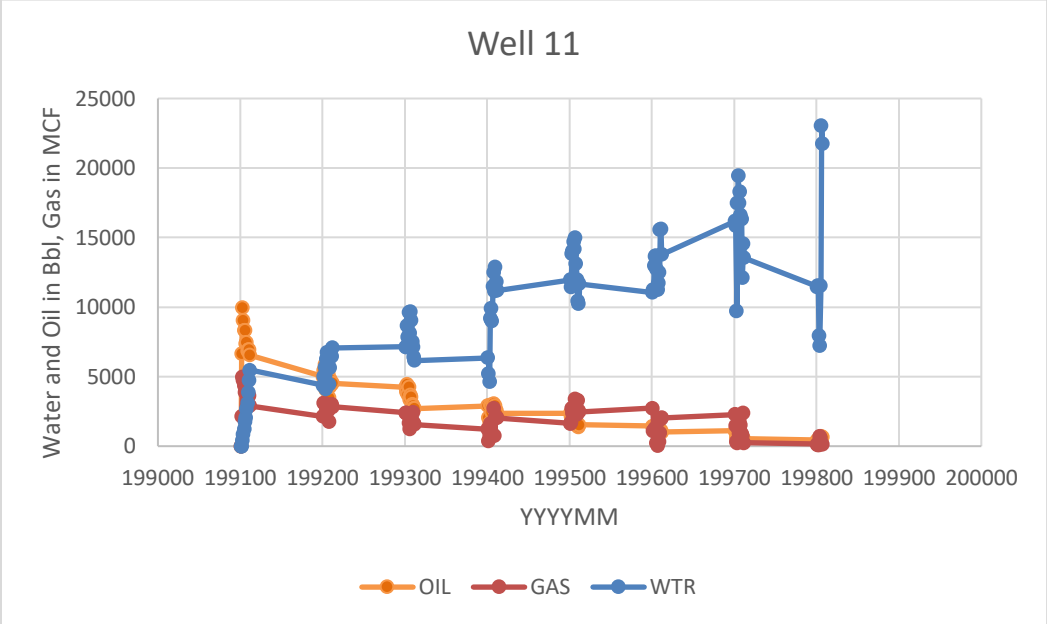

Appendix 18: Well 11 original primary production data.

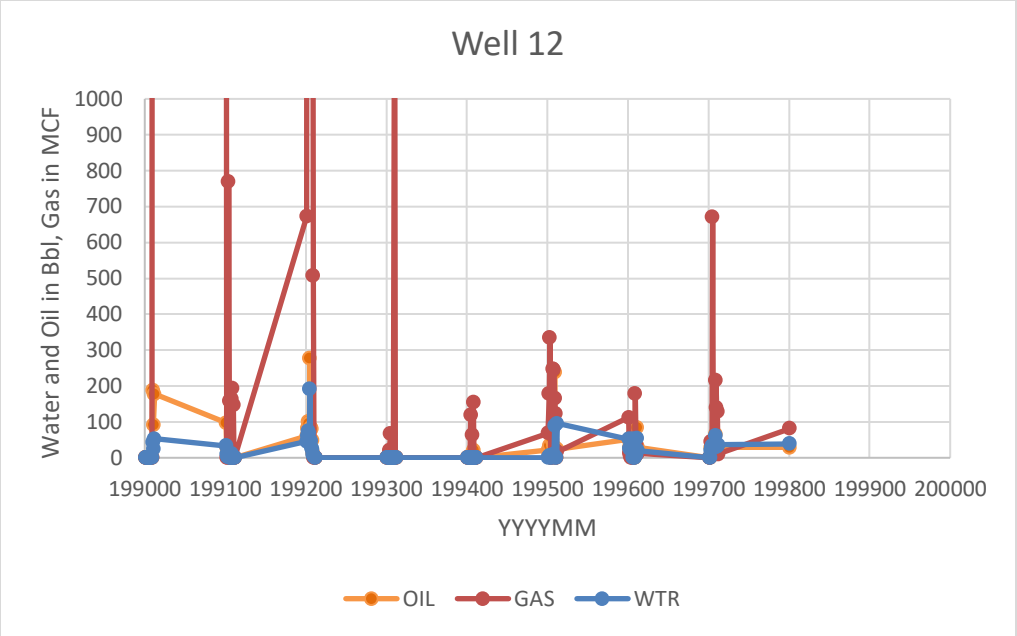

Appendix 19: Well 12 original primary production data. Gas production is out of range because it was too high to display oil trend.

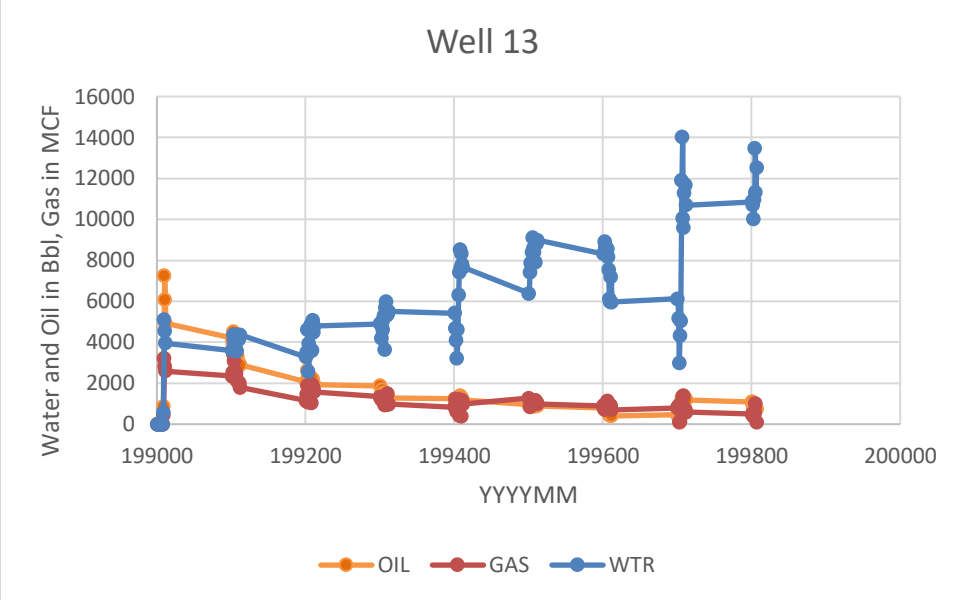

Appendix 20: Well 13 original primary production data.

Glossary

Anthropogenic: Created by human activity.

Aggradation: accumulation of stratigraphic sequences during a period of balance between sediment supply and accommodation.

Anticline: a large fold of stratified rock in which the oldest layers are in the core.

Capillary Force: Force caused by curved surface of the interface between liquid and a solid.

Cenozoic: Current geologic era starting 66 million years ago.

Clastic: pieces of pre-existing rocks created by weathering processes.

Continental Margin: Edge of the continental crust, separating it from the deep ocean floor.

Density Porosity Log: Log that measures the electron density of rock along a well path.

Displacement efficiency: Fraction of oil recovered from a zone swept by a displacement process.

Gamma Ray Log: Log that measures electromagnetic radiation of rock along a well path.

Horst and Graben: A system of upthrown (horst) and downthrown blocks as the result of normal faults on either side of the blocks.

Interfacial tension: surface tension the result of cohesive forces at the surface separating two immiscible fluids.

Jurassic: Geologic period that occurred approximately 201-145 million years ago.

Minimum miscibility pressure: The minimum pressure at which a crude oil will be miscible with carbon dioxide at reservoir temperature.

Miocene: The first geological epoch of the Neogene period occurring 23.03 to 5.33 million years ago.

Miscible: Ability of two substances to mix unto a homogeneous mixture.

Neogene: Geological period occurring 23.03 to 2.58 million years ago.

Neutron Porosity Log: Log that measures hydrogen concentration of rock along a well path.

Orogeny: A mountain building event caused by lateral compression.

Progradation: accumulation of stratigraphic sequences by deposition during a period when sediment supply exceeds accommodation. Results in the position of the shoreline migrates into the basin.

Regression: a geologic event during which the shoreline moves seaward, and the sea level falls relative to the land.

Resistivity Log: Log that measures electrical resistivity of rock along a well path.

Retrogradation: accumulation of stratigraphic sequences by deposition during a period when sediment supply is too low to fill the available accommodation space. Results in the position of the shoreline migrating backwards.

Spontaneous Potential Log: Log that measures electric potentials of rocks along a well path.

Transgression: a geologic event during which shoreline moves landward and the sea level rises relative to the land.

Triassic: Geologic period occurring approximately 252 to 201 million years ago.

References

26 U.S. CODE § 45Q (2018)

AAPG, 2016, February 24, Reservoir drive mechanisms. Retrieved from https://wiki.aapg.org/Reservoir_drive_mechanisms

Asquith, G., and Krygowski D., 2004, Basic Relationships of Well Log Interpretation, in G. Asquith and D. Krygowski, Basic Well Log Analysis: AAPG Methods in Exploration 16, p. 1–20.

Beckham, E. C., 2018, CO2 Storage in Deltaic Environments of Deposition: Integration of 3Dimensional Modeling, Outcrop Analysis, and Subsurface Application (Master Thesis): The University of Texas.

Bradshaw, B. E., and Watkins, J. S., 1994, Growth-fault evolution in offshore Texas: Gulf Coast Association of Geological Societies Transactions, v. 44, p. 103–110.

Carr, D. L., Wallace, K. J., Nicholson, A. J., and Yang, C., 2017, Chapter 5: Regional CO2 static capacity estimate, offshore Miocene saline aquifers, Texas State Waters, in Treviño, R. H., and Meckle, T. A., eds., Geological CO2 sequestration atlas for Miocene strata offshore Texas State Waters: The University of Texas at Austin, Bureau of Economic Geology Report of Investigations No. 283, p. 37-46.

CCS Network, 2019. Sleipner CO2 Injection. Retrieved from https://ccsnetwork.eu/projects/sleipner-co2-injection

Combellas-Bigott, R. I., and Galloway, W. E., 2006, Depositional and structural evolution of the middle Miocene depositional episode, east-central Gulf of Mexico: AAPG Bulletin, v. 90, no. 3, p. 335–362.Galloway, W. E., 2006, Depositional and structural evolution of the middle Miocene depositional episode, east-central Gulf of Mexico: AAPG Bulletin, v. 90, no. 3, p. 335–362.

Choi, J., Nicot, J., Hosseini, S.A., Clift, S.J., Hovorka, S. D., 2013, CO_2 recycling accounting and EOR operation scheduling to assist in storage capacity assessment at a U.S. gulf coast depleted reservoir: International Journal of Greenhouse Gas Control, v. 18, p. 474–484.

Dalane, K., Dai, Z., Mogseth, G., Hillestad, M., & Deng, L., 2017, Potential applications of membrane separation for subsea natural gas processing: A review. Journal of Natural Gas Science and Engineering, 39, 101-117. doi:10.1016/j.jngse.2017.01.023.

DeAngelo, M., 2016, May 16. Time-to-Depth Conversion. Unpublished report for Department of Energy.

DeAngelo, M. V., Fifariz, R., Meckel, T., Trevino, R. H., 2019, A seismic-based CO.sub.2-sequestration regional assessment of the Miocene section, northern Gulf of Mexico, Texas and Louisiana. International journal of greenhouse gas control, v. 81, p. 29–37.

Department of Energy, (n.d.). Enhanced Oil Recovery. Retrieved from https://www.energy.gov/fe/science-innovation/oil-gas-research/enhanced-oil-recovery

EIA, 2019., Energy Infrastructure with Real-time Storm Information. Retrieved from https://www.eia.gov/special/gulf_of_mexico/

EIA, 2009 April 8, Energy Infrastructure with Real-time Storm Information. Retrieved from https://www.eia.gov/special/gulf_of_mexico/

Fifariz, R., 2019. Personal Interview.

Fowler, J., 1987, High Island 10-L Field, Houston Geological Society Typical Oil and gas Fields of South East Texas, v. 2, p. 286–290.

Galloway, W. E., 1989, Genetic stratigraphic sequences in basin analysis II: application to northwest Gulf of Mexico Cenozoic Basin: AAPG Bulletin, v. 73, no. 2, p. 143–154.

Galloway, W. E., Ganey-Curry, P. E., Li, X., and Buffler, R. T., 2000, Cenozoic depositional history of the Gulf of Mexico basin: AAPG Bulletin, v. 84, no.11, p. 1743–1774.

Galloway, W. E., 2005, Gulf of Mexico basin depositional record of Cenozoic North American drainage basin evolution: International Association of Sedimentologists Special Publication, v. 35, p. 409–423.

Galloway, W. E., Whiteaker, T. L., and Ganey-Curry, P., 2011, History of Cenozoic North American drainage basin evolution, sediment yield, and accumulation in the Gulf of Mexico basin: Geosphere, v. 7, no. 4, p. 938–973.

Heiskanen, E., 2006, Case 24: Snohvit CO 2 capture & storage project. Create Acceptance Project Report. http://www.createacceptance.net. Horlick-Jones, T., Walls, J., Kitzinger, J., 2007. Bricolage in action: learning about, making sense of, and discussing, issues about genetically modified crops and food. Health, Risk & Society 9 (1), 83–103.

Henriques, C. C. D., Joia, C.-J. B., Guedes, F., & Baptista, I. P., 2012, April 30, Material Selection for Brazilian Presalt Fields. Offshore Technology Conference. doi:10.4043/23320-MS.

IEAGHG, 2017, IEAGHG Information Paper 2017-IP63; CSLF Report on Offshore CO2-EOR https://ieaghg.org/docs/General_Docs/Information_Papers/2017-IP63_CSLF_Report_on_Offshore_CO2-EOR.pdf

Lake, L. W., & Society of Petroleum Engineers of AIME., 2014, Fundamentals of enhanced oil recovery ([2nd]. ed.). Richardson, Tex: Society of Petroleum Engineers.

Latson, J., 2015, August 27. History of the American Oil Industry: When Drake Struck Oil. Retrieved from http://time.com/4008544/american-oil-well-history/

Leiserowitz, A., Maibach, E., Roser-Renouf, C., Rosenthal, S., Cutler, M., and Kotcher, J., May 8, 2018, Politicals and Global Warming, March 2018. Yale University and George Mason University. New Haven, CT: Yale Program on Climate Change Communication.

Lewis, A. R., Marchant, D. R., Ashworth, A. C., Hemming, S. R., and Machlus, M. L., 2007, Major middle Miocene global climate change: evidence from East Antarctica and the Transantarctic Mountains: Geological Society of America Bulletin, v. 119, no. 11-12, p. 1449–1461.

Lindsey, R., 2018, August 01. Retrieved from https://www.climate.gov/news-features/understanding-climate/climate-change-atmospheric-carbon-dioxide

Malone, T., Kuuskra, V., DePietro, Phil., 2014, June 05., CO2-EOR Offshore Resource Assessment, DOE/NETL-2014/1631

McDonnell, A., Hudec, M. R., and Jackson, M. P. A., 2009, Distinguishing salt welds from shale detachments on the inner Texas shelf, western Gulf of Mexico: Basin Research, v. 21, p. 47–59.

Metcalfe. R.S., 1981. Effects of Impurities on Minimum Miscibility Pressure and Minimum Enrichment Levels for CO2 and Rich-Gas Displacements. SPE J. 22(2), 219-225

Melzer, L. S., 2012. Carbon Dioxide Enhanced Oil Recovery (CO2 EOR): Factors Involved in Adding Carbon Capture, Utilization and Storage (CCUS) to Enhanced Oil Recovery.

MIT, 2016, Snohvit Fact Sheet: Carbon Dioxide Capture and Storage Project, https://sequestration.mit.edu/tools/projects/snohvit.html

Mufson, S., 2018. ExxonMobil to give $1 million to promote a carbon tax-and-dividend plan.The Washington Post

National Energy Technology Laboratory, (n.d.). Enhanced Oil Recovery. Retrieved from https://www.netl.doe.gov/oil-gas/oil-recovery

National Energy Technology Laboratory, 2010, Carbon Dioxide Enhanced Oil Recovery Untapped Domestic Energy Supply and Long Term Carbon Storage Solution

Nunez-Lopez, V., Gil-Egui, R., Gonzalez-Nicolas, A., & Hovorka, S., 2017, August 18., Carbon Balance of CO2-EOR for NCNO Classification. Retrieved from https://www.sciencedirect.com/science/article/pii/S1876610217320052

Ogbuabuo, P.C., 2015, The role of methane in limiting CO_2 EOR : case study of offshore Gulf of Mexico oil reservoirs (Master Thesis): The University of Texas 930029306

Okuno, R., Lake, L. W., Gould, T. L., & McGuire, P. L., 2017, Ethane-based enhanced oil recovery: An innovative and profitable enhanced-oil-recovery opportunity for a low-price environment. *SPE Reservoir Evaluation & Engineering*, *20*(1), 042-058. doi:10.2118/179565-PA

Olariu, M. I., Deangelo, M., Dunlap, D., Trevino, R. H., 2019, Early Miocene High Island delta system, offshore Texas and Louisiana. In Review

Perera, M., Gamage, R., Rathnaweera, T., Ranathunga, A., Koay, A., & Choi, X. 2016, A review of CO2-enhanced oil recovery with a simulated sensitivity analysis. *Energies*, *9*(7), 481. doi:10.3390/en9070481

Petrowiki, 2015, January 3. Solution Gas Drive Reservoirs. Retrieved from https://petrowiki.org/Solution_gas_drive_reservoirs

Petrowiki, 2018, January 15. Oil and gas processing. Retrieved January 15, 2018, from https://petrowiki.org/Oil_and_gas_processing

Ramirez-Garcia, O., 2019, Geologic Characterization and Modeling for CO2 Storage Reseource Assessment of the High Island Field 10L in Texas State Waters, Offshore Gulf of Mexico (Master Thesis): Unpublished.

Richards, J. V., 1998 High Island State Tract 60-S Field Jefferson County, Texas, Gulf Of Mexico: 3-D Seismic Case Histories From the Gulf Coast Basin: a GCAGS Special Publication. 139-146

Ruhe R. W., Griffin, P., 1970. Adaptation of Fixed Platform Rig Instrumentation to Floating Vessels, Offshore Technology Conference, 22-24 April. 1308-MS. http://dx.doi.org/10.4043/1308-MS

Ruiz, I., 2019., Characterization of the High Island Field 24L Field for Modeling and Estimating CO2 Storage Capacity in the Offshore Texas State Waters, Gulf of Mexico (Master Thesis), University of Texas at Austin,

Salim, M., Harley, J., & Faizal, Z. 2012, January 1. Process Design Aspects for Taking CO2 Enhanced Oil Recovery Offshore. Society of Petroleum Engineers. doi:10.2118/155527-MS

Salvador, A., 1987, Late Triassic-Jurassic paleogeography and origin of Gulf of Mexico Basin: AAPG Bulletin, v. 71, no. 4, p. 419–451.

Schlumberger, 2009, Log Interpretation Charts. Retrieved from http://pages.geo.wvu.edu/~tcarr/pttc/schlumberger_chartbook.pdf

Schlumberger., 2018, Secondary Recovery. Retrieved from https://www.glossary.oilfield.slb.com/en/Terms/p/secondary_recovery.aspx

Schlumberger, 2018, Primary Production. Retrieved from https://www.glossary.oilfield.slb.com/en/Terms/p/primary_production.aspx

Seni, S. J., Geological Survey of Alabama, & University of Texas at Austin, Bureau of Economic Geology, 1997, Atlas of northern Gulf of Mexico gas and oil reservoirs: The University of Texas at Austin, Bureau of Economic Geology.

Sills, S. R., 1993. AAPG Methods in Exploration Series, No. 10, AAPG. 9780891816607

Taber, J. J., Martin, F. D., Seright, R. S., 1997. EOR screening criteria revisited—Part 2: Applications and impact of oil prices. SPE Reservoir Engineering, 12(03), 199- 206.

Treviño, R. H., and Rhatigan, J.-L. T., 2017, Chapter 1: Regional geology of the Gulf of Mexico and the Miocene section of the Texas near-offshore waters, in Treviño, R. H., and Meckle, T. A., eds., Geological CO2 sequestration atlas for Miocene strata offshore Texas State Waters: The University of Texas at Austin, Bureau of Economic Geology Report of Investigations No. 283, p. 3-5.

Tutton, P.M., 2018, Carbon capture and storage network optimization under uncertainty (Master Thesis) University of Texas at Austin

Varhaug, S., 2016., Basic Well Log Interpretation, Oilfield Review, The Defining Series, Schlumberger

Vogler, H. A., and Robison, B. A., 1987, Exploration for deep geopressured gas—Corsair trend, offshore Texas: AAPG Bulletin, v. 71, no.7, p. 777–787.

Wallace, K. J., 2013, Use of 3-dimensional dynamic modeling of CO2 injection for comparison to regional static capacity assessments of Miocene sandstone reservoirs in the Texas State Waters, Gulf of Mexico: The University of Texas at Austin, M.S. Thesis, 152 p.

Winker, C. D., and Edwards, M. B., 1983, Unstable progradational clastic shelf margins, in Stanley, D. J., and Moore, G. T., eds., The shelf break: critical interface on continental margins: SEPM Special Publication, v. 33, p. 139–157.